Durham University

Durham E-Theses

An evaluation of imagery from an unmanned aerial vehicle (UAV) for the mapping of intertidal macroalgae on Seal Sands, Tees Estuary, UK

Stephen James Dugdale

How to cite:

Dugdale, Stephen James (2007) An evaluation of imagery from an unmanned aerial vehicle (UAV) for the mapping of intertidal macroalgae on Seal Sands, Tees Estuary, UK. Masters thesis, Durham University.

Use policy

The full-text may be used and/or reproduced, and given to third parties in any format or medium, without prior permission or charge, for personal research or study, educational, or not-for-profit purposes provided that:

- a full bibliographic reference is made to the original source
- a https://etheses.durham.ac.uk/id/eprint/2879/ is made to the metadata record in Durham E-Theses
- the full-text is not changed in any way

The full-text must not be sold in any format or medium without the formal permission of the copyright holders.

Please consult the full Durham E-Theses policy for further details.

Academic Support Office, The Palatine Centre, Durham University, Stockton Road, Durham, DH1 3LE
e-mail: e-theses.admin@durham.ac.uk Tel: +44 0191 334 6107
https://etheses.durham.ac.uk

An evaluation of imagery from an unmanned aerial vehicle (UAV) for the mapping of intertidal macroalgae on Seal Sands, Tees Estuary, UK

The copyright of this thesis rests with the author or the university to which it was submitted. No quotation from it, or information derived from it may be published without the prior written consent of the author or university, and any information derived from it should be acknowledged.

Thesis submitted for Master of Science (MSc) by Research

0 6 OCT 2008

Stephen James Dugdale, December 2007

Abstract

The Seal Sands area of Teesmouth is designated a Special Protection Area under the habitats directive because guideline concentrations of nutrients in coastal waters are exceeded. This may be responsible for extensive growth of the green filamentous macroalgae *Enteromorpha sp.*, and literature suggests that algal cover in the intertidal zone is detrimental to the feeding behaviour of wading bird species. Although numerous studies have highlighted the causes and consequences of macroalgal cover, the complex spatial and temporal dynamics of macroalgal bloom growth are not as well understood, and hence there is a need to develop a precise and cost effective monitoring method for the mapping and quantifying of algal biomass. Previous studies have highlighted several image processing techniques that could be applied to high resolution airborne imagery in order to predict algal biomass. In order to test these methods, high resolution imagery was acquired in the Seal Sands area using a lightweight *SmartPlanes SmartOne* unmanned aerial vehicle (UAV) equipped with a near-infrared sensitive 5-megapixel *Canon IXUS* compact camera, a standard 6-megapixel *Canon IXUS* compact camera and a *Garmin Geko 201* handheld GPS device. Imagery was acquired in November 2006 and June 2007 in order to examine the spectral response of *Enteromorpha sp.* at different time periods within a macroalgal growth cycle. Images were mosaicked and georeferenced using ground control points located with a *Leica 1200* differential GPS and processed to allow for analysis of their spectral and textural properties. Samples of macroalgal cover were collected, georeferenced and their dry biomass content obtained for ground truthing. Although textural entropy and inertia did not correlate significantly with macroalgal biomass, normalised green-red difference index (NGRDI), normalised difference vegetation index (NDVI) and colour saturation computed on the imagery showed a good degree of linear correlation with *Enteromorpha sp.* dry weight, achieving coefficients of determination in excess of $r^2 = 0.6$ for both the November 2006 and June 2007 image sets. Linear regression was used to establish predictive models to estimate macroalgal biomass from image spectral properties. *Enteromorpha sp.* biomass estimations of 71.4 g DW m^{-2} and 7.9g DW m^{-2} were established for the November 2006 and June 2007 data acquisition sessions respectively. Despite a lack of previous biomass quantification for Seal Sands, the favourable performance of a UAV in terms of operating cost and man hours required for image acquisition suggests that unmanned aerial vehicles may present a viable method for the mapping of intertidal algal biomass on an annual basis.

Contents

List of figures

List of Tables

List of Equations

Chapter 1. Introduction and Literature Review

1.1 Introduction

1.1.1 Ecological Monitoring

Well informed ecological management and decision-making requires accurate and reliable information on the causes and consequences of environmental change (Vos *et al.*, 2000). The gathering of data pertaining to ecological change is often seen as reactionary (Spellberg, 1991), and the increasingly complex response of the global environment to perceived anthropogenic impacts has necessitated the establishment of regional, national and international programmes with which to derive such information (eg. Scanlan *et al.*, 2007; Tegler *et al.*, 2001; Vos *et al.*, 2000). However, effective ecological monitoring is necessary not only to account for human influences on the environment, but also to gain a further insight into the spatial and temporal behaviour of the natural environment (Spellberg, 1991), with a view to advancing our knowledge of ecosystem dynamics.

Current ecological monitoring programmes are often viewed as time consuming, costly, and environmentally intrusive (Caughlan & Oakley, 2001; Gray, 1980). However, this represents something of a paradox, as the very purpose of ecological monitoring is to establish regular, detailed measurements of environmental conditions, usually over a long time period (Vaughan *et al.*, 2001). In light of this, although the length of time over which an ecological monitoring programme takes place is usually pre-determined, the time and cost required to perform measurements or surveys *within* a monitoring programme may be subject to change. Prior to the widespread use of proxy or remote monitoring efforts, Gray (1980) noted the prevalence of 'massive surveys [with] countless hours spent identifying and counting species...repeated as often as is practical'. Furthermore, Grey (1980) highlighted the need for alternative ecological monitoring techniques, in order to assuage the criticism of contemporary methods.

Remote sensing has, to some extent, been employed as a technique to resolve this issue, thus simultaneously increasing the spatial coverage and reducing the time and associated labour costs of conducting an ecological monitoring programme (eg. Scanlan *et al.*, 2007). However, for the purposes of smaller monitoring tasks, the cost of repeated 'standard' remote sensing surveys can

still be prohibitively expensive (Guichard *et al.*, 2000). It is therefore appropriate to look towards less conventional remote sensing methods by which ecological data can be gathered in a cost-effective, efficient manner, whilst still maintaining the regularity of measurement needed for the data produced to be fit for purpose. Within this thesis, I describe the application of a high resolution, cost effective remote sensing technique with a view to resolving the need for efficient, readily available ecological monitoring.

1.1.2 Macroalgal blooms as a case study for Ecological Monitoring

The role of the coastal ecosystem as a centre of human activity, coupled with the shortage of information about coastal habitats (Burke *et al.*, 2001) are chief motivators for the monitoring of estuarine systems. Although macroalgal blooms represent just one facet of the coastal ecosystem, their monitoring may help to identify the linkages between chemical pollution, estuarine eutrophication and widespread habitat loss within the intertidal zone (Scanlan *et al.*, 2007). Although a number of papers address appropriate means of quantifying macroalgal dynamics (eg. Brouwer *et al.*, 1995; Guichard *et al.*, 2000; Jeffrey & Hayes, 2005; Scanlan *et al.*, 2007), the rationale behind macroalgal monitoring is often site-specific (eg. Jeffrey & Hayes, 2005), or driven by a need to mitigate against the various environmental problems associated with bloom events (eg. Cabral *et al.*, 1999; Donoghue *et al.*, 2004a; McGlathery, 2001).

Jeffrey & Hayes (2005) present five chief reasons to assess the productivity of intertidal ecosystems: Quantification of intertidal carbon sequestration, quantification of estuarine material cycles, determination of resources available to secondary production, determination of the trophic status of the ecosystem and the need to assist the management of intertidal areas (Jeffrey & Hayes, 2005). As a major constituent of the intertidal environment, the rationale behind macroalgal monitoring can be explained using these terms. Potentially the most significant reason for determining intertidal primary productivity (and hence macroalgal productivity) is addressed first. Intertidal ecosystems are a fundamental component of the global carbon cycle (Jeffrey & Hayes, 2005), and because of this, the accurate monitoring and quantification of macroalgal biomass may help in determining the ability of intertidal ecosystems to sequester carbon dioxide. Observing the reaction of macroalgal blooms to enhanced carbon dioxide concentrations is also of importance

when attempting to assess the response of coastal ecosystems to global environmental change, as increased global atmospheric carbon may act to increase intertidal ecosystem productivity (Jeffrey & Hayes, 2005). Similarly, repeated observations of macroalgal habitats may help to highlight the complex effects of sea-level change on the coastal environment (Smith *et al.*, 1998), and the accurate monitoring of macroalgal blooms may help to highlight the response of intertidal ecosystems to global climatic change.

Jeffrey & Hayes' (2005) second and third points address pollutants, eutrophication and their associated impacts on secondary trophic levels. Macroalgae, especially *Ulva sp.* and *Enteromorpha sp.* are established bio-indicators. The tissues of a number of algal species readily absorb heavy metals and can be used to identify the bio-availability of heavy metal pollutants in an estuarine environment (Fytianos *et al.*, 1999; Villares *et al.*, 2001). Similarly, because the response of macroalgae to estuarine eutrophication is well established (Bjornsater & Wheeler, 1990; Fong *et al.*, 1996; Grall & Chauvaud, 2002; Martins *et al.*, 2001; Patricio *et al.*, 2004), the regular monitoring of intertidal algal biomass is necessary for highlighting areas affected by estuarine eutrophication. The response of macroalgae to eutrophication and estuarine nutrient influx is also of importance towards secondary trophic levels, as availability of both oxygen and dissolved organic matter are directly linked to macroalgal abundance (eg. Grall & Chauvaud, 2002; Trimmer *et al.*, 2000). Hence, the nutrients available to secondary producers are directly governed by the presence of macroalgae, and regular monitoring may help to identify the level of potential resources available for secondary productivity (Jeffrey & Hayes, 2005).

Determination of whether an estuarine system is autotrophic (self-sustaining) or heterotrophic (requires nutrient inputs) is addressed in Jeffrey & Hayes' (2005) fourth point. This item is of special significance to coastal ecosystems suffering from a high influx of pollutants, as highly polluted estuarine locations are likely to be heterotrophic owing to nutrient discharges. The monitoring of such areas is of high importance as it may help to advise management techniques for vulnerable heterotrophic coastal ecosystems (Jeffrey & Hayes, 2005). Jeffrey & Hayes' (2005) final point complements this: Through gaining an understanding of the primary productivity of an intertidal ecosystem, it possible to achieve a more complete insight into the environmental quality of the area in general. Intertidal communities have (in the past) been used as a proxy by which to determine more general environmental quality (Jeffrey & Hayes, 2005; Plater & Appleby, 2004), and the regular observation of macroalgal bloom behaviour as a facet of the coastal ecosystem could

facilitate enhanced understanding of the interactions between vegetation, sediment and topography of the intertidal environment as a whole (Smith *et al.*, 1998).

1.2 Literature Review

1.2.1 Causes of macroalgal blooms

With a view to constructing a methodological framework within which macroalgal blooms can be monitored, it is appropriate to review the literature relating to the growth of intertidal algal cover (Scanlan *et al.*, 2007). Although no comprehensive list of controlling and limiting factors has been devised, authors have stressed the importance of certain conditions in facilitating bloom development (eg. Fong *et al.*, 1996; Grall & Chauvaud, 2002; Martins & Marques, 2002; Martins *et al.*, 2001; Scanlan *et al.*, 2007).

Estuarine eutrophication is noted as a key contributor to macroalgal growth in most European intertidal environments (Patricio *et al.*, 2004) and nutrient limitation, particularly measured by nitrogen:phosphorus ratios, is regarded as one of the foremost factors in controlling macroalgal bloom growth (Bjornsater & Wheeler, 1990; Fong *et al.*, 1996; Grall & Chauvaud, 2002; Martins *et al.*, 2001). Grall & Chauvaud (2002) suggest that increased nutrient concentration, primarily from riverine flux, stimulates a growth in macroalgal biomass, although this is accompanied by associated variations in species distribution (Grall & Chauvaud, 2002). Under laboratory conditions, *Ulva fenestrata* and *Enteromorpha intestinalis* have shown to be limited by both nitrogen and phosphorus concentrations (Bjornsater & Wheeler, 1990). Field studies have also suggested that pulses of nitrogen associated with effluent and agricultural runoff stimulate *Enteromorpha sp.* growth (Fong *et al.*, 1996). However, it is possible that nitrogen:phosphorus ratios are only limiting in regions of low estuarine salinity (Martins & Marques, 2002; Martins *et al.*, 2001): The optimum salinity range for *Enteromorpha sp.* growth is 18-22 ppm (Martins & Marques, 2002), and *Enteromorpha sp.* shows sustained growth in waters of up to 30 ppm (relatively high salinity; (Martins *et al.*, 2001). Hence, because N:P ratios in estuarine environments are inversely proportional to salinity (Martins *et al.*, 2001), it is likely that nitrogen is only limiting in low salinity environments. Grall & Chauvaud

(2002) also suggest that the concept of nutrient limitation and eutrophication is widely oversimplified, and the response of algal blooms to eutrophication is subject to a range of biotic and abiotic factors. Grall & Chauvaud (2002) argue that intertidal hydrology and topography have a significant impact on the establishment of macroalgal blooms. The flushing potential of an estuarine or intertidal environment can act to influence the growth of eutrophication-forced algal blooms (Grall & Chauvaud, 2002), as areas with more efficient flushing have a reduced ability to accumulate nutrients (Schramm, 1999). Intertidal topography can also control algal bloom extent, as *Enteromorpha sp.* and *Ulva sp.* populations are also limited to areas where the estuarine altitude is below the level of mean high tide and above the light penetration depth (Scanlan *et al.*, 2007).

In nutrient-rich environments, light is considered a major controlling influence for algal bloom development (Grall & Chauvaud, 2002; Leland *et al.*, 2001). Leland *et al.* (2001) show that under nutrient rich conditions, summer light levels become the limiting factor for growth, as the photosynthetic demand for light exceeds available insolation. Grall & Chauvaud (2002) argue that this effect is due to high benthic productivity, which increases shading, and reduces the depth penetration of incident light. Similarly, Schramm (1999) noted that floating or semi-attached macroalgae can often out-compete hardier algae or seagrasses, simply by occupying locations on the substrate that are more conducive to light penetration. Light penetration can also be influenced by the ability of the water column to attenuate light. In a wholly marine environment, the maximum colonisation depth of macroalgae is limited not only by the turbidity of the water, but also the depth at which light is attenuated (Middelboe & Markager, 1997). Although this effect is diminished in an intertidal environment which is subject to patterns of cyclical inundation, water column attenuation can still affect macroalgal growth (Hanelt *et al.*, 1997). For similar reasons, it is also possible that longer periods of inundation can limit the exposure of macroalgae to potentially harmful radiation. Hanelt *et al.* (1997) note that estuarine environments are vulnerable to UV influenced photoinhibition, a physiological stress resulting from high photon flux densities (Adir *et al.*, 2003; Martins & Marques, 2002). Hence, the depth of the water column can directly influence the level of photoinhibition to which macroalgae are subject, both through the attenuation of UV light, and spectral changes in insolation received by the algal mat (Hanelt *et al.*, 1997).

Martins & Marques (2002) note that the photosynthetic response of algae to temperature follows a unimodal distribution, with a clearly defined optimum temperature range, although globally, *Enteromorpha sp.* is able to tolerate temperatures from 1.8°C to c. 30°C (Graham & Wilcox, 2000). Laboratory studies suggest that above 5°C, *Enteromorpha sp.* germination rates increase tenfold for every 6°C rise in temperature, with an optimum growth temperature of approximately 15°C (Lotze & Worm, 2002), although the temperature under which optimum growth occurs has been shown to vary according to location (Espinosa & Guerra-García, 2005). Lotze & Worm (2002) also noted that grazer populations increase in line with temperature, emphasising the difficulty in attempting to quantify the response of algal growth rates to temperature. The response of algal growth to grazers is also of importance when considering factors affecting bloom development. Although Scanlan *et al.* (2007) suggest that grazers do not have a significant impact on macroalgal growth, Schramm (1999) suggested that zooplankton and other marine fauna can lead to a signification reduction in macroalgal cover. However, anoxia resulting from the decomposition of large algal blooms may actually reduce grazer populations, leading to enhanced bloom development (Schramm, 1999). Anoxic conditions can also impair macroalgal growth rates, by limiting the ability of algae to compensate for biomass lost through grazing (Schramm, 1999).

Although *Enteromorpha sp.* and *Ulva sp.* are known to grow on a wide variety of surfaces and sediment types (Bold & Wynne, 1978), substrate is generally considered an important influence on macroalgal growth (Donoghue *et al.*, 2004a; Grall & Chauvaud, 2002; Kamer *et al.*, 2004; Scanlan *et al.*, 2007; Trimmer *et al.*, 2000). Grall & Chauvaud (2002) suggest that the nutrient concentrations in sediments are determined by grain size, and field studies have quantified a significant correlation between sediment porosity and organic carbon concentration (Trimmer *et al.*, 2000). Hence, substrates with larger void-spaces (eg. sand) tend to support elevated levels of organic carbon (Trimmer *et al.*, 2000) and may facilitate larger growths of macroalgae cover than those with smaller void-spaces (eg. mud/silt). Laboratory research has shown that *Enteromorpha intestinalis* grew faster when nurtured with intertidal sediments than with sand (Kamer *et al.*, 2004). It is, however, necessary to note that algal growth could also result from the recycling of either allochthonous or in-situ organic carbon (Trimmer *et al.*, 2000); therefore, the presence of algal cover could simply be a result of an already high carbon content rather than the ability of the sediment to store nutrients. Substrate stability is also likely to affect macroalgal growth. The

presence of *Enteromorpha sp.* on the tidal flat acts to bind sediment, increasing its stability and protecting from erosion (Friend *et al.*, 2003). This positive feedback is likely to further aid bloom development. Likewise, slope angle may also affect development of algal communities, although previous studies have only shown a ~4% difference in *Enteromorpha sp.* biomass between slope angles of 0° and 45° (Somsueb *et al.*, 2001).

To summarise, although there is broad agreement between the role of nutrients (nitrogen:phosphorus ratios), salinity, light and substrate on macroalgal bloom growth, the complex response of *Enteromorpha sp.* to estuarine grazer species is less well understood. Similarly, the varying roles of intertidal topography and temperature on limiting macroalgal development appear to vary in importance between geographical locations, indicating that *Enteromorpha sp.* behaviour may be site-specific.

1.2.2 Effects of macroalgal blooms

The response of intertidal environments to macroalgal blooms is generally considered a complex and spatially-dependent process (Raffaelli *et al.*, 1998), with chiefly detrimental consequences (Scanlan *et al.*, 2007) which are often cited as the major rationale behind macroalgal monitoring (eg. Scanlan *et al.*, 2007). Although it is difficult to produce an exhaustive analysis of the various influences of 'green-tide' events (Raffaelli *et al.*, 1998), the impacts of macroalgal blooms can largely be separated into biotic (ecosystem response; eg. Cabral *et al.*, 1999; McGlathery, 2001; Pihl *et al.*, 1999; Valiela *et al.*, 1997) or abiotic (sedimentary or nutrient response; eg. Bolam *et al.*, 2000; Eriksson *et al.*, 2002; Grall & Chauvaud, 2002; Trimmer *et al.*, 2000) factors.

A variety of literature addresses the biotic effects of algal blooms. Seagrass decline is generally noted as one of the most visible consequences of macroalgal expansion (McGlathery, 2001; Valiela *et al.*, 1997), primarily through shading and light attenuation (McGlathery, 2001). Macroalgal growth is often found associated with seagrass colonies due to the nitrifying ability of macrophyte roots (Valiela *et al.*, 1997). However, seagrass species are generally out competed, as algae can utilise incident radiation more efficiently (Valiela *et al.*, 1997). Pihl *et al.* (1999) suggest that such species competition propagates throughout the intertidal ecosystem, causing significant changes in the complexity of the intertidal ecosystem.

These changes in invertebrate species composition also affect higher trophic levels. The role of algal bloom cover on wader bird species diversity and behaviour is addressed by Bolam *et al.*, 2000, Cabral *et al.*, 1999, Lewis & Kelly, 2001, and Scanlan *et al.*, 2007, and although often species-specific (Lewis & Kelly, 2001), there are a number of common consequences of macroalgal matting. Anoxia resulting from macroalgal decomposition reduces the diversity of invertebrate prey (Cabral *et al.*, 1999; Lewis & Kelly, 2001). However, the abundance of prey available to bird taxa is also dependent on species (both bird and invertebrate): Certain invertebrate species favour algal matting (Bolam *et al.*, 2000; Cabral *et al.*, 1999), resulting in a larger food source for predators, whereas other species suffer a decline in numbers. Such changes in invertebrate community composition will inevitably lead to a change in feeding behaviour at higher trophic levels (Cabral *et al.*, 1999; Lewis & Kelly, 2001). Lewis & Kelly (2001) also note that the presence of macroalgal matting affects the ability of bird species to penetrate the sediment. Thicker/denser patches of algal matting provide a physical barrier between the wader and food source, inhibiting the ability of the bird to feed (Lewis & Kelly, 2001).

Bolam *et al.* (2000) note that the abiotic impacts of macroalgal mat development are largely predictable and generally site independent. Artificial plantations of *Enterormopha sp.* have shown to cause widespread changes in substrate composition, with significant increases in the percentage of water, organic, and minerogenic sediment content (Bolam *et al.*, 2000). Changes in the chemical composition of the substrate by the presence of algal mats are generally considered adverse for faunal and floral populations (Schramm, 1999). Hydrogen sulphide produced through respiration and decay of macroalgae is released into sediments beneath algal matting (Norkko *et al.*, 2000; Trimmer *et al.*, 2000), presumably altering the substrate pH balance. Anoxia resulting from the either the large respiratory demand of algal matting (Trimmer *et al.*, 2000) or from decaying macrophyte populations (Schramm, 1999) results in water column stratification and the presence of a distinct oxygen profile within the littoral zone. Such disoxia may also result in a 'vertical particle flux' (Grall & Chauvaud, 2002), affecting the mineralisation of organic particulate matter. The affects of macroalgae on the mineralisation of nutrients within the water column is widely noted (eg. Grall & Chauvaud, 2002; Trimmer *et al.*, 2000). Detrital matter released from decaying macroalgae results in the net export of organic carbon to the litteral zone, where rapid mineralisation occurs (Grall & Chauvaud, 2002). Further to the minerogenic effects of macroalgal

cover, the presence of *Entermorpha sp.* matting works to enhance bed stability by binding sediment and presenting a boundary layer between the substrate and water column (Brown *et al.*, 2000; Friend *et al.*, 2003), as well as by reducing flow velocities through increased turbulence (Brown *et al.*, 2000). It is fairly safe to assume that such a reduction in flow velocity would result in increased sedimentation rates (Allen, 2000).

Because the causes and consequences of macroalgal growth are determined by the interplay of a wide variety of complex factors (detailed above), present scientific understanding of the precise effects of bloom development is limited (Scanlan *et al.*, 2007). Although a number of papers address the causes of macroalgal growth, (eg. Fong *et al.*, 1996; Grall & Chauvaud, 2002; Martins & Marques, 2002; Martins *et al.*, 2001; Scanlan *et al.*, 2007), most studies concentrate on the individual factors, rather than addressing the complex interactions among possible causal mechanisms. Similarly, although a variety of literature has addressed the problems associated with macroalgal matting (eg. Bolam *et al.*, 2000; Cabral *et al.*, 1999; McGlathery, 2001; Raffaelli *et al.*, 1998), there is a tendency to view many of the consequences as isolated and site-specific.

In order to address the above shortfalls in our understanding of the causes and consequences of macroalgal mats, it is necessary to look for ways of better observing the development of blooms. Although the application of various monitoring techniques to studying bloom development has generally resulted from the need to assess estuarine eutrophication (Scanlan *et al.*, 2007), regular monitoring also allows for the study of the dynamic behaviour of algal mats. Through regular monitoring, it may be possible to quantify the behaviour of macroalgal matting in response to various forcing mechanisms.

1.2.3 Techniques for quantifying macroalgal blooms

Scanlan *et al.* (2007) describe a number of methods through which macroalgal cover can be monitored and quantified, either by percentage cover or total algal biomass. Conventional transect surveys are primarily used for detailed multitemporal monitoring (eg. Donoghue *et al.*, 2004a), and are generally deemed the most accurate and highest resolution monitoring technique for assessing macroalgal cover or biomass (Berglund *et al.*, 2003), but they are usually considered expensive

(Caughlan & Oakley, 2001; Gray, 1980), highly labour intensive (Berglund *et al.*, 2003; Scanlan *et al.*, 2007), and around 10 times slower than remote sensing methods (Berglund *et al.*, 2003). Such methods can also be environmentally insensitive and intrusive both in terms of the disturbance caused by the presence of humans at an ecologically sensitive site, and the survey techniques employed, which often involve bulk sampling of algal tissues (Foley *et al.*, 1998). Vaughan *et al.* (2001) suggest that proxy or surrogate monitoring can be used to infer measurements, in the absence of data pertaining to the required variable. It is possible that this method could be used to avoid the intrusion/disturbances inflicted by conventional transect surveys. However, there is little data regarding the use of surrogate observations in the field of macroalgal monitoring. Similarly, although proxy records are often used in the absence of adequate long-term monitoring records (Vaughan *et al.*, 2001), giving good *temporal* resolutions, the ability of proxy records to infer *spatial* trends is not clear.

The use of remote sensing as an ecological monitoring tool is suggested as a means of resolving the above issues (eg. Scanlan *et al.*, 2007). Remote sensing is regarded as relatively cheap and less labour intensive (Berglund *et al.*, 2003), and can be applied at a number of different spatial and temporal scales (Scanlan *et al.*, 2007). Similarly, remote sensing, by its very nature, is a means by which environmental processes can be monitored from a distance, thereby limiting ecological disturbance. For this reason, remote sensing provides an ideal compromise between spatial coverage, accuracy and cost, and is widely advocated as a method for cost-effective monitoring of estuarine and intertidal environments at easy replicable temporal and spatial scales (eg. Berglund *et al.*, 2003; Cracknell, 1999; Donoghue *et al.*, 2004a; Guichard *et al.*, 2000; Scanlan *et al.*, 2007; Smith *et al.*, 1998). The very use of remote sensing to monitor a fundamentally biological process also brings about an element of interdisciplinarity, highlighting the applicability of remote sensing techniques outside the remit of purely geospatial research.

1.2.4 Remote sensing for macroalgal bloom monitoring

Cracknell (1999) notes that a number of recent advances in remote sensing techniques (eg. airborne imaging spectrometers, sub-1m resolution satellite imagery and bathymetric lidar) have facilitated repeatable environmental monitoring on a large spatial scale (Smith *et al.*, 1998). Because the uses

of SAR and LiDAR in estuarine environments are generally limited to the creation of topographic and bathymetric data (Cracknell, 1999), most papers relating to monitoring intertidal macrophyte and macroalgal blooms focus on optical remote sensing systems (eg. Cracknell, 1999; Guichard *et al.*, 2000; Scanlan *et al.*, 2007; Smith *et al.*, 1998). There are a number of theoretical considerations involved in the use of optical data to discriminate algal blooms. Temporal and seasonal changes in light conditions can produce significant variation in the amount of radiation received from the same surface during different time periods (Smith *et al.*, 1998), through changes in atmospheric conditions and the seasonal alteration in the angle of incident radiation (Smith *et al.*, 1998). Surface moisture, sediment entrainment (Carrère *et al.*, 2004) and period of inundation (Smith *et al.*, 1998) can also affect the spectral response of intertidal vegetation. When monitoring macroalgal blooms, it is also pertinent to account for temporal variations in algal growth. The gamete release patterns of both *Ulva sp.* and *Enteromorpha sp.* is determined by the lunar cycle, with gamete release occurring immediately prior to spring tide (Graham & Wilcox, 2000; Lee, 1999). This occurrence is marked by a change in vegetation colour (Haxo & Clendenning, 1953), altering the spectral response of the macroalgae. Similarly, photoacclimation of macroalgae to incident radiation is also likely to influence spectral response by altering cellular chlorophyll concentrations (Falkowski & LaRoche, 1991).

Studies concerned with the use of multispectral remote sensing data have previously focused on the need to discriminate the various algal species spectrally. The use of portable spectrometers to assess coastal zone biodiversity has shown good correlation with expert survey data, suggesting that it is possible to identify macroalgal species spectrally (Forster & Jesus, 2006). Similarly, Carrère *et al.* (2004) show that portable spectrometers can be used to assess chlorophyll-*a* concentrations in microphytobenthos (high chl-a concentrations are marked by strong absorption at ~623nm; (Carrère *et al.*, 2004)), highlighting the possibility of using spectral data to detect species abundance. Although portable spectrometers have been shown capable of producing cost-effective, accurate data (Forster & Jesus, 2006), the need to cover large intertidal areas means that airborne or satellite based sensing platforms are often favoured (eg. Cracknell, 1999; Scanlan *et al.*, 2007; Smith *et al.*, 1998). Smith *et al.* (1998) show that the Compact Airborne Spectrographic Imager (CASI) can adequately identify general areas of macroalgal matting, although difficulties associated with the geocorrection of CASI imagery (Smith *et al.*, 1998), as well as the variable pixel size makes adequate discrimination of macroalgal features difficult. Similarly, although the Landsat TM sensor

has been shown to discriminate between different intertidal habitats with a relatively high degree of accuracy (Larsen *et al.*, 2004), higher spatial resolution is recommended for coastal areas with 'complex habitat heterogeneity' (Larsen *et al.*, 2004), and even the relatively small pixel sizes of the IKONOS (c. 5m) and Quickbird (c. 2.5m) satellite-based multispectral images are too large to be amenable to small-scale macroalgal monitoring.

Guichard *et al.* (2000) notes the lack of research addressing the gap in spatial scales between low-resolution monitoring projects (eg. Landsat; Larsen *et al.*, 2004), and experimental or lab-based coastal observation work (eg. Bjornsater & Wheeler, 1990; Bolam *et al.*, 2000; Fong *et al.*, 1996; Forster & Jesus, 2006), and recommends that for detailed biological study, data with a ground resolution of < 0.5m is required (Guichard *et al.*, 2000). Although conventional aerial photography can provide imagery with spatial resolutions of this order, the cost and time constraints of data acquisition is generally not amenable to interannual or multi-temporal monitoring purposes (Guichard *et al.*, 2000; Hunt *et al.*, 2005). It is therefore necessary to look for alternate platforms which can simultaneously provide low-cost, high resolution aerial imagery 'able to match the rich spectral and spatial diversities observed in coastal systems' (Malthus & Mumby, 2003).

1.2.5 Unmanned aerial vehicles (UAVs) as an alternative coastal monitoring platform

Remote sensing solutions can largely be separated into airborne and satellite-borne sensors (Mather, 2004). As discussed previously, satellite platforms do not offer the spatial resolution amenable to detailed biological monitoring, and must be rejected in favour of aerial platforms. Airborne platforms can be further categorised in terms of their spatial, spectral, radiometric and temporal resolutions (Mather, 2004). Although manned aircraft offer a wide variety of spectral and radiometric resolutions (eg. Airborne Visible/Infrared Imaging Spectrometer (AVIRIS), 224 bands; Vane *et al*, 1993), as well as the spatial resolutions required to observe detailed biological trends, the cost of manned survey flights can affect the practicalities of gaining an adequate temporal resolution. Instead, unmanned aerial vehicles can largely negate the problems associated with high-temporal resolution monitoring. Current UAVs in use as remote sensing platforms can be largely separated into four categories: High-Altitude Long-Endurance (HALE) systems capable of

large-swath geostationary monitoring (eg. MERCATOR-1; Delauré *et al*, 2007), lightweight fixed-wing platforms used for small-scale agricultural and environmental applications (eg. Labbé *et al*, 2007; Hunt *et al.*, 2005; Quilter & Anderson, 2000), small Helicopter systems (eg. Lambers *et al* (2007) and experimental balloon/blimp platforms (eg. Guichard *et al.*, 2000).

Malthus & Mumby (2003) note that the use of unmanned aerial vehicles (UAVs) for monitoring in the coastal zone 'offers benefits in terms of frequency of coverage, spatial resolution, flexibility in spectral resolution and maintenance and calibration' (Malthus & Mumby, 2003). However, there is a relative lack of material detailing the use of UAVs in coastal environments, with most UAV-based work dominated by agricultural (eg. Hunt *et al.*, 2005; Quilter & Anderson, 2000) or military (eg. Holland *et al.*, 2002; Lomax *et al.*, 2005) research. Although much of the major research into UAVs focuses on large, high-endurance craft (Lomax *et al.*, 2005), there is a growing amount of material espousing the benefits of lightweight fixed-wing radio-controlled UAVs (eg. Hunt *et al.*, 2005). Because of the relatively small size and weight, lightweight UAVs lend themselves well to coastal monitoring operations, where rapid deployment and image acquisition may be necessary (Lomax *et al.*, 2005). Similarly, labour costs involved in operating and maintaining lightweight UAVs are significantly lower than conventional aerial photography (Lomax *et al.*, 2005), and the ease of launch and recovery enables the use of UAVs in environments that are inaccessible to conventional aircraft (Lomax *et al.*, 2005). Peterson *et al.* (2003) note that when compared with satellite-based imaging platforms, UAV systems offer greater reliability and flexibility. The ability of the UAV operator to remove, calibrate and repair sensor systems means that UAV imaging systems do not suffer from the degradation problems associated with satellite imagers (Peterson *et al.*, 2003). Similarly, the design of most UAVs is such that they allow the user to choose from a variety of sensors, allowing greater flexibility than satellite systems (Peterson *et al.*, 2003). This also adds an element of 'future-proofing' to the UAV concept, as newer and more advanced sensors could be chosen to reflect improving technologies.

There are, however, a number of limitations to UAVs which must be addressed. Although it is established that the cost of UAV imagery is significantly lower than standard aerial imagery (Guichard *et al.*, 2000; Hunt *et al.*, 2005; Lomax *et al.*, 2005; Peterson *et al.*, 2003; Quilter & Anderson, 2000), it is possible that the labour costs involved in frequent UAV monitoring flights could actually be greater than the costs of imagery from satellites with a fast revisit rate (Peterson *et al.*, 2003). Peterson *et al.* (2003) also suggest that the small scene-size produced by UAV systems

(compared to larger satellite scenes) can make mosaicking difficult and time consuming, and inhibit data processing efforts. Lomax *et al.* (2005) also note the multitude of purposes for which UAVs may be used in a coastal monitoring context: Because macroalgal monitoring may require different image processing techniques to those used when monitoring, for example, oil spills, it is likely that different image resolutions, and hence, different flying altitudes will be used (Lomax *et al.*, 2005). This is of significance for two reasons: first, because data acquired for one purpose may be inadequate for others, necessitating further UAV flights of the same area. Secondly, obtaining imagery at a precise altitude may be difficult, owing to atmospheric conditions in coastal areas. This may mean that imagery acquired from a UAV in a coastal location may require a significant amount of geometric correction, leading to further image degradation, because the greater affect of atmospheric turbulence at low levels may contribute greater distortions to the dataset, requiring increased image post-processing (Peterson *et al.*, 2003).

1.2.6 Derivation of biological information from UAV-based imagery

In order to derive metrics with which to quantify macroalgal biomass from aerial imagery, it is necessary to look at the suitability of various processing techniques that can be applied to UAV-based imagery. The majority of previous studies aimed at deriving algal or floral biomass from UAV imagery used either commercial 35 mm film cameras with filters sensitive to visible or near-infrared light or similar digital data using a CCD (eg. Guichard *et al.*, 2000; Hunt *et al.*, 2005; Peterson *et al.*, 2003; Quilter & Anderson, 2000). Although data of this type could be considered multispectral, the limited number of discrete spectral bands within imagery of this type and the lack of separate detectors for different wavelengths means that alternate or unconventional image processing techniques must be considered with a view to extracting the maximum amount of data possible from commercial 'off-the-shelf' camera equipment.

1.2.6.1 Normalized Green-Red Difference Index (NGRDI) and Normalized Difference Vegetation Index (NDVI)

Curran & Steven (1983) state that pigments within vegetation cause the absorption of blue and red wavelengths and the reflectance of green wavelengths. Near-infrared wavelengths are also strongly reflected by cellular refraction. Although substrate and shadow also have distinct spectral signatures, vegetation shows the highest spatial and temporal variability (Curran & Steven, 1983), and has the greatest influence on spectral response. Curran & Steven (1983) showed that green leaf area index exhibits a negative correlation with red reflectance and a positive correlation with near-infrared reflectance. In light of this, ratios can be used in order to express this increasing difference between the NIR/green and red bands.

Hunt *et al.* (2005) suggest that the difference in spectral response between the red and green bands over vegetation and soil can be used to relate ground biomass to image digital number intensity (DN) values. They used a lightweight radio-controlled aircraft equipped with a 4 megapixel digital camera to acquire imagery of crop plantations from an altitude of ~200 m. Imagery was separated into red, green and blue components by the Bayer mask coating on the CCD, and radiometrically calibrated using a monochromatic light source. The Normalized Green-Red Difference Index (NGRDI) was then applied to the images:

$$\mathrm{NGRDI} = \frac{(\mathrm{Green} - \mathrm{Red})}{(\mathrm{Green} + \mathrm{Red})} \qquad (1.1)$$

(where *Green* and *Red* are the intensity values of the green and red bands respectively) in order to analyse the difference in red and green spectral response with a view to assessing crop biomass.

When compared to ground truth data, Hunt *et* al (2005) observed that NGRDI values exhibited a level of linear correlation to alfalfa crop biomass values (R^2 = 0.47), although the quality of data varied according to crop species and date of image acquisition. Corn and soybean crops also exhibited a correlation with NGRDI, but indicated a threshold above which biomass could not be related to NGRDI. Substrate moisture was also shown to influence the spectral response measured by the detector. Although application of this technique in a coastal context is limited, it is possible that this method may provide a similar degree of correlation with macroalgal biomass.

Guichard et al. (2000) used a helium-filled blimp at an altitude of ~100m to acquire colour infrared photography using a standard 35 mm camera equipped with professional infrared EIR film. Although radiometric calibration was not carried out, they computed a *relative* Normalized Difference Vegetation Index (NDVI) on the near-infrared and red channels of the EIR film in order to estimate intertidal macroalgal biomass:

$$NDVI = \frac{(NIR - Red)}{(NIR + Red)} \tag{1.2}$$

where *NIR* and *Red* are the intensity values of the near-infrared and red bands respectively.
NDVI showed a strong positive correlation with algal biomass (R^2=0.73; Guichard *et al.*, 2000) on smooth substratum (eg. sand/silts). NDVI/biomass correlation was poor on complex substrate (eg. boulders), showing significant deviation from the ground-calibration data (Guichard *et al.*, 2000). This was noted to be a result of dense biomass matting within boulder crevices that was outside of the biomass range of the ground truth calibration set.

1.2.6.2 HSV (or HSI) colour transformations

In the absence of a clearly established method for the derivation of algal biomass data from UAV-based digital imagery, it is prudent to examine a wide variety of image processing techniques to provide metrics. A small number of papers have looked towards colour transformations as a way of extracting agricultural vegetation percentage cover data from standard 3-band (RGB) aerial imagery (eg. Casadesús *et al.*, 2007; Catani *et al.*, 2005; Karcher & Richardson, 2003; Laliberte *et al.*, 2006; Laliberte *et al.*, 2007; Li *et al.*, 2005) with varying degrees of success. Although a considerable number of colour transformations are available (Li *et al.*, 2005), the Hue-Saturation-Value (or Hue-Saturation-Intensity) transformation is widely used, because it a) approximates human colour perception (Laliberte *et al.*, 2007; Li *et al.*, 2005), highlighting the relative dominance (hue) and purity (saturation) of a certain colour (Laliberte *et al.*, 2007), and b) reduces the band intercorrelation observed when using standard RGB colours helping to differentiate between

vegetation types that would normally be difficult to discriminate when using the RGB colourspace (Laliberte *et al.*, 2007).

The HSV colourspace transformation can be described using the equations:

$$H = \begin{cases} 60\left(\dfrac{G-B}{MAX(R,G,B)-MIN(R,G,B)}\right) & \text{if } MAX(R,G,B)=R \\ 60\left(2+\dfrac{B-R}{MAX(R,G,B)-MIN(R,G,B)}\right) & \text{if } MAX(R,G,B)=G \\ 60\left(4+\dfrac{R-G}{MAX(R,G,B)-MIN(R,G,B)}\right) & \text{if } MAX(R,G,B)=B \end{cases} \quad (1.3)$$

$$S = \frac{MAX(R,G,B)-MIN(R,G,B)}{MAX(R,G,B)} \quad (1.4)$$

$$V = MAX(R,G,B) \quad (1.5)$$

where *H*, *S* and *V* are hue, saturation and value, respectively, *R*, *G* and *B* are green, red and blue DN, respectively, and *MAX* is equal to the maximum of (R,G,B) and *MIN* the minimum. Figure 1.1 is a visual representation of the HSV model.

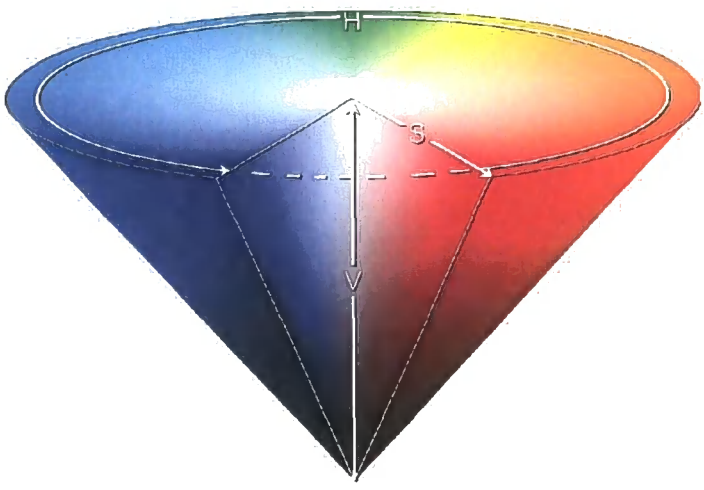

Figure 1.1 Visual representation of the HSV colour space model.

Both the Hue and Saturation components of the HSV transformation have been shown to correlate well with *percentage cover* of vegetation (R^2 = 0.7 - 0.9; Laliberte *et al.*, 2006; Li *et al.*, 2005). However, there is a paucity of data relating either macroalgal *percentage cover* or, more significantly, *biomass* to the HSV colour transformation.

1.2.6.3 Image Texture

It is possible that images with a sufficiently high spatial resolution, such as those obtained using a UAV, can impair 'normal' spectral classification efforts, because 'single pixels no longer capture the characteristics of classification targets' (Yu *et al.*, 2006). Pixels in an image with coarser resolution may facilitate spectral classification because each pixel represents the average spectral response over a larger area, aiding classification efforts (Yu *et al.*, 2006), and in light of this, it is pertinent to look towards region-based methods of image analysis in order to supplement or supplant conventional spectral analysis.

Image texture is '...concerned with the spatial distribution of the image intensities and discrete tonal features' (Haralick & Shapiro, 1992); little variation in tonal features within an image is described as sparsely textured whereas an image with wide variation in tonal features is regarded as highly textured. Image textural analysis is therefore concerned with the conversion of an image into a texture map where pixel intensity represents textural variation in the original image (Carbonneau *et al.*, 2005). The tonal variation within an image is described within the grey level co-occurrence matrix (GLCM), 'a matrix of relative frequencies...with which two neighbouring pixels ...occur on the image' (Haralick & Shapiro, 1992).

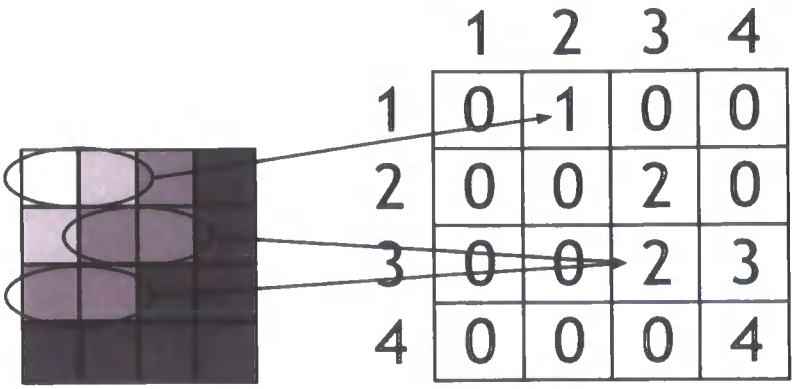

Figure 1.2 Simple schematic of gray level co-occurrence matrix (GLCM). Describes the frequency with which a grey level occurs alongside a neighbouring grey level within an image.

Figure 1.2 illustrates the creation of the grey level co-occurrence matrix. The image to the left of the schematic shows a small subset of a larger image, composed of four grey levels. The matrix to the right is the GLCM computed from the image subset. The image shows one occurrence of a grey level of 1 (white) next to a grey level of 2 (light grey), and two occurrences of a gray level of 3 (medium gray) next to another grey level of 3. These instances are marked as 'counts' in the appropriate cells. It is necessary to note that the figure 1.2 GLCM has been computed in 90° direction, so only the horizontal relationship of the pixels has been noted into the GLCM.

Once the GLCM has been computed on an image, the role of texture analysis is to condense the GLCM to a single number which represents local image texture (eg. Carbonneau *et al.*, 2005; Haralick & Shapiro, 1992). Although there are numerous texture measures which can perform this analysis, the derivation of biomass information from image texture measures is rarely studied (Lu & Batistella, 2005), and the paucity of information regarding the use of specific texture measures and kernel sizes for biomass assessment (Lu & Batistella, 2005) justifies the need for further study.

The *entropy* and *inertia (contrast)* texture measures are relatively widely used for biological/ecological image analysis purposes (eg. Lu, 2005; Lu & Batistella, 2005; Wikantika *et al.*, 2004). Entropy has been shown to correlate well with forest biomass (Lu, 2005) and vegetation cover change (Wikantika *et al.*, 2004), and is a measure of the tonal disorder within an image (Wikantika *et al.*, 2004); the lower the tonal variation within an image, the higher the entropy value (Carbonneau *et al.*, 2005). Entropy is defined as:

$$E = \sum_{ij} P_{ij} \log P_{ij} \quad (1.6)$$

where *E* is the entropy calculation and *P* is the GLCM.

Lu & Batistella (2005) also noted a significant correlation between inertia and mature forest biomass. Inertia (or contrast) is a calculation of 'the difference between the highest and the lowest values of a continuous set of pixels' (Wikantika *et al.*, 2004), and is defined as

$$I = \sum_{ij} (i - j)^2 P_{ij} \quad (1.7)$$

where *I* is the inertia value and *P* is the GLCM.

Hence, although the usefulness of texture to derive macroalgal or coastal biomass has not been assessed, the good correlations demonstrated between texture measures and vegetation biomass (eg. Hudak & Wessman, 2001; Lu & Batistella, 2005) suggest that image texture analysis may yield further information from either standard RGB or greyscale imagery, highlighting its potential as a method for the extraction of quantitative biomass data from imagery with limited spectral information.

1.3 Research Questions & Objectives

In light of the above, it is plausible that unmanned aerial vehicles could be used as an alternative source for the acquisition of data amenable to ecological monitoring. However, relatively little research has been undertaken in this domain, and in the absence of any previous detailed investigations into the application of UAVs for the purpose of monitoring macroalgal blooms, it is necessary to consider the appropriate research questions with which to assess the benefits of unmanned aerial vehicles to the field of ecological monitoring.

1.3.1 Research Questions

1. In order to synthesize usable monitoring data from UAV-derived imagery, it is pertinent to examine the relationship between UAV image metrics and ground truth data. To this end, it is necessary to establish whether there is a significant relationship between image metrics and ground truth data, and to what extent can this relationship be accounted for?

2. The quality of the data produced by the UAV is of key importance with regards to the use of unmanned aerial vehicles for ecological monitoring. In order to evaluate the suitability of the UAV for ecological monitoring, it is necessary to establish whether the data is sufficient for adequate correlation with ground truthing: Does the image processing methodology produce data that is adequate for correlation with ground truthing?

3. Once suitably robust techniques have been established with which algal biomass can be correlated to aerial imagery, it is necessary to test the validity of these methods by applying them to acquired imagery. Can macroalgal biomass be modelled using the above relationships between image metrics and ground truth data?

4. The time and cost involved in producing usable data for ecological monitoring is regarded as a key reason for the uptake of alternative remote sensing technologies, and more cost-effective methods may facilitate the increased use of remote sensing for ecological monitoring purposes. Would the use of an unmanned aerial vehicle (UAV) to monitor macroalgae represent a realistic time/cost benefit over more traditional remote sensing approaches?

5. The use of unmanned aerial vehicles as a tool with which to observe macroalgal bloom dynamics can only provide a limited insight into the suitability of unmanned aerial vehicles for the much broader scope of ecological monitoring. In mind of the above questions, could unmanned aerial vehicles (UAVs) be used as a feasible source of high resolution imagery for ecological monitoring purposes?

1.3.2 Research Objectives

1. To acquire high resolution imagery of a suitable site using a lightweight radio-controlled unmanned aerial vehicle (UAV) in order to identify macroalgal coverage.

2. To obtain accurate ground control and ground truthing for the imagery.

3. To identify and establish an image processing methodology to derive metrics that can be used to correlate with ground truth data.

4. To test the relationship between image metrics and ground truth data and use this to assess macroalgal biomass at the site.

5. To evaluate the feasibility of using such techniques for ecological monitoring.

Chapter 2. Methodology

2.1 Study Area

Seal Sands comprises a section of the Teesmouth National Nature Reserve (NNR) in the Cleveland Coast, and is the most extensive area of intertidal mudflat on the East Coast of England in a ~230 km stretch of coastline between Humberside and Lindisfarne (Natural England, 2001).

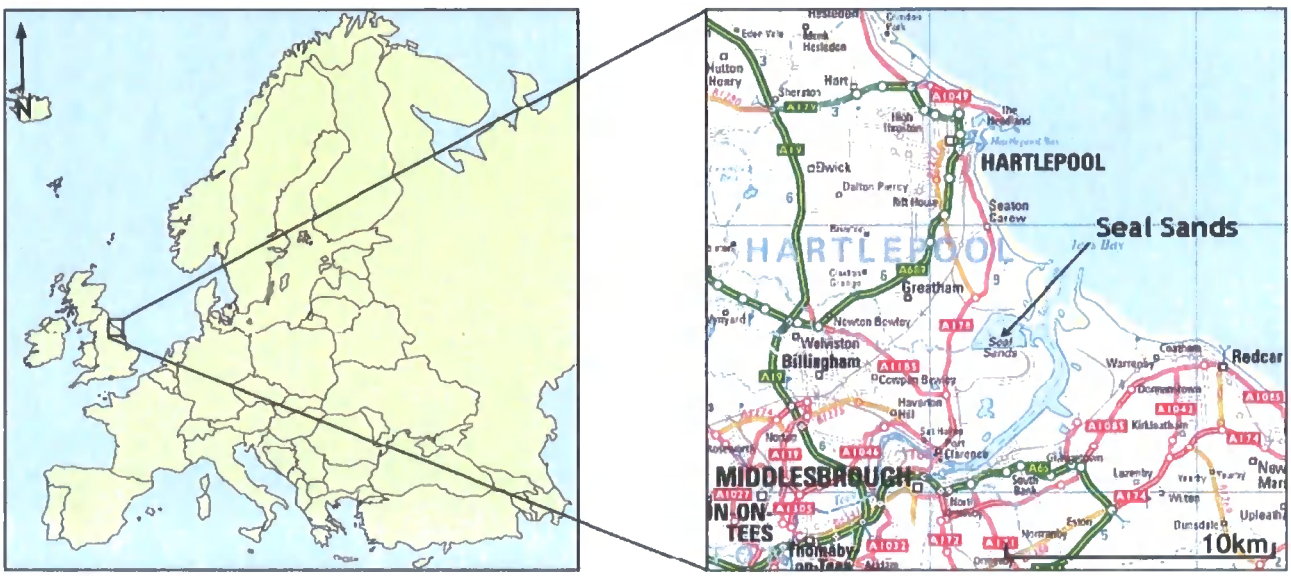

Figure 2.1 Location of Seal Sands SPA. Source: EDINA, 2004

Large scale land reclamation at Seal Sands prior to 1975 greatly reduced the area of land subject to tidal influence (Doody, 2004), from ~2500 ha in 1820 to ~400 ha by 1970 (Evans *et al.*, 1999). The remaining area of intertidal flats was partitioned by the deposition of a slag wall, leading to the annexing of the southern intertidal sector, and the subsequent formation of brackish or freshwater marshland in the absence of regular tidal inundation. The majority of the Seal Sands mudflat is exposed for ~7.5 - 8.5 hours of each tidal cycle (Davidson & Evans, 1986). The site is bordered by reclaimed wetlands on the south and west sides (Davidson & Evans, 1986), and is enclosed to the east by a grassed embankment and access road. When inundated, the intertidal area drains into Seaton on Tees Channel to the north, through a large number of creeks and channels, the largest of which, Greatham Creek, divides the mudflat area in the south-west corner (see figure 2.3). The Seal Sands area has been severely impacted by the effects of agricultural expansion, industrial

development, and channel dredging (Davidson *et al.*, 1991; Evans *et al.*, 1999), and is subject to a number of international, European and national protocols regarding further anthropogenic encroachment. Teesmouth and Cleveland Coast is listed as a Wetland of International Importance under the Ramsar Convention (Ramsar Convention, 2007), and the Seal Sands area is recognised as a site of international significance under the European Community Directive on the Conservation of Wild Birds due to the presence of a number of rare wading bird and migratory wildfowl species (Davidson *et al.*, 1991; Evans *et al.*, 1999; Natural England, 2001; Ratcliffe, 1977). The area is also a Site of Special Scientific Interest (SSSI) under the Wildlife and Countryside Act (1981), with particular notice given to the internationally significant counts of knot and redshank wading bird species.

Seal Sands is designated as a Special Protection Area (SPA) under the habitats directive, because guideline concentrations for nutrients in coastal waters, resulting largely from effluent and sewage discharge, (Donoghue *et al.*, 2004a) are exceeded. The intertidal area supports extensive growth of the attached green filamentous macroalgae *Enteromorpha sp.* (see figure 2.2), and there is concern that intertidal algal cover is deleterious to the feeding behaviour of wading bird species (Donoghue *et al.*, 2004a).

Aside from affluent discharge, lead and zinc compounds are seen as the major contaminants of the tees estuary, resulting from 19th century mining of the North Pennines ore field (Plater & Appleby, 2004). Quantities of arsenic and potassium found within the substrate at Seal Sands are noted as a consequence of fertiliser production within Teesside, as are a number of other heavy metal compounds, resulting from post-1920s chemical and metallurgic industries located near the site (Plater & Appleby, 2004).

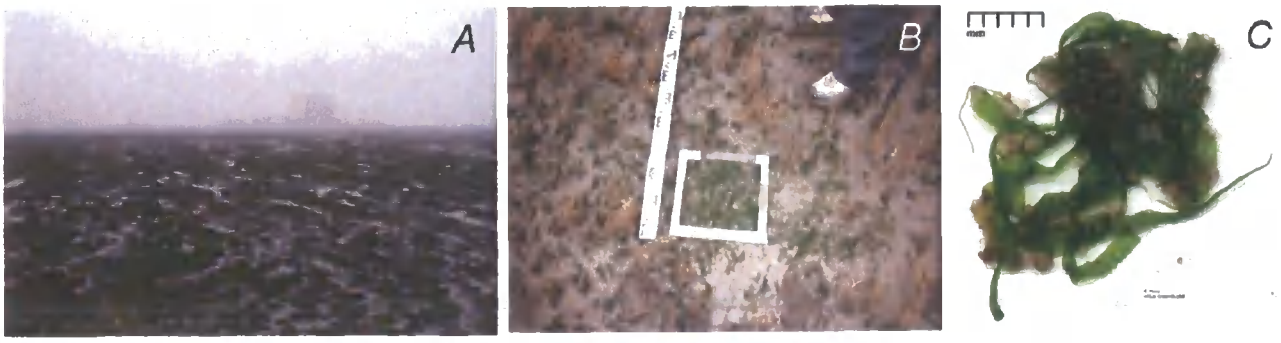

Figure 2.2 (A & B) *Enteromorpha sp.* cover at Seal Sands. **(C)** Laboratory sample of *Enteromorpha sp.* Source: Perry, 2001.

Figure 2.3 Aerial photograph of Seal Sands. 1:5000 scale. Source: Donoghue *et al.*, 2004a

The SSSI area is divided into three units (see figure 2.4) based on conservation status (Natural England, 2007). Of the two smaller areas, unit 2 is classed as 'destroyed', owing to major land reclamation, and unit 3 is considered 'favourable', with little macroalgal disturbance (Natural England, 2007). Unit 1, a ~245 ha area of littoral sediment (comprising ~82% of the total SSSI area), is significantly larger, encompassing the majority of the Seal Sands intertidal area, and is regarded as 'unfavourable - no change', because of extensive *Enteromorpha sp.* cover at the site. However, the most recent unit assessment (May 2007) notes the requirement for more detailed quantification of macroalgal cover (Natural England, 2007).

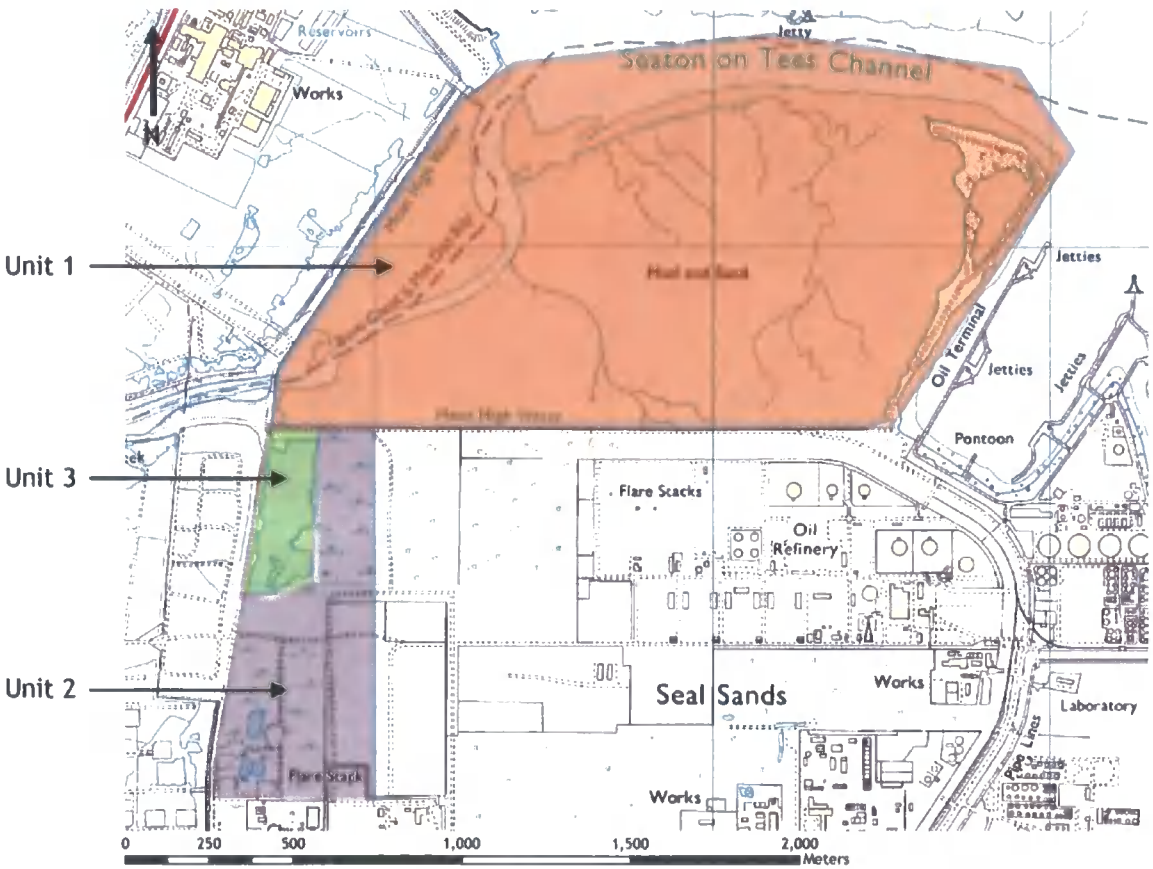

Figure 2.4 SSSI Unit coverage of Seal Sands. Modified from: Natural England, 2007.

Of the three SSSI units present, Unit 1 is the most obvious site for monitoring. Previous studies of *Enteromorpha sp.* cover in this unit have shown a gradual increase in percentage macroalgal cover from 1992 (11.2% in 1992 to 36.9% in 1996; EA, 1999), followed by a peak (~50% coverage) and subsequent decline following 1999 (Donoghue *et al.*, 2004a; see figure 2.5). Regular monitoring of macroalgal cover may therefore help to shed light on the annual patterns of growth and decline exhibited by *Enteromorpha sp.* populations at Seal Sands, highlighting the need for a precise and

cost-effective method through which macroalgal growth can be monitored, with a view to improving scientific understanding of the role of macroalgae within the coastal ecosystem.

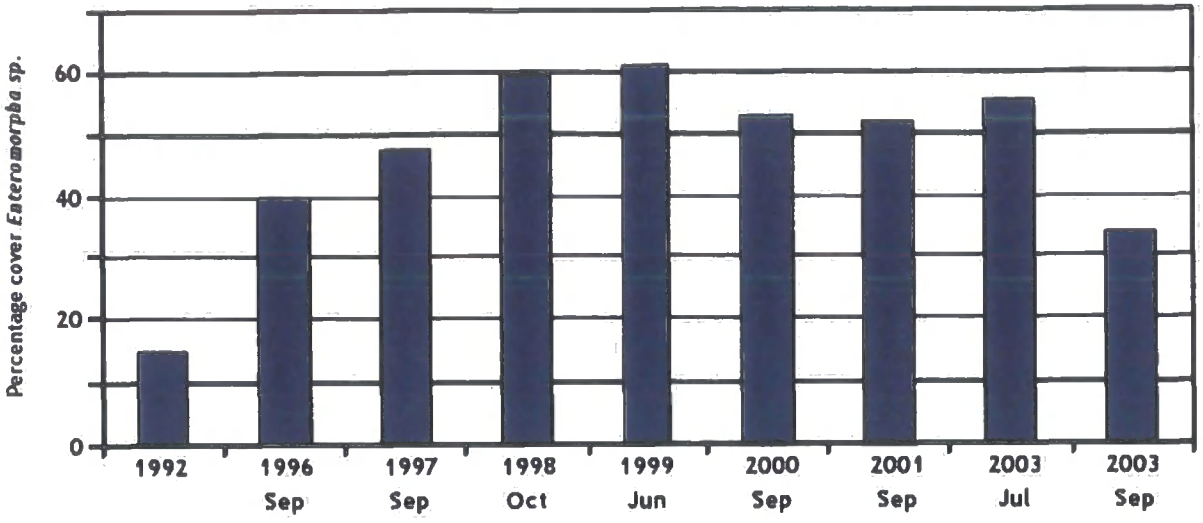

Figure 2.5 Variation in Seal Sands *Enteromorpha sp.* cover between 1992 and 2003. Modified from: Donoghue *et al.* (2004a)

2.2 Fieldwork Preparation

2.2.1 Unmanned Aerial Vehicle (UAV)

The platform used in this study was a SmartPlanes SmartOne UAV. The aircraft has a 1.2m wingspan and can support a payload of ~300g, usually a digital camera in one wing, and a GPS instrument in the other. Lithium-polymer batteries give ~20-40 mins endurance, with a nominal velocity of ~15 ms^{-1} (SmartPlanes, 2006). The aircraft is controlled using a standard 35MHz radio transmitter, and flight stabilisation is provided by an *FMA FS8 Co Pilot* horizon sensor, which steadies pitch and roll movement (FMA, 2004).

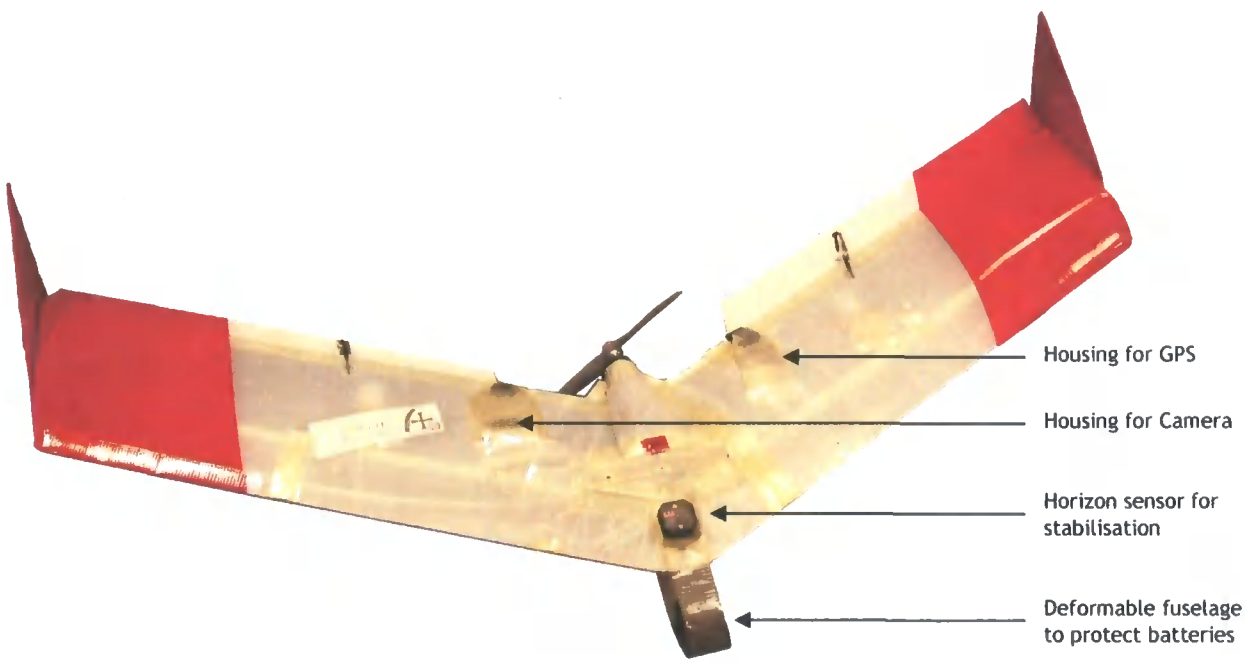

Figure 2.6 SmartPlanes SmartOne UAV

Although SmartPlanes (2006) suggest a typical altitude of ~250 m, image acquisition can be performed at any altitude below 300 m (the recommended service ceiling; Hagner, O, pers. comm.) In the absence of radio telemetry between the controller and the aircraft, flying height is controlled visually by the user. This means that it is difficult to maintain a precise altitude, although the onboard GPS allows the user to ascertain the aircraft's altitude on a *post-hoc* basis. For all flights,

the UAV was equipped with either a Canon IXUS 60 or 50 camera (normal RGB *or* infrared; see section 3.1.2) and a Garmin Geko 201 GPS, for navigation and altitudinal information. The GPS unit is WAAS/EGNOS enabled, with a typical accuracy of between ±3 m and ±10 m (Garmin, 2003). Camera shutter operation was controlled remotely by means of a button on the radio transmitter and associated servo controller in the plane wing, allowing images to be required when flying over the desired location.

2.2.2 Camera calibration

A total of three digital cameras were used to obtain aerial imagery of the site, because of the varying availability of equipment at the time of data acquisition. These were: Canon IXUS 60 6-megpixel CCD camera, Canon IXUS 50 5-megapixel CCD camera, and a modified Canon IXUS 50 where the infrared filter had been removed from the Bayer mask coating on the CCD, rendering it sensitive to infrared wavelengths.

Central to image acquisition is a need to geometrically calibrate the sensor device, in order to obtain precise measurements from the aerial photographs (Guichard *et al.*, 2000; Peterson *et al.*, 2003). Camera calibration was performed using PhotoModeler 5.0 (Eos, 2003), and subsequently used to establish the angular field-of-view (FOV) of the camera, given by:

$$\alpha_{(rad)} = 2 \arctan \frac{d}{2f} \qquad (2.1)$$

where a is the angular field-of-view (in radians), d is the chosen CCD dimension (in millimetres) and f is the effective focal length (in millimetres).

The linear (or dimensional) FOV of the camera could then be calculated using the equation:

$$L = 2h * \tan \frac{\alpha_{(rad)}}{2} \qquad (2.2)$$

where L is the linear field of view (in metres) a is the angular field-of-view (in radians) and h is the distance to object/flying height (in metres). Using this measurement, it was possible to estimate the GSD (ground spatial distance) covered within each image, and ascertain the spatial resolution of the imagery. This can then be used to inform the appropriate altitude from which to obtain imagery. Table 2.1 shows calibration data for the two camera systems.

	Camera	
	Canon IXUS 60	Canon IXUS 50
Focal length (mm)	5.8009	5.7932
CCD size x (mm)	5.5974	5.5019
CCD size y (mm)	4.1989	4.1275
No. of detectors x	2816 cols.	2592 cols.
No. of detectors y	2112 rows	1944 rows
Angular FOV x	51.5109°	50.8022°
Angular FOV y	39.7922°	39.2155°
Linear FOV x @ 200m altitude (m)	192.9838	189.9434
Linear FOV y @ 200m altitude (m)	144.7672	142.4946
Pixel size x @ 200m altitude (m)	0.068	0.073
Pixel size y @ 200m altitude (m)	0.068	0.073

Table 2.1 Calibration data for cameras used onboard UAV. Note both the standard and modified infrared cameras share the same lens and CCD, so calibration data can be considered the same.

2.2.3 Preliminary site assessment

Prior to airborne or ground-based data acquisition, it was necessary to identify areas of Seal Sands SSSI Unit 1 which were amenable to monitoring. Four potential zones with varying land cover types were selected, in order to test the capabilities of the UAV (see figure 2.7a). zone 1 (figure 2.7b) consisted of dense *Enteromorpha sp.* coverage with deep water-filled channels. The majority of zone 2 comprised medium *Enteromorpha sp.* coverage interspersed with a large number of bivalve shells, again with deep channelling. zone 3, to the north of the Seal Sands area showed more consistent macroalgal cover, and the marginally higher altitude of this zone put it outside the influence of the deep channelling. zone 4 (figure 2.7c) was covered with a mixture of dense and sparse *Enteromorpha sp.* matting and widespread dead or decaying *Salicornia sp.*, and was at an altitude similar to that of zone 3.

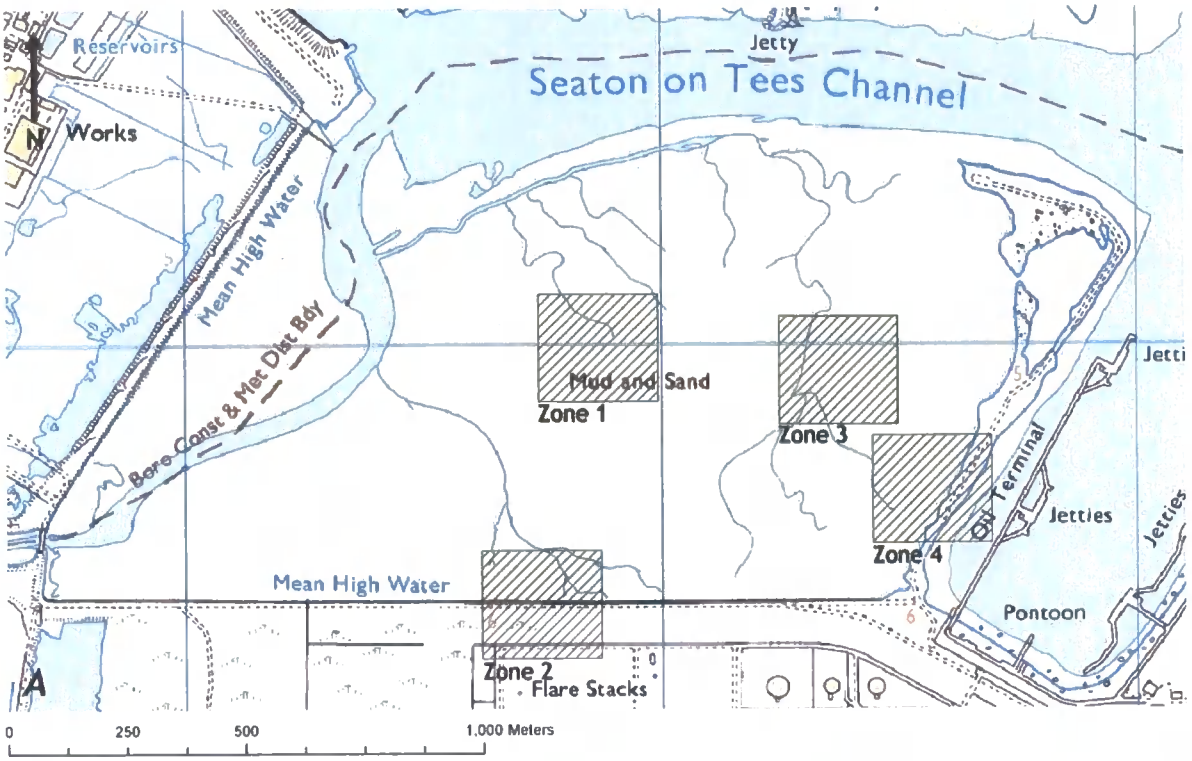

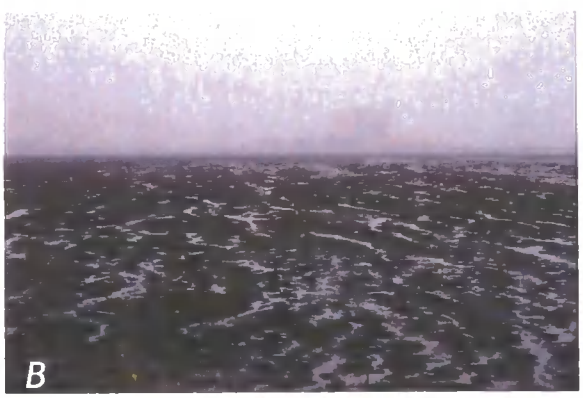

Figure 2.7(A) Approximate locations of potential monitoring zones at Seal Sands. Source: EDINA, 2004. **(B)** Zone 1 with *Enteromorpha sp.* matting and deep channelling. **(C)** Zone 4: Interspersed algae and *Salicornia sp.* cover.

Zones 1 and 2 were judged unsuitable for data acquisition; zone 1 because deep channelling made access difficult, and zone 2 because its proximity to industrial sites on the southernmost side of Seal Sands was deemed a risk to flying the UAV. In addition to this, the marginally lower altitude at which these zones were situated meant that the tidal 'window' within which imagery could be obtained was significantly smaller than that of zones 3 and 4. Although zone 3 was at an altitude favourable to extended tidal exposure, access to this section of the mudflat was difficult, due to the long distance from the roadway/embankment, coupled with the presence of soft mud.

Zone 4 was therefore deemed the most appropriate site for data acquisition due to a) ease of access, b) free of risks to UAV flying, c) higher altitude, giving longer tidal exposure, and d) mixed land cover types.

2.3 Data Acquisition

Data was acquired on two occasions to examine the affects of season on imagery and ground truth measurements. Several appropriate low tidal 'windows' were identified for each data acquisition session, and imagery was obtained during the tidal cycle that coincided with the optimum weather conditions. Imagery was acquired on two dates, November 2006 and June 2007, in order to establish relationships between macroalgal samples and image metrics under spectrally-dissimilar conditions. Because of seasonal differences between the two acquisition sessions, it was possible to capture imagery of a macroalgal bloom in two different states of development, from decay (in November) to new growth (in June).

2.3.1 Fieldwork session 1: November 2006

Initial data acquisition took place at the end of the growth season, between 16th November and 24th November 2006. Imagery was acquired on 16th November when weather conditions and tidal exposure was optimal. Macroalgal data for ground truthing was acquired on 24th November, the next occasion on which tide and weather conditions were favourable.

2.3.1.1 Aerial Photography

Imagery was acquired using both the standard *Canon IXUS 60* camera and the modified *Canon IXUS 50* for infrared photography. Photographs were acquired at a range of altitudes above zone 4, although the majority of images were taken from ~200 m. This represented a good trade-off

between spatial resolution and ground coverage, and the relatively high altitude minimised motion blur. The bulk of the imagery was taken using the *IXUS 60* camera, and tidal inundation later in the day limited the area that was covered by the modified infrared *IXUS 50* camera.

At the time of acquisition, sun angle was low, and cloud cover was close to 100%. Image exposure times were increased to compensate for the relatively low-light conditions. Ground control was provided by 30 A4-paper-sized (~30 cm x ~20 cm) panels of plywood (see figure 2.8), distributed at random over the study area. These were painted with high-visibility orange paint to aid georeferencing. At ~200 m altitude, these panels were visible as ~4.4 x 2.9 pixel rectangles in the 6-megapixel imagery and ~4.1 x 2.7 pixel rectangles in the 5-megpixel images. The ground control points (GCPs) were then recorded in UTM format using a *Leica GPS1200 Series* differential GPS system, with a typical accuracy of ±25 cm (Leica, 2006a).

Figure 2.8 Panel used for ground control points (GCPs)

2.3.1.2 Ground Truthing

Intertidal macroalgal coverage was sampled using 30x30 cm quadrats, as it was not logistically feasible to sample larger quantities. Jeffrey & Hayes (2005) note the necessity of sampling each yield class consistently: quadrats were distributed in a pseudo-random pattern around the area that had previously been imaged, and the contents of each quadrat was recorded as either *control*

(zero), *sparse*, *medium* or *dense* macroalgal cover, ensuring that a roughly equal number of samples of each yield class were taken. It was not possible to take samples from the same locations as the ground control points used during the image acquisition session, because the control points were removed to prevent them being washed away by the incoming tide. Scanlan *et al.* (2007) suggest that only the surface layer of macroalgae should be sampled, in order to establish the optimum correlation with aerial photography. The surface layer of *Enteromorpha sp.* matting within each quadrat was removed with a knife and placed in a sample bag (after Jeffrey & Hayes, 2005), and the location of each quadrat was demarcated with the differential GPS (figure 2.9). Prior to commencing lab work, the macroalgal samples were stored in a refrigerator to limit decomposition.

Figure 2.9 30 cm^2 quadrat and GPS used to denote position

2.3.2 Fieldwork session 2: June 2007

Secondary data acquisition took place towards the start of the new growth season. Imagery and data for ground truthing were both acquired on 20th June 2007, when spring tide conditions allowed for a large window of time in which measurements could be collected.

2.3.2.1 Aerial Photography

Imagery was acquired using the standard *Canon IXUS 50* camera; the standard *IXUS 60* and the modified infrared *IXUS 50* were not available. Photographs were taken from the same area as in the previous data acquisition session, and comprised a range of altitudes. The majority of images were taken from ~230 m, allowing for very wide spatial coverage. The total area covered in this session encroached onto zone 3, while the extremely low tide meant that it was possible to walk to this area of the Seal Sands mudflat. Although images were taken from a higher altitude, and with a lower resolution camera, the extremely low cloud cover ~5%, and high sun angle at midday led to a large reduction in the motion blur visible in images, giving a similar effective resolution to the images obtained in the previous session. Ground control was provided by the same plywood panels, visible as ~3.5 x 2.4 pixel rectangles. Panels were distributed in an approximate grid pattern, in order to provide more uniform georeferencing. Ground control points were demarcated using a *Leica TPS1200 Series* total station, with a typical accuracy of ±5 mm (Leica, 2006b). The relative total station measurements were then converted to UTM coordinates by means of a reference point with a known UTM location.

2.3.2.2 Ground Truthing

Enteromorpha sp. coverage was again sampled using 30x30 cm quadrats. Samples were removed, placed in sample bags, and stored prior to labwork. On this occasion, quadrats were distributed to the immediate north-west corner of each ground control point. This acted to reduce the error involved in locating algal sample points on the georeferenced image, as each sample was taken next

to a visible 'target'. Although this meant that yield classes were not sampled as consistently as in the first data acquisition session, the ease with which samples were geolocated greatly benefited image processing (see below), and was deemed an acceptable compromise. Allowing samples to be taken next to the existing GCPs also greatly reduced the time needed for fieldwork, and all measurements were recorded during the same day. Figure 2.10 shows the distribution of ground control points for both the November 2006 and June 2007 data acquisition sessions.

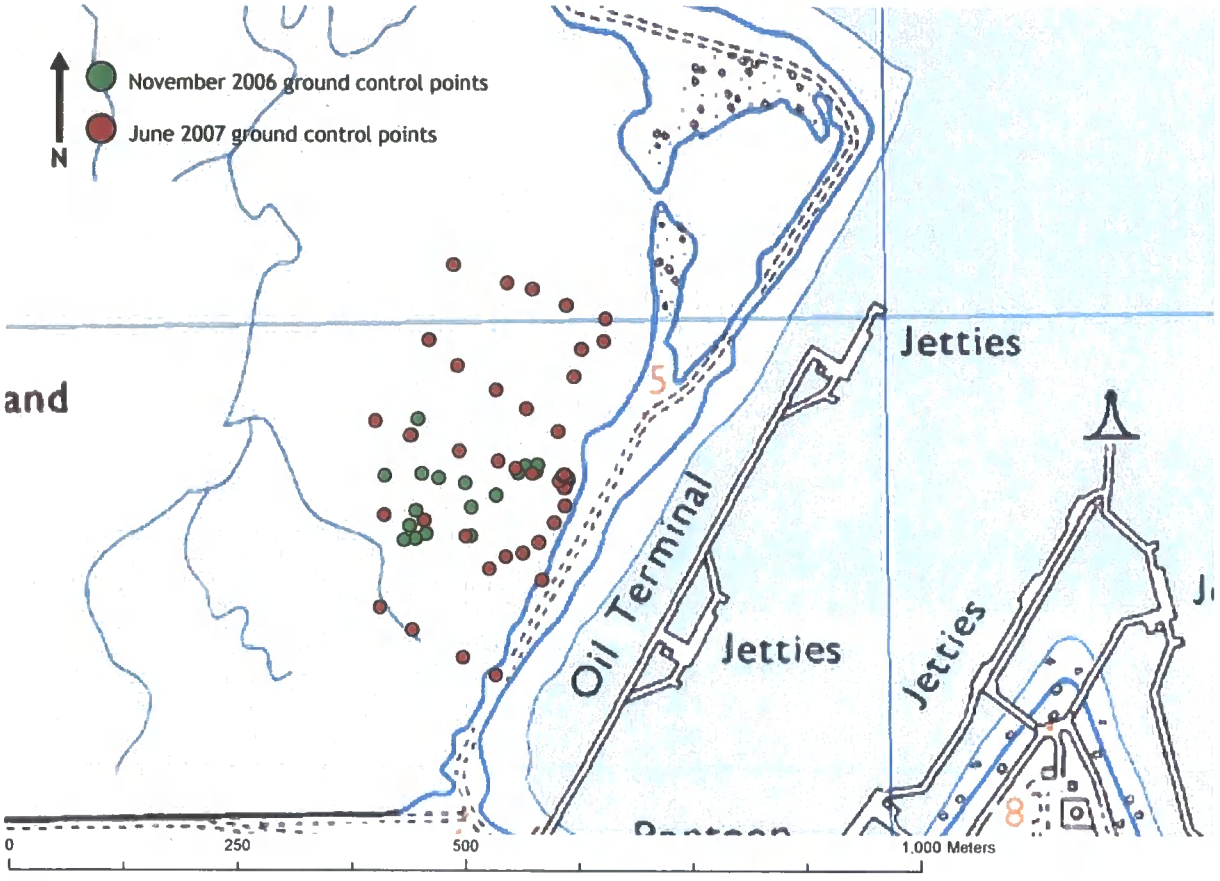

Figure 2.10 Distribution of ground control points across portion of Seal Sands

2.4 Laboratory Processing

A number of different methods have been advocated for the derivation of accurate biomass measurements from samples of macroalgal matting. Scanlan *et al.* (2007) note that 'the collection of algal samples for biomass estimation is inherently inexact', and suggest that *wet weight per square metre (g WW m^{-2})* represents an accurate and time-efficient method of calculating macroalgal biomass, citing a good correlation with *dry weight per square metre (g DW m^{-2})* . A

number of other authors have used this approach to ascertain *Enteromorpha sp.* biomass (eg. Espinosa & Guerra-García, 2005; Fong *et al.*, 1996; Kamer *et al.*, 2004; Norkko *et al.*, 2000; Schaadt *et al.*, 2003), and have generally produced acceptable variations in biomass yield. However, Fong *et al.* (1996) and Norkko *et al.* (2000) complemented this technique with dry weight data for improved accuracy in nitrogen and carbon measurements, and Schaadt *et al.* (2003) noted that the *wet weight* did not produce a suitable estimation of biomass, because the absorbent nature of *Enteromorpha sp.* led to a high variation in water content between samples (Schaadt *et al.*, 2003). *Dry weight per square metre* is more commonly used to accurately establish macroalgal biomass (eg. Berglund *et al.*, 2003; Bolam *et al.*, 2000; Fytianos *et al.*, 1999; Jeffrey & Hayes, 2005; Lyngby *et al.*, 1999; Martins *et al.*, 2001; Pihl *et al.*, 1999; Villares *et al.*, 2001). However, the exact details of the methodology varies between studies. Bolam *et al.* (2000), Fytianos *et al.* (1999) and Jeffrey & Hayes (2005) all note the need to wash samples prior to drying, to remove sediment. However, Bolam *et al.* (2000) suggest washing in seawater in seawater is sufficient, Fytianos *et al.* (1999) recommend the use of deionized water to remove excess salts, and Jeffrey & Hayes (2005) do not advocate a specific cleaning technique. Similarly, the manner in which *Enteromorpha sp.* samples should be dried is also open to debate; temperatures of 60°C (Pihl *et al.*, 1999), 70°C (Berglund *et al.*, 2003) and 80°C (Fytianos *et al.*, 1999), as well as ash-free-dry-weight (AFDW) produced through loss on ignition at 550°C (Martins *et al.*, 2001; Morris, 2005) are all suggested. However, although there does not appear to be consensus on the exact methodology behind calculating macroalgal *dry weight per square metre*, this technique appears to produce more robust data than *wet weight*, because it is not susceptible to bias by algal water content.

2.4.1 Session 1

Wet *Enteromorpha sp.* samples were removed from sample bags and placed in glass beakers. The beakers were labelled and placed in an oven at 60°C (the lowest temperature recommended in the literature) for a minimum of 24 hours (see figure 2.11a & b). Although the smaller samples dried rapidly within this period, some of the larger samples took considerably longer, and had to be laid out on a tray to aid drying.

Figure 2.11 (A) Macroalgal samples were placed in beakers, **(B)** dried in oven and **(C)** weighed using analytical balance

After all samples were dry, the contents of the beaker (including sediments, shells) were weighed using an analytical balance with an accuracy of ±0.01 g (see figure 2.11c).

In order to remove unwanted sediments and shells from the samples, all samples were rehydrated in a mixture of two-thirds distilled water and one-third ethyl-alcohol (ethanol). The lower density of ethanol (0.79 @ 20°C; Fisher Scientific, 2005) compared to water (1.00 @ 20°C), caused sediment entrained in the algae to separate more readily, and descend to the bottom of the beaker, allowing the macroalgae to be easily 'skimmed' off the surface (see figure 2.12). Any sediment or shells still entrained in the algae was sieved and removed, and placed back in the beaker.

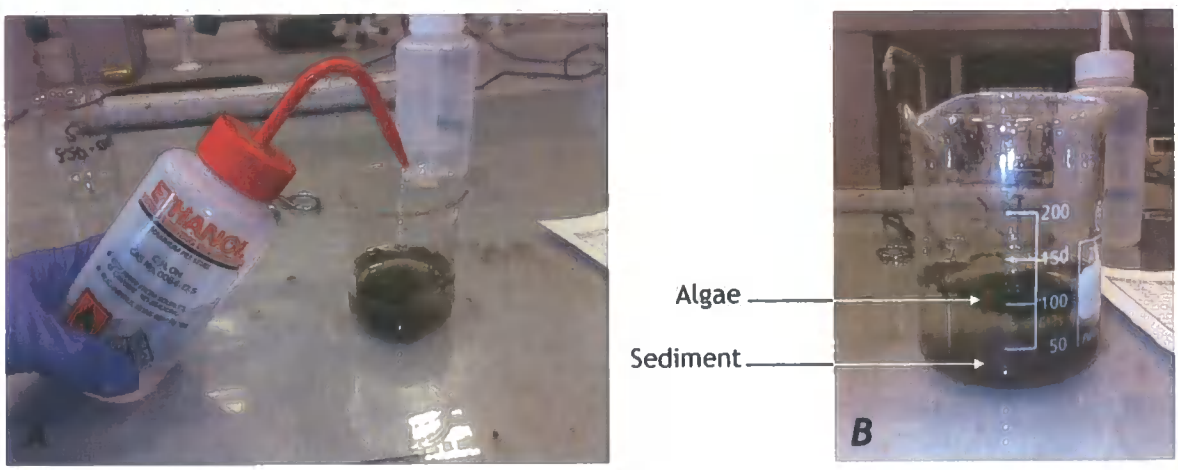

Figure 2.12(A) Ethanol added to beaker to separate algal mass from sediment. **(B)** Visible separation of algae and unwanted detritus.

This process was repeated until the algal mass and minerogenic material was completely separated. The remaining residue or sediment present in the beaker was then dried at 60°C, reweighed, and subtracted from the total weight of the entire sample, to give the dry biomass of the macroalgal content of the sample.

2.4.2 Session 2

Although the method detailed above was thorough and ensured that all sediment was removed from the sample, it was both time consuming (~1.5 hours sieving/skimming per sample), and relatively uneconomical, because of the large quantities of ethanol consumed in the process. It is also possible that some macroalgal biomass was leached into the solution, as the ethanol turned the solution green, indicating that algal material was being dissolved, although this is unlikely to represent a significant biomass loss.

For the second group of samples, laboratory restrictions limited the amount of time available for analysis. Instead of drying the samples prior to removing biomass content for weighing, samples were sieved before drying. Because the samples had not disintegrated as a result of the drying process, the algal tissue was able to withstand a more thorough sieving process, and it was not necessary to use the ethanol-water solution to remove sediment. Remaining residue was then discarded, and the macroalgal mass placed in beakers, and dried at 60°C. Because the sediment was removed before the drying process, samples were desiccated considerably faster than previously. Samples were than weighed using an analytical balance, and biomass was recorded and tabulated. This method was considerably less time consuming than previously (~0.5 hours per sample), with little visible difference in results.

2.5 Image Pre-processing

2.5.1 Creation of mosaics

Due to the relatively small area covered by each aerial photo (~190 m x ~140 m at 200 m altitude) and the scarcity of ground control points or distinguishing features within the each individual image, it was necessary to create a mosaic of a number of aerial photos in order to more accurately georeference the dataset. Extended File Information (EXIF) headers were extracted from each JPEG image using the Matlab Image Processing Toolbox (MathWorks, 2007). The EXIF timestamps were

then compared with the log file taken from the GPS receiver onboard the UAV (see figure 2.13), allowing each image to be tagged with an approximate altitude and geographical location.

	A	B	C	D	E	F
1	**Image no.**	**EXIF Time**	**GPS Log time**	**X**	**Y**	**Z**
2	IMG_259.jpg	12:16:06	12:16:06	618008.2	6054532.4	183.749023
3	IMG_283.jpg	12:17:20	12:17:20	618031.5	6054647.7	183.749023
4	IMG_333.jpg	12:20:01	12:20:01	617986.1	6054422	183.749023

Figure 2.13 EXIF timestamp from imagery matched to GPS log to give approximate UTM coordinates and altitude of photograph.

2.5.1.1 Session 1

Images taken using the *Canon IXUS 60* camera were grouped by approximate altitude and visually inspected. Images with motion blur, artefacts, or those taken noticeably off-nadir were removed from the dataset. As imagery from 200m appeared to offer a good tradeoff between resolution and coverage, those taken from between ~190 m and ~210 m altitude (200±10 m, representing the vertical accuracy of the GPS) were selected. *AutoPano Pro 1.3.1* (Kolor, 2007) was used to produce photomosaics. The scale-invariant feature transform algorithm (SIFT; Lowe, 2004) implemented within the software allows for 'reliable matching of panoramic image sequences despite rotation, zoom and illumination change' (Brown & Lowe, 2007), enabling the mosaicking of imagery acquired from a range of different altitudes and flight directions, as well as providing a level of 'compensation' for image distortions caused by in-flight pitch, roll and yaw movements.

Images taken using the modified infrared *Canon IXUS 50* were again grouped by altitude and visually inspected. Motion blur was more common in this dataset, and a large number of images were discarded from the dataset. Because of advancing tidal inundation, it was not possible to image the entire area from 200m altitude, and was necessary to include some imagery taken from below 200m to create a suitable mosaic.

2.5.1.2 Session 2

Beneficial weather conditions during data acquisition facilitated coverage of a larger area of Seal Sands from a higher altitude; most suitable imagery was taken between ~210 m and ~250 m. Photos taken from between 220 m and 240 m (230±10 m, representing the vertical accuracy of the GPS) were selected and visually inspected. Because of the amenable lighting conditions, it was not necessary to remove so many images from the dataset. However, the large number of images present adversely affected the mosaicking process, producing visible artefacts and 'seams' in the resulting image. In order to reduce the occurrence of these, it was necessary to further reduce the images within the dataset, by the removal of those images that appeared to cause distortions.

2.5.2 Georeferencing

2.5.2.1 Georeferencing mosaics

In order to ensure precise correlation between image pixel coordinates and ground truth metrics, it was necessary to accurately georeference the mosaicked imagery to ground control points. Imagery was first registered to visible landmarks with known UTM coordinates to aid more precise orientation. The mosaics were then referenced to the temporary plywood GCPs distributed over the monitoring zone during fieldwork, and warped to fit using a 2^{nd}-order polynomial model.

Root mean square error (RMSE) of the polynomial fit for mosaics from the first image acquisition session were low (1.5), suggesting a minor level of image distortion. However, the mosaic from the second data acquisition session gave a significantly higher RMSE (3.7), suggesting that the georeferencing was less accurate, even though the GCPs were more uniformly distributed. This may be because the mosaic acquired during the second data acquisition session covered a significantly larger area than that of the first mosaic. Hence, even though the GCPs were more evenly distributed, the large majority of the mosaic lacks any from of ground control, and inevitably increases the RMSE. Although the overall RMSE is higher, it is likely that the area of interest bounded by the GCP locations is more rigorously georeferenced, so the relatively large RMSE should not be problematic.

2.5.2.2 Obtaining pixel coordinates for raw images

Although image mosaics are suitable for spectral analysis, distortions introduced into the imagery through the successive mosaicking and georeferencing processes rendered them unacceptable for texture analysis: blurring and warping of an image changes the distribution of grey levels within the grey level co-occurrence matrix, leading to biased texture calculations. Because it was unfeasible to georeference single images, it was necessary to 'backtrack' the transformations introduced by the mosaicking and georeferencing processes in order to ascertain image pixel coordinates (ie. column, row) from given geographical coordinates, in order to relate ground truthing (with known geographical coordinates) to specific points within the raw images.

Mosaics were re-processed and output as layered TIFF mosaic files using *AutoPano Pro 1.3.1* (Kolor, 2007), so that each TIFF layer constituted a single image within the mosaic. The raw JPEG images were then co-registered to each corresponding TIFF layer in order to 'backtrack' the image transformation. Once the image transformation was established, it was possible to manually calculate the desired image pixel coordinates from given UTM coordinates, and hence extract texture information from given pixel coordinates in the raw JPEG files. Figure 2.14 is a schematic of this process. Figure 2.15 is a flow diagram representing the various steps of the image selection procedure.

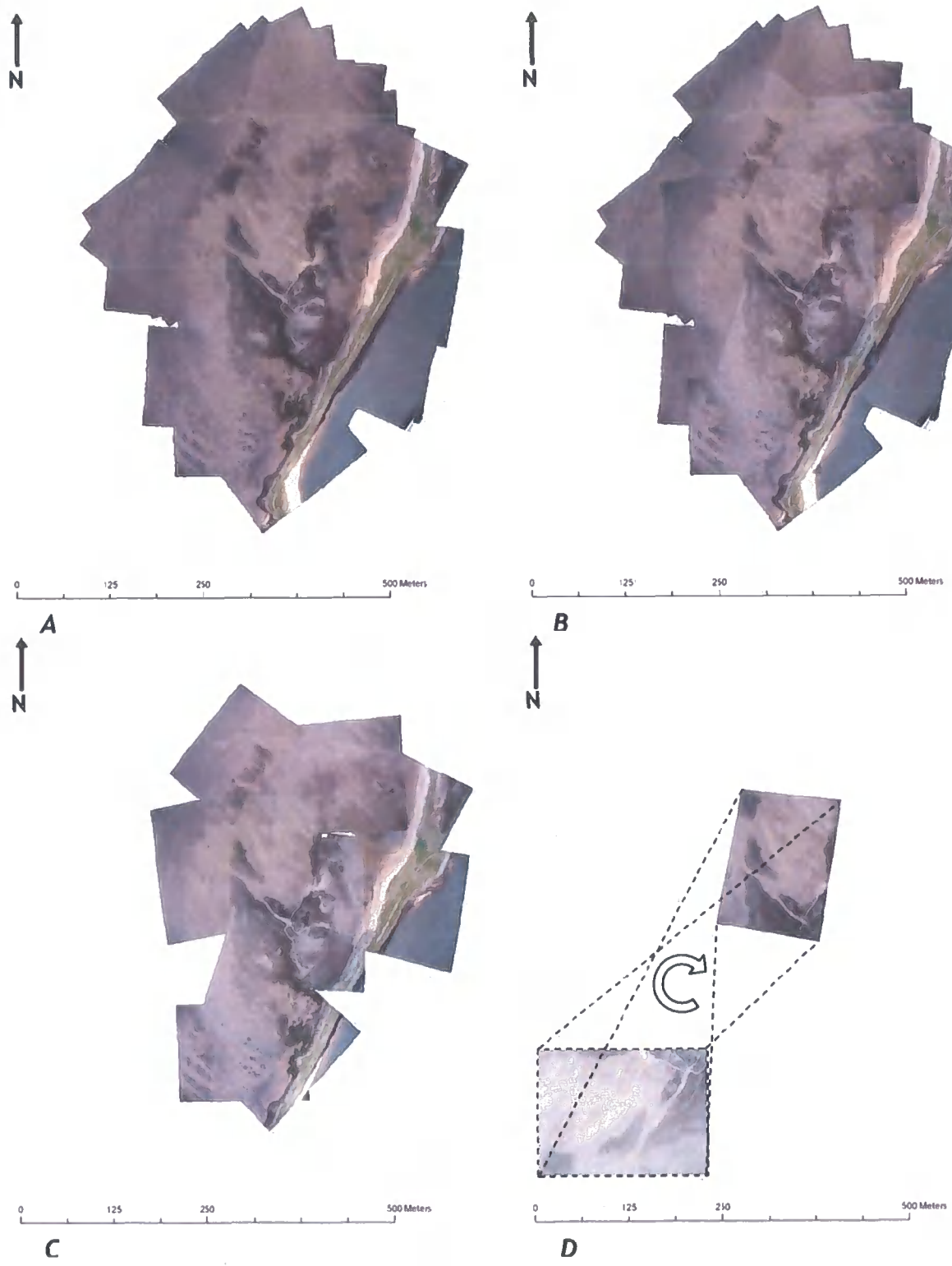

Figure 2.14 (A) Original image mosaic. Removal of unwanted TIFF layers **(B & C)** to leave the required image. **(D)** Raw JPEG image is rotated around its centre and co-registered to mosaicked TIFF file, giving the required transformation.

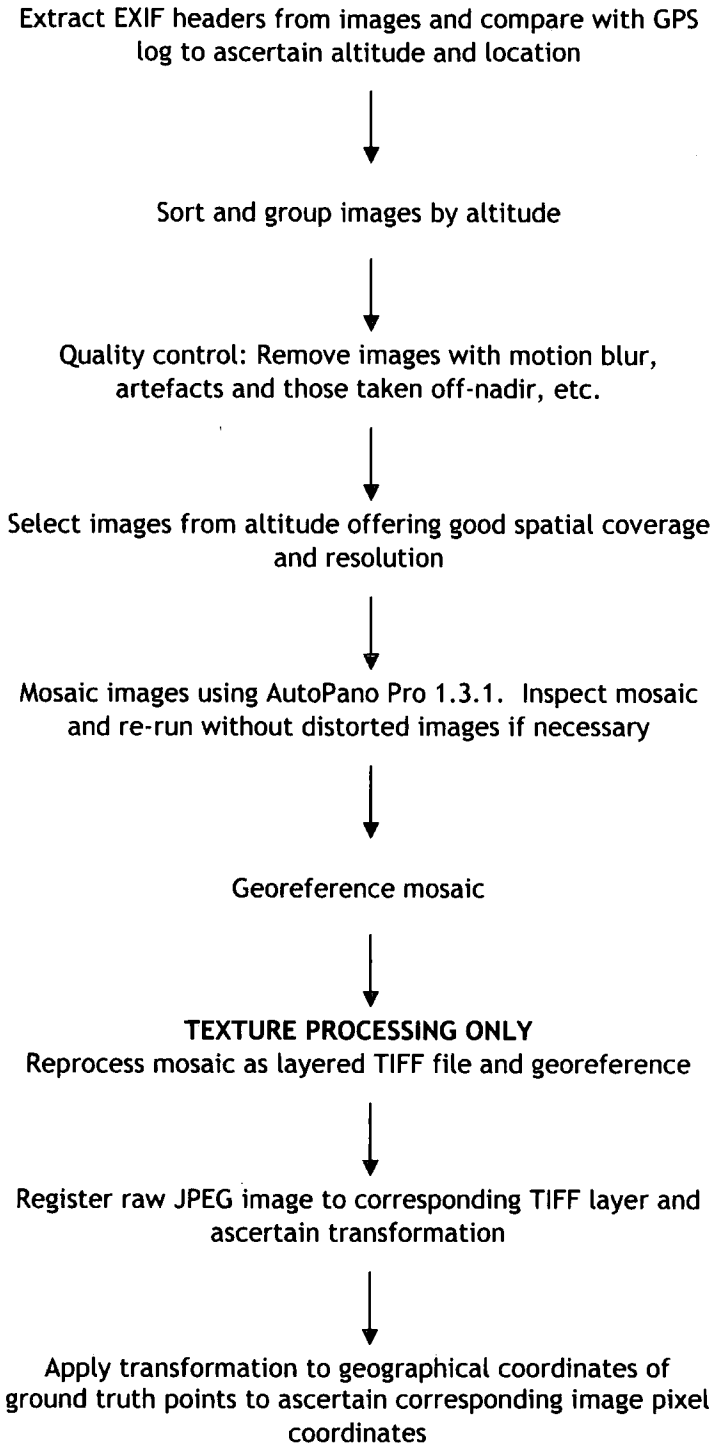

Figure 2.15 Flow diagram showing image selection procedure

2.6 Image Processing and Analysis

2.6.1 *Relative* Normalised Green-Red Difference Index and Normalised Difference Vegetation Index

Although the spectral response of intertidal algal vegetation has been widely studied (eg. (Ben Moussa *et al.*, 1989; Guichard *et al.*, 2000; Larsen *et al.*, 2004; Smith *et al.*, 1998) and the reflectance of macroalgal communities (including *Enteromorpha sp. and Ulva sp.*) has been assessed using portable spectrometers (Forster & Jesus, 2006; Morris, 2005), the derivation of precise spectral data from consumer-grade digital cameras is problematic, owing to the paucity of information regarding the response of specific CCDs and the wide variations in spectral sensitivity between different camera makes and models (Hong *et al.*, 2001). Although the spectral sensitivity of the *Canon IXUS* cameras used in this study has not previously been established, broadly similar Canon cameras have shown peak spectral sensitivities at ~480 nm, ~520-550 nm and ~580-600 nm for the blue, green and red channels respectively (Labbé *et al.*, 2007; Ritter & Wueller, 1999). The removal of the IR-cut filter from an *EOS 350D* camera model yielded near-infrared sensitivity between ~700-900 nm, with a peak at ~820 nm (Labbé *et al.*, 2007), and spectral sensitivity in the modified *IXUS 50* is likely to exhibit a similar pattern. Because intertidal algal biomass is known to reflect infrared light between these wavelengths (Ben Moussa *et al.*, 1989; Guichard *et al.*, 2000), the modified infrared *IXUS 50* may be able to detect macroalgal biomass to a greater degree than a standard RGB camera.

The relative spectral response of macroalgal sample points was extracted using ArcGIS 9.1 (ESRI, 2006). UTM coordinates for the locations of sample points were converted to shapefile format, and the red, green and blue DN values were extracted from the mosaicked imagery at the appropriate locations. Near-infrared DN values were also extracted from imagery taken using the modified *IXUS 50* camera. This process was repeated for all datasets, and the spectral response of all sample points to be recorded and tabulated. The red and green components of the mosaics (from both data acquisition sessions) were used to calculate a *relative* normalised green-red difference index (NRGDI).

Mosaicked false-colour near-infrared (NIR) imagery taken using the modified *IXUS 50* camera was used to compute a *relative* normalised difference vegetation index (NDVI) of the study area. Because the modification to the camera damaged accurate spectral response in the conventional RGB channels, it was not possible to calculate an NDVI using the NIR mosaic alone. Instead, the NIR mosaic was accurately co-registered to the existing true-colour mosaic acquired during the same field session, and an NDVI created by combining the red band of the true-colour together with the NIR band of the NIR mosaic. Although minor georeferencing errors were introduced into the NDVI image through the co-registration of the NIR mosaic to the true-colour image, NDVI values from the mosaicked imagery showed good agreement from test NDVI performed on raw imagery.

2.6.2 Image Saturation

True-colour mosaics from both data acquisition sessions were converted to hue-saturation-value colour space using the Matlab Image Processing Toolbox (MathWorks, 2007). The saturation component was separated from the dataset, and pixel values rescaled to unsigned 8-bit integer format (1-255 scale) for easier visualisation and processing. The resulting saturation mosaic was filtered in order to a) remove anomalies within the mosaic resulting from JPEG compression artefacts and b) enhance contrast between macroalgal cover and bare sediment. Filter kernel sizes were designed to reflect the dimensions of the sampling quadrats: imagery acquired using the *IXUS 60* camera was filtered using a 5 x 5 and a 16 x 16 pixel moving window (equivalent to 30 cm^2 and 100 cm^2 GSD respectively at 200 m altitude), and imagery acquired using the *IXUS 50* was filtered with a 3 x 3 and a 10 x 10 pixel moving window (equivalent to 30 cm^2 and 100 cm^2 GSD respectively at 230 m altitude). Saturation DN values for ground sample locations were extracted from the raw saturation mosaic and for the images produced by the three filters used (averaging, zonal maximum and zonal minimum) and tabulated for analysis.

2.6.3 Image Texture

Because of the time-consuming nature of the texture analysis process, it was necessary to condense the dataset to the smallest number of images necessary for processing. Most ground truth sample points were visible on several of the images in the datasets, so those images with only a small number of sample points were discarded, greatly reducing the number of images necessary for processing (see figure 2.16). For the November 2006 imagery, the total image dataset was reduced from 47 to 10 images covering all necessary sample points; for the June 2007 imagery, the dataset was reduced from 21 to 14 images.

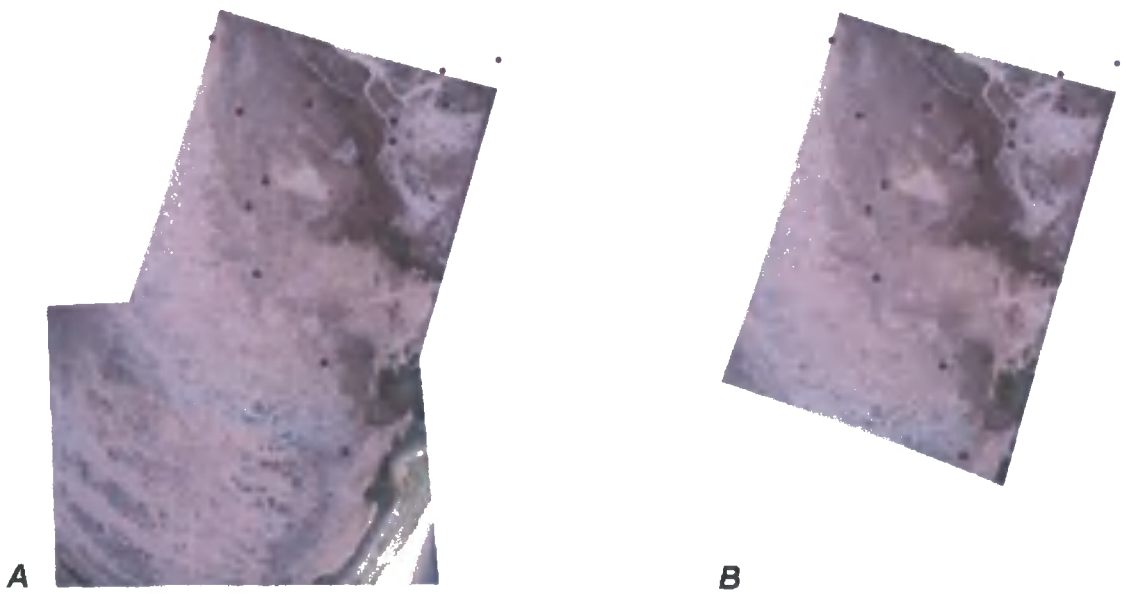

Figure 2.16(A) Although sample points occur across both images, it is unnecessary to process both photos, because all points are covered by a single image **(B)**, reducing processing time.

Image texture maps were produced using Matlab R2007a for a variety of input parameters. Raw imagery was resampled to 32 grey levels to speed up computation of the grey level co-occurrence matrix (GLCM) (eg. Carbonneau *et al.*, 2005). Textural entropy for the raw images was calculated for the area of image subset by the moving window, and the resulting value mapped to the corresponding pixel in the texture map. The moving window was then transposed by a user defined 'step' and direction, and entropy calculated for the next image subset. This process was repeated for the entire image, generating a matrix of values, each of which represents the local entropy of the portion of image subset by the moving window. Textural inertia was calculated in a similar manner.

Entropy and inertia operations were performed on the chosen raw images from both data acquisition sessions. The sizes of the 'moving window' and the transposition 'step' were iterated to explore the relationship between different textural primitives and macroalgal biomass. Window sizes were iterated from 4 x 4 pixels (reflecting the spatial dimensions of the sampling quadrats) to 50 x 50 pixels (even numbers only), and the transposition step was varied between 2 and 10 pixels, giving 216 permutations of window and step size for each image. This process was repeated for both entropy and inertia operations, giving a total of 432 textural permutations.

Because of the complex nature of the entropy and inertia computations, the number of permutations for each image, and the project time constraints, it was necessary to accelerate the image processing procedure. The Condor High Throughput Computing System (Thain *et al.*, 2005) was used to distribute image processing jobs to otherwise idle CPUs within a 'cluster' of networked computers , greatly reducing the overall processing time for the datasets. The speed at which data was output therefore allowed for a much greater number of images to be processed than would otherwise have been possible, aiding more detailed analysis and conclusions to be drawn.

Chapter 3. Results and Analysis

3.1 Qualitative results/description of raw mosaics

3.1.1 Session 1

Figure 3.1 shows the final true-colour mosaic produced from the first image acquisition session. Imagery was taken in late November, towards the end of the bloom season, and this is reflected in the non-contiguous nature of the macroalgal cover present. The largest expanse of dense algal matting present in the mosaic is situated towards the south of the image, and can be clearly distinguished as a vibrant green patch of colour, approximately 30 m in diameter. Secondary areas of moderate *Enteromorpha sp.* matting are present towards the centre of the image alongside a large drainage structure. Extensive areas of sparse macroalgal growth are visible as grey patches (each measuring ~40 m across) against the lighter coloured sand, the three largest patches of which are situated towards the north-west of the image. Stratified 'stripes' of sparse cover ~7 m in width are also present towards the extreme south of the image, presumably separated by channelling which is not visible at low tide. The substantial area of mauve-brown coloration towards the centre and southern sections of the image highlights the extent of the season's *Salicornia sp.* growth. The seagrass' brown colour is a result of the seasonal decline following the summer growth period; this facilitates the easy visual characterisation and separation of macrophyte (green/grey) from vascular plant (brown) communities.

Although imagery appears to be relatively sharp, allowing for good visual characterisation of different cover types, relatively long exposure periods were needed to compensate for the low-light conditions. Coupled with the adverse effects of cloud cover on the Co-Pilot stabilisation system, this induced an amount of blurring into some of the images. Although it was possible to discard the worst-affected images, the blurring visible towards the south of the mosaic made discrimination of small algal features difficult (see figure 3.2).

Figure 3.1 Final true-colour mosaic produced from November 2006 imagery

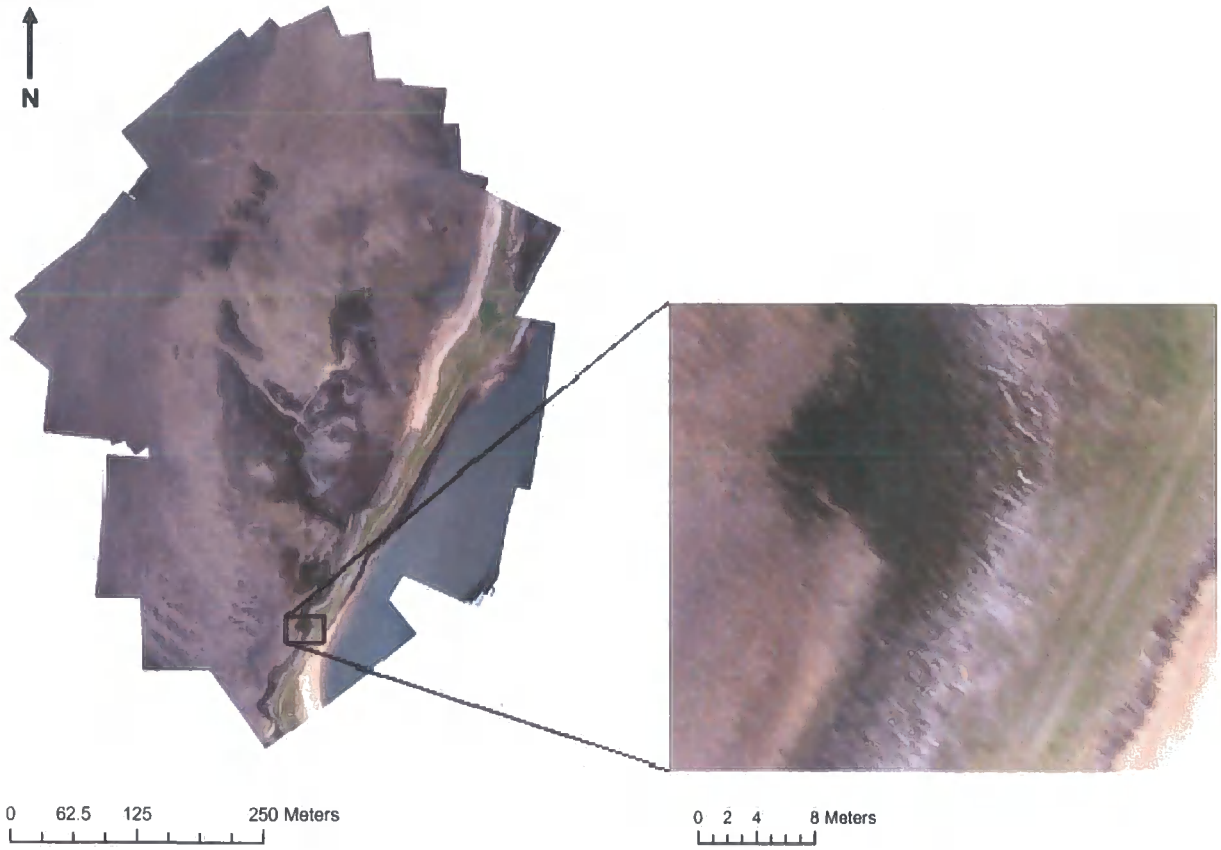

Figure 3.2 Example of blurring present within November 2006 mosaic

Figure 3.3 shows the near-infrared (NIR) false-colour mosaic taken using the modified *Canon IXUS 50* camera. To produce the false-colour image, the red and green image constituents were mapped to the green and blue channels respectively, and the NIR wavelengths were mapped to the red channel. Imagery used to generate this mosaic was taken during the same data acquisition session as above, and algal cover exhibits marked similarity to the true-colour mosaic. The most dense algal matting, situated towards the south of the image can be distinguished as a bright red patch of colour, indicating maximum spectral response in the near-infrared. A further strip of dense *Enteromorpha sp.* cover next to the drainage structure is visible as a high near-infrared reflectivity feature, and moderate macroalgal cover around the drainage structure is visible as a less intense shade of red, indicating a diminished NIR response. The area of *Salicornia sp.* visible as mauve shades in figure 3.1 is represented by grey colouration in figure 3.3; the lack of an NIR response in this area highlights the absence of chlorophyll to be expected towards the end of the *Salicornia sp.* growing season.

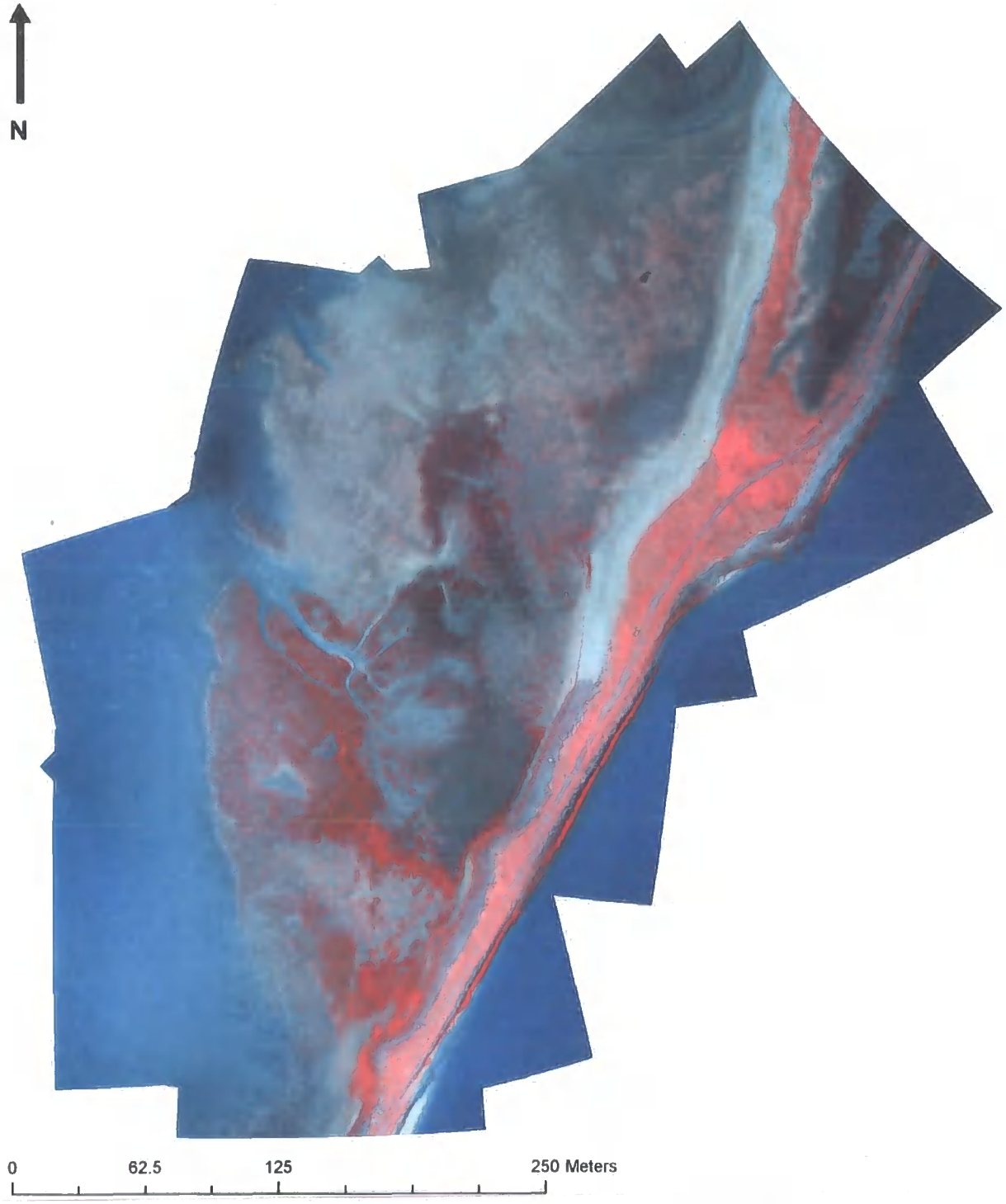

Figure 3.3 Final NIR false-colour mosaic produced from November 2006 imagery

The large section of light-red colouration towards the south-west of the image highlights the need for ground truthing: in figure 3.1 (true-colour mosaic), this area shows mixed green/grey and brown hues, indicating a mix of *Enteromorpha sp.* and decaying *Salicornia sp.* cover. However, figure 3.3 (NIR false-colour mosaic) shows consistent near-infrared reflectivity, suggesting an area of contiguous *Enteromorpha sp.* cover (see figure 3.4). This discrepancy emphasises the need for accurate ground-based measurements to aid more rigorous image interpretation.

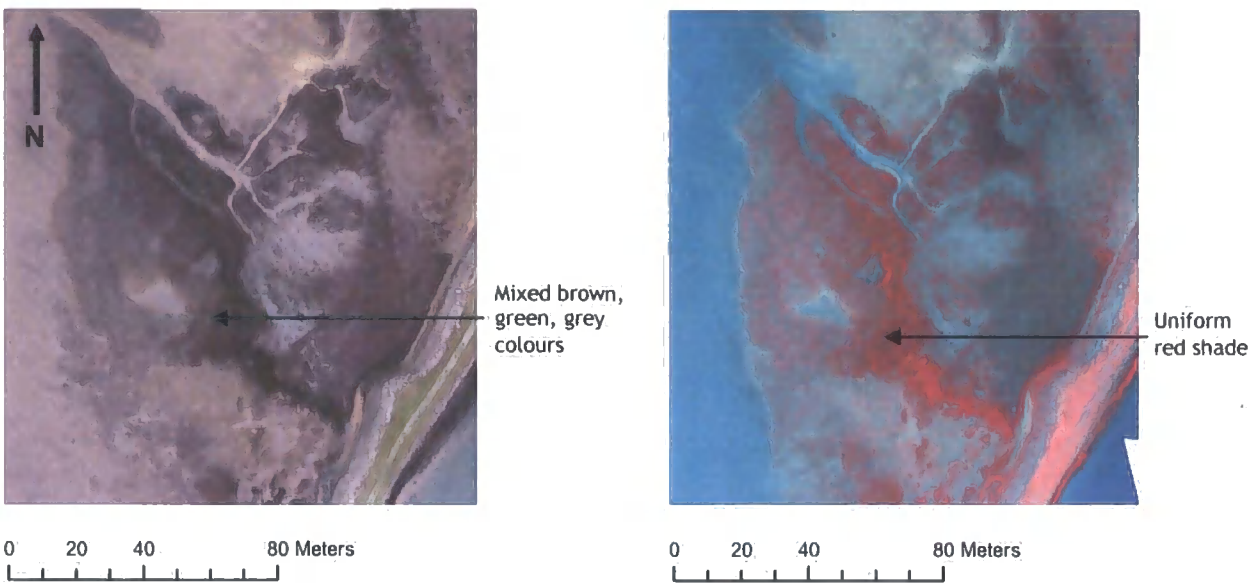

Figure 3.4 Example illustrating how vegetation reflects differently under true-colour and NIR false colour imagery

The NIR imagery was acquired towards the end of the tidal 'window' and a large section of the mosaic is obscured by inundation. Because of this, large patches of sparse macroalgal cover, particularly those towards the north of figure 3.1, are not visible, and so the infrared response of such cover types cannot be assessed qualitatively. However, the general pattern of macroalgal distribution is visually similar to the true-colour mosaic, and the green and NIR components of the true-colour and false-colour mosaics appear to show broadly similar spectral features.

3.1.2 Session 2

Figure 3.5 shows the finalised true-colour mosaic produced from the second image acquisition session. Imagery was taken in mid-June, at the beginning of the new bloom season, prior to the formation of the most extensive algal matting. The absence of cloud cover and good visibility aided image acquisition and reduced necessary exposure times, allowing for clear photography. Similarly, low wind speeds aided flight stabilisation, reducing the number of off-nadir images.

Because of the time of year, the spectral response of *Salicornia sp.* is similar to that of the macroalgal matting. This is most notable towards the centre of the image near the drainage structure, where small areas of dense *Enteromorpha sp.* mat ~2-5 m in diameter, visible as dark green shades, are surrounded by an expanse of *Salicornia sp.*, characterised by vibrant lighter green shades. Extensive (~50-150 m across) contiguous areas of dense macroalgal cover are also present towards the extreme north and south-east edges of the mosaic, again visible as dark green patches. The area towards the extreme north is actually a section of the proposed monitoring zone 3 (see figure 2.7); the long period of tidal exposure facilitated sampling and image acquisition further out onto the flats. More moderate macroalgal coverage is evident as scattered dark-green patches of *Enteromorpha sp.* between ~0.5 m and ~1 m in diameter, situated towards the south of the drainage structure. A similar texturing is visible towards the immediate north of the drainage structure, indicating a further area of moderate algal cover. Grey colouration towards the central- and north-west of the mosaic, representing sparse macroalgal coverage, show a similar distribution to figure 3.1. However, Figure 3.5 also shows sparse *Enteromorpha sp.* cover extended towards the north of the mosaic, mirroring channel formations. This was not present in the first dataset, and is likely to represent a new macroalgal growth.

Figure 3.5 Finalised true-colour mosaic produced from June 2007 imagery

3.2 Supervised classification of raw mosaics

3.2.1 Session 1

Supervised classification (see figure 3.6) of the November 2006 true colour mosaic revealed broadly similar features to those discussed in section 3.1.1. Algal material is situated towards the centre of the study area, in close proximity to the drainage structure, with the most dense patches of *Enteromorpha sp.* situated towards the south of the site. Secondary patches of medium and sparse *Enteromorpha sp.* were also highlighted towards the north of the study area, with dimensions similar to those observed in section 3.1.1. Seasonal Salicornia sp. growth was also classified towards the centre and east of the image.

Visual interpretation suggests that a significant area of substrate was misclassified as shrub/grassland. This misclassification is notable, as the presence of extensive shrub/grasslands within a tidal mudflat is not logically feasible. Similarly, areas classified as *Enteromorpha sp.* and Salicornia sp. were interspersed with incorrectly classified areas of substrate, particularly the more dense Salicornia sp. beds towards the central-north of the image. This highlights the difficulty of using simple spectral classification to adequately determine land cover type using 3-band imagery. However, it is necessary to note that because no extensive ground survey of the site was made, it was not possible to quantify the extent of incorrect classification.

	November 2006		June 2007		Difference (m^2)
	Area (m^2)	% cover	Area (m^2)	% cover	
Dense *Enteromorpha sp.*	1237.446	0.627	4938.720	1.880	1.253
Medium *Enteromorpha sp.*	8208.538	4.160	5327.390	2.028	-2.132
Sparse *Enteromorpha sp.*	3092.294	1.567	23359.170	8.893	7.326
Salicornia sp.	1824.474	0.925	15035.610	5.724	4.800
Shrub/Grassland	31090.662	15.756	7883.150	3.001	-12.755
Water	68310.611	34.618	20364.520	7.753	-26.865
Substrate	83562.797	42.347	185760.120	70.720	28.373
Total	197326.822		262668.680		

Table 3.1 Coverage extent of classification categories for November 2006 and June 2007 mosaic

Table 3.1 shows the approximate coverage extent of the various land cover classes. When compared to qualitative analysis of the study area, the abnormally high pixel counts/coverage areas for the substrate and shrub/grassland classes suggest that the classification signatures do not adequately discriminate different cover types. Similarly, the dense, medium and sparse *Enteromorpha sp.* classes are largely arbitrary, and are not sufficient to establish a realistic biomass estimate for the site. Of the three *Enteromorpha sp.* classes present, 'medium' cover is the most common, occupying 4.16% of the imaged area. The relatively high percentage cover attained by the 'shrub/grassland' class in comparison to the 'substrate' class again emphasises the misclassification present within the image.

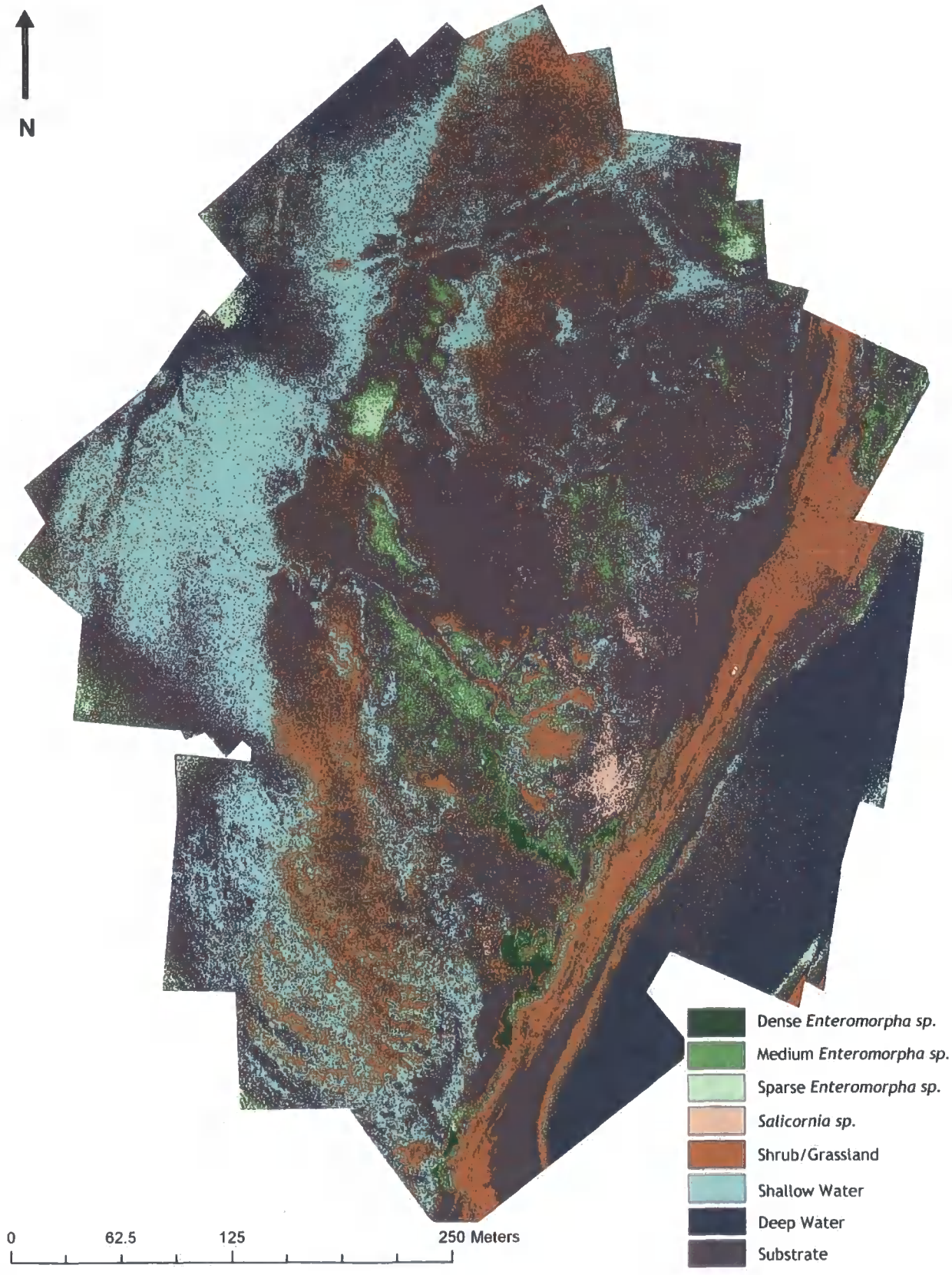

Figure 3.6 Supervised classification of November 2006 true-colour mosaic

3.2.2 Session 2

Figure 3.7 shows supervised classification of the June 2007 mosaic. This again shows parity with the qualitative analysis of the study area. Although the spectral response of *Salicornia sp.* was similar to that of *Enteromorpha sp.* during this time of year, they appear to be adequately discriminated by simple spectral classification. The majority of *Salicornia sp.* cover is located towards the centre of the site, and is fringed by sparse macroalgal cover. Extensive dense *Enteromorpha sp.* cover is located towards the extreme north-west and south edges of the image, in a pattern similar to that described in section 3.1.2. Classification also shows extensive sparse *Enteromorpha sp.* cover towards the central and north-east of the mudflat area. These were not visible in the simple qualitative analysis of the image, and are likely to represent incorrect image classification. However, macroalgal quadrats surveys in this area showed sparse algal cover, so this may indicate that supervised classification can discriminate visually indistinct *Enteromorpha sp.* cover. There appears to be a lesser degree of misclassification than exhibited by the November 2006 imagery, and the *shrub/grassland* class is not as overvalued.

Table 3.1 suggests that although the 'dense' and 'sparse' classes of *Enteromorpha sp.* cover have increased following the November 2006 dataset, the 'medium' class has experienced a reduction of 2.13%. However, it is again necessary to stress that the cover classes are arbitrary, and this may not indicate a biomass increase. The 4.80% increase in *Salicornia sp.* is plausible, because the previous imagery was taken towards the end of the growing season. Similarly, the significant decrease in pixels classed as 'water' (26.86%) is likely to be an accurate reflection of the tidal cycle in comparison to the November 2006 dataset. However, as evidenced by the significantly greater area classed as 'substrate' within the June 2007 dataset, any variation in percentage cover may simply be a reflection of the larger GSD coverage of the June 2007 dataset.

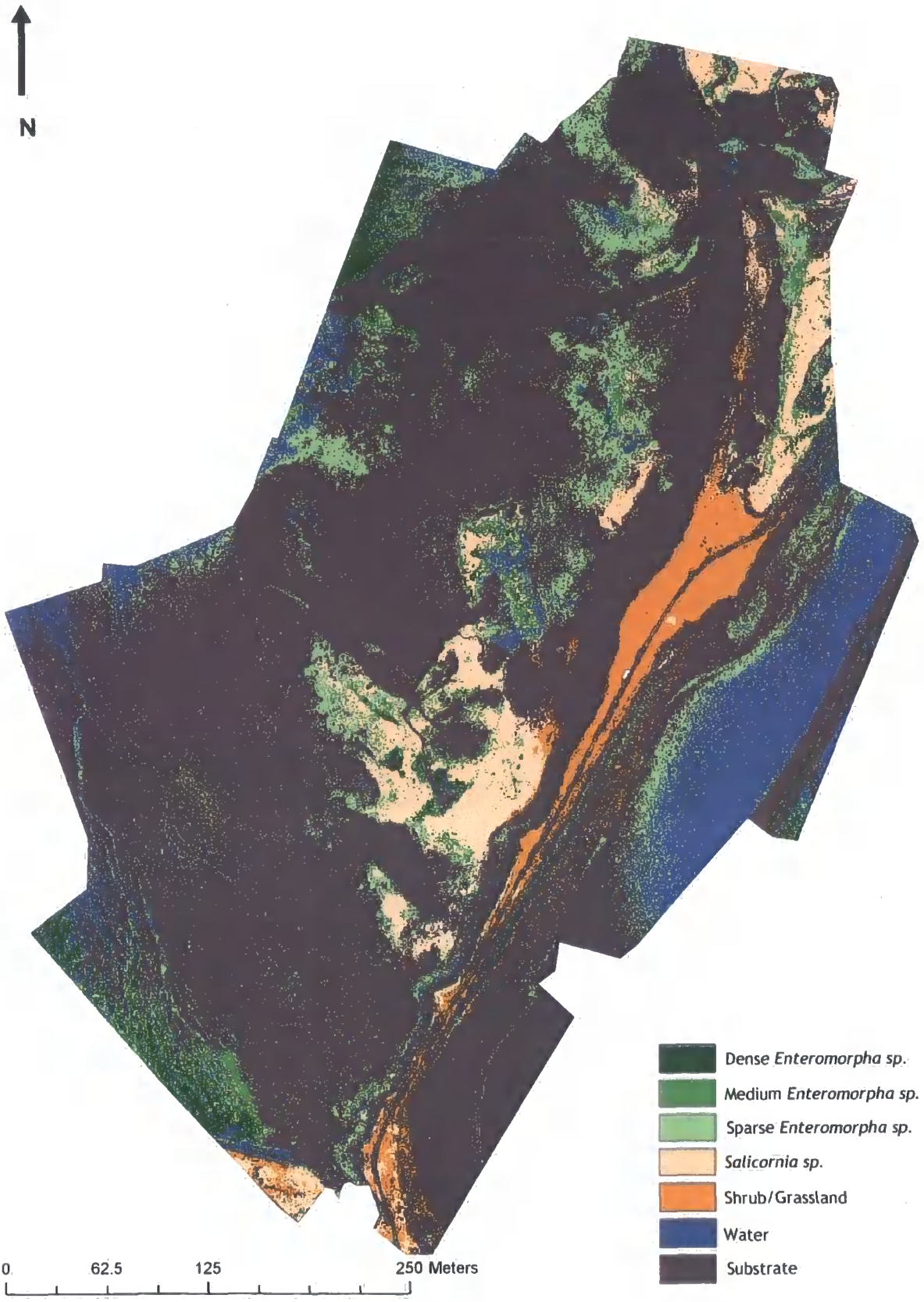

Figure 3.7 Supervised classification of June 2007 true-colour mosaic

3.3 *Enteromorpha sp.* dry weight results

3.3.1 Session 1

Figure 3.10 (p. 63) shows *Enteromorpha sp.* sample locations superimposed on the November 2006 mosaic. A total of 32 samples were collected. Macroalgal *dry weight per square metre* (g DW m^{-2}) measurements show a large variation (standard deviation σ = 130.3 g) in biomass across the surface of the study area. The highest biomass samples (greater than 500 g DW m^{-2}) were situated towards the centre and south of the study area, coinciding with the areas of high green reflectivity noted in section 3.1.1. Although it is possible that the highest biomass samples (see figure 3.8A) represent autochthonous growth, the presence of several superimposed layers of *Enteromorpha sp.* matting at these locations suggests that algal material may originated elsewhere prior to being transported to the edges of the mudflat by tidal activity. Sampling of the more dense matting proved problematic, as older algal growth below the surface layer had started to decay (presumably because samples were taken towards the end of the growth season).

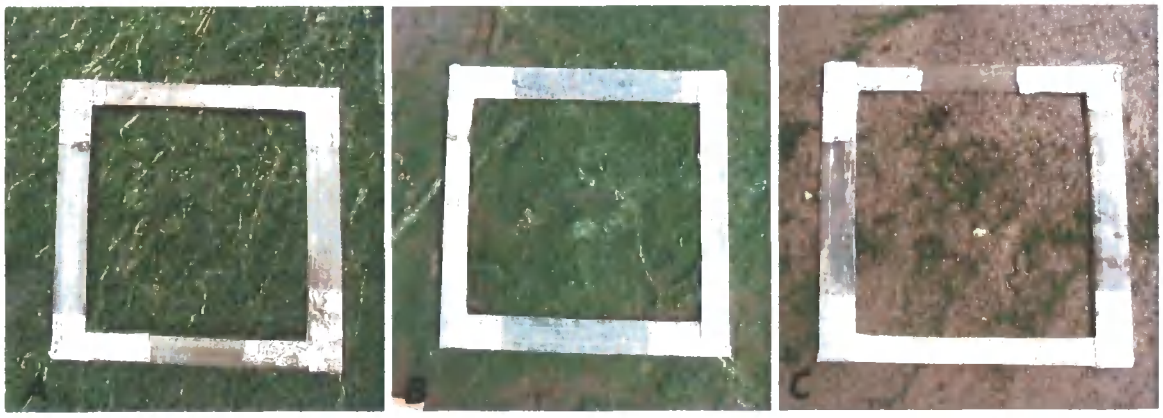

Figure 3.8 *Enteromorpha sp.* sample quadrats. **(A)** Dense biomass/cover, **(B)** moderate biomass/cover, **(C)** sparse biomass/cover

Moderate biomass samples (75 - 100 g DW m^{-2}) are located towards the immediate east of the drainage structure noted in figure 3.1. *Enteromorpha sp.* cover at these locations is likely to have

developed in-situ, as algal matting is generally thinner, and does not appear to be stratified as several layers (see figure 3.8B). The lowest biomass samples (1 - 25 g DW m^{-2}) are situated towards the south-west and north of the mosaic. *Enteromorpha sp.* cover at these locations has not developed into mats, and consists mainly of a number of smaller independent filaments (see figure 3.8C).

Figure 3.9 shows *Enteromorpha sp.* dry biomass plotted against altitude relative to the dGPS reference station. A 'zero' altitude was established at the point where the dGPS station was placed, and altitude was established relative to this point. Although there appears to be no significant correlation between sample altitude and macroalgal dry biomass (R^2 = 0.0961), samples with a relatively high biomass (<50 g DW m^{-2}) were all located at altitudes lower than 0.6 m. However, samples with lower dry weight measurements display a much greater altitudinal spread (~0.3 m - 1.2 m), although this trend is potentially due to the absence of a larger number of high-biomass samples. The shallow gradient of the regression line is likely to be a result of outlying high-biomass samples. This is supported by the high ANOVA *p* value, which shows that the correlation is *not* significant at the 99% confidence level.

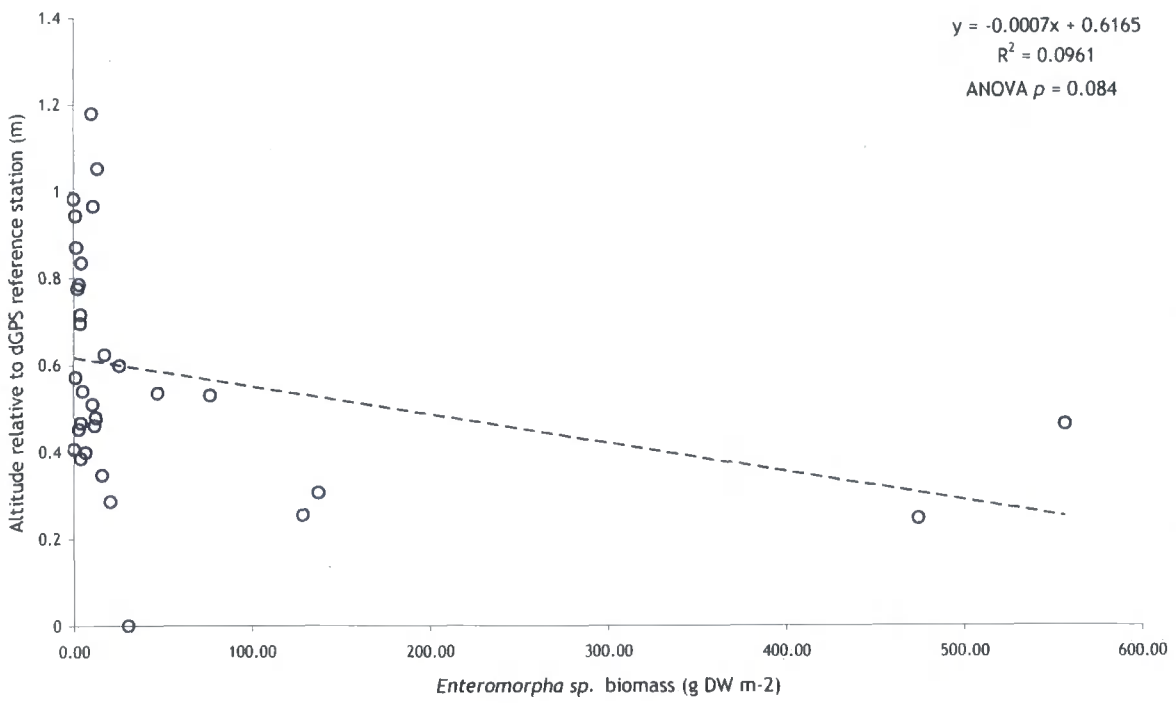

Figure 3.9 *Enteromorpha sp.* against altitude relative to dGPS reference station.

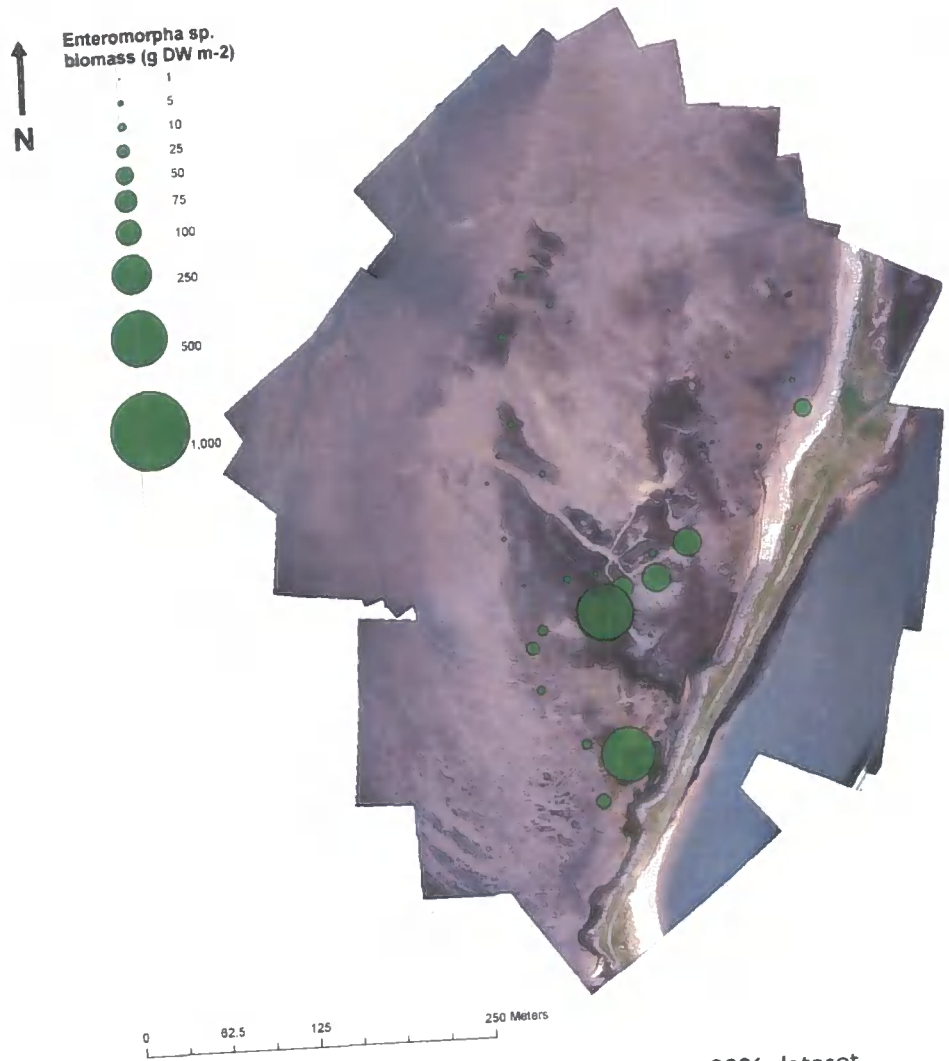

Figure 3.10 *Enteromorpha sp.* samples from November 2006 dataset

Figure 3.11 *Enteromorpha sp.* samples from June 2007 dataset

3.3.2 Session 2

Figure 3.11 shows *Enteromorpha sp.* sample locations superimposed on the June 2007 mosaic. A total of 27 samples were collected. Although macroalgal *dry weight per square metre* (g DW m^{-2}) measurements suggest a similar distribution to figure 3.10, there is significantly less variation in sample biomass (standard deviation σ = 25.5 g). Overall sample weights were also significantly lower than those taken in November 2006; it is likely that this is because the seasonal growth of macroalgal matting had only just started to develop at the time samples were taken. The highest biomass samples (>50 g DW m^{-2}) were clustered towards the centre of the mosaic, near the drainage structure, although the large dark-green reflectivity feature towards the extreme north of the image (see section 3.1.2) yielded a high biomass value. Biomass values were significantly lower further away from the drainage feature. Moderate samples (10 - 50 g DW m^{-2}) were situated towards the north of the site, coinciding with areas of lower green reflectivity. However, the majority of samples towards the north and west of the site generally varied between 1 and 10 g DW m^{-2}, and were formed as multiple 'strands' of *Enteromorpha sp.* (figure 3.8c), rather than the thicker matted samples found nearer to the centre of the site.

Figure 3.12 suggests that *Enteromorpha sp.* biomass exhibited similar altitudinal trends to the previous survey. Although there is no significant correlation between biomass and altitude (R^2 = 0.0035), larger samples (>50 g DW m^{-2}) were generally situated at lower altitudes. Again, those samples with a lower biomass exhibited a greater altitudinal spread, although the absence of a greater number of high-biomass samples limits the conclusions that can be drawn from this. Similarly, the flatness of the trendline suggests that there is little or no biomass variation with altitude. The dearth of sample points within close proximity of the trendline, and the high ANOVA *p* value show the association to be insignificant. However, it is also pertinent to note that the majority of larger samples in both instances (November 2006 and June 2007) were taken near to the drainage structure, and it is plausible that this may act to reduce any biomass-altitude correlation that may have been present.

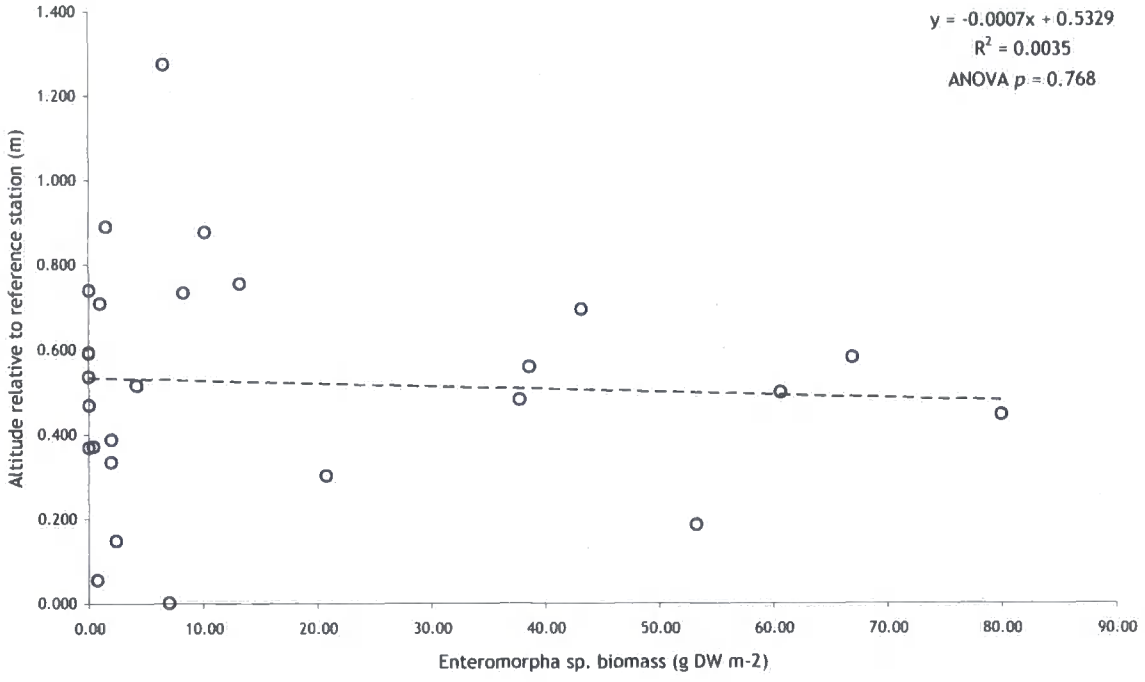

Figure 3.12 *Enteromorpha sp.* against altitude relative to reference station.

3.4 Image analysis and biological calibration

3.4.1 Image Spectral Properties

3.4.1.1 Session 1

Quantitative analysis of the November 2006 mosaics indicates that *Enteromorpha sp.* biomass variation is associated with spectral behaviour. Figure 3.13 shows how reflectivity DN values for the red, green, blue and NIR bands varies with respect to macroalgal biomass. Red, green and blue DN values were extracted from the true-colour mosaic; NIR response values were extracted from the NIR mosaic. Although the NIR mosaic also contained red and green components in addition to the NIR band, the

modification performed on the *Canon IXUS 50* in order to obtain NIR imagery rendered these bands unsuitable for analysis.

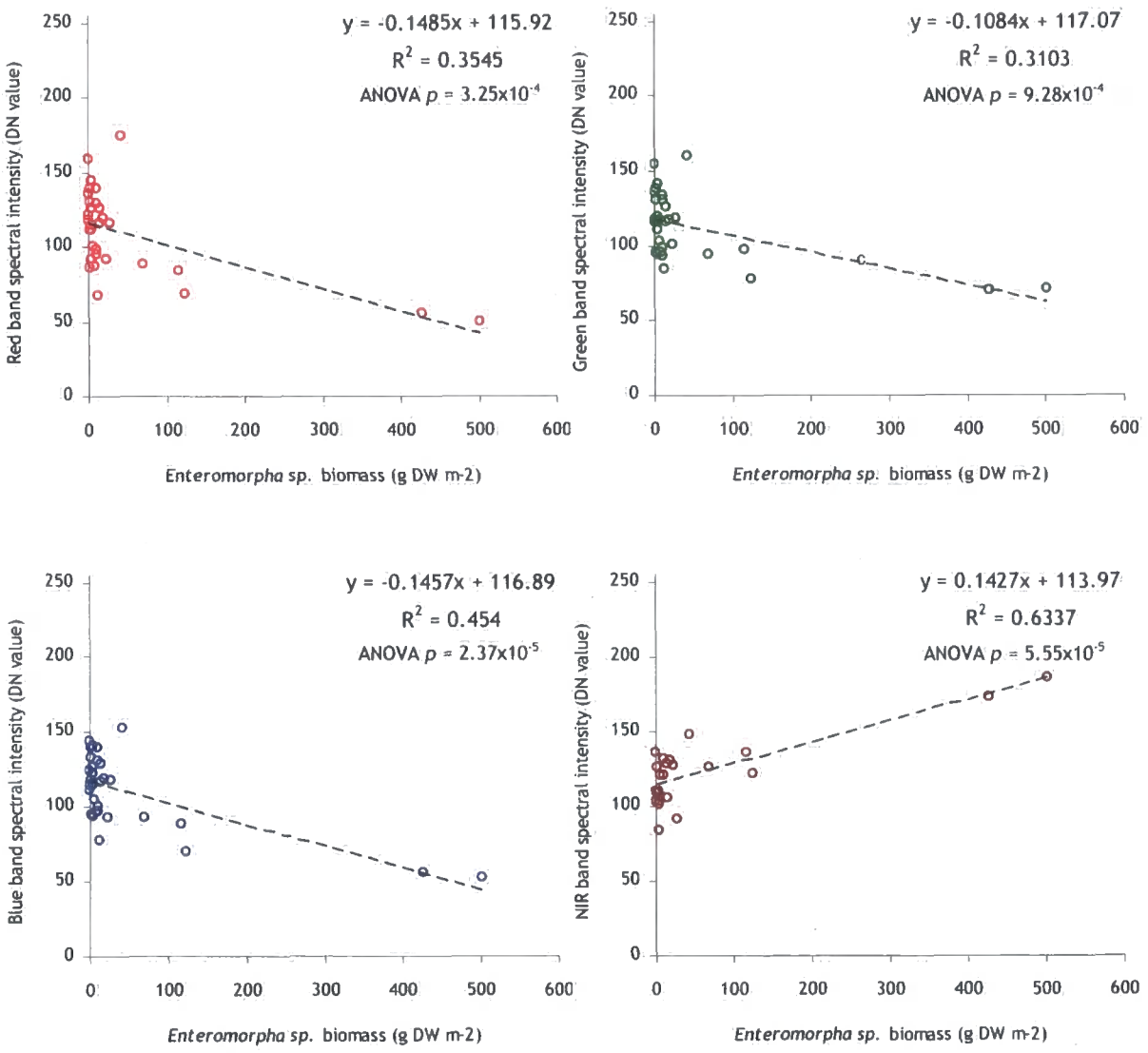

Figure 3.13 *Enteromorpha sp.* biomass against red, green, blue and NIR reflectivity DN for November 2006 mosaic.

The red, green and blue bands all show similar trends: The low R^2 values (less than 0.5) indicate a weak negative correlation between spectral response and biomass, suggesting that spectral response in the visible wavelengths is inversely proportional to macroalgal biomass. Although the data indicates that lower biomass values yield a greater range of DN values, it is likely this is due (in part) to the absence

of a greater number of high biomass samples, especially in the range of ~45 - 140 g DW m^{-2}. The lower R^2 of the red and green bands (~0.3 - 0.35) when compared to the blue band (0.454) also highlights a potential fallacy of the data, as it is usually the red and green components of RGB imagery that are correlated with biomass/vegetation cover (eg. Ben Moussa *et al.*, 1989; Curran & Steven, 1983; Guichard *et al.*, 2000; Hunt *et al.*, 2005; Larsen *et al.*, 2004; Smith *et al.*, 1998), whereas the blue band is commonly disregarded. Hence, because the blue band shows the strongest correlation, the significance of the red/green band - biomass plots is questionable. The relatively shallow gradient of the trendline would also indicate that spectral response only varies a small amount with regards to biomass. However, ANOVA *p*-values for the red, green and blue DN - biomass plots are all lower than 0.01, suggesting that the R^2 values *are* significant at the 99% confidence level.

The trends exhibited by the near-infrared component of the NIR mosaic are more conventional. The relatively strong positive correlation (R^2 = 0.6337) between NIR spectral response and biomass indicates that biomass variation can be explained by the NIR band. Although the trendline gradient is again relatively shallow, the points appear to follow a more linear distribution than the red, green and blue bands. The range of spectral intensities yielded by lower biomass values also appears smaller than that of the red, green or blue bands, possibly accounting for the low ANOVA *p*-value, indicating a significant correlation at the 99% confidence level. However, this is due (in part) to the obscuration of part of the NIR mosaic by tidal inundation, so that it was not possible to extract spectral values from nine sample points (see figure 3.3). Although higher macroalgal biomass appears to cede higher spectral DN values (as is to be expected), the absence of samples in the range of ~45 - 140 g DW m^{-2} is likely to have introduced bias into the coefficient of determination.

Although figure 3.13 suggests a weak linear correlation between reflectivity DN and biomass, the dense distribution of low biomass samples *above* the regression lines and subsequent higher biomass samples below the lines may indicate that the biomass - reflectivity relationship is non-linear. Log_{10} transformation of the red, green and blue bands (see figure 3.14) leads to a marginal improvement in correlation with macroalgal biomass, supporting the hypothesis that the relationship may be curvilinear. An R^2 improvement of ~0.10 - 0.15 is noted for the true-colour bands. The plots also show

an increase in clustering of low-biomass samples and the placement of higher-biomass samples in closer proximity to the regression line.

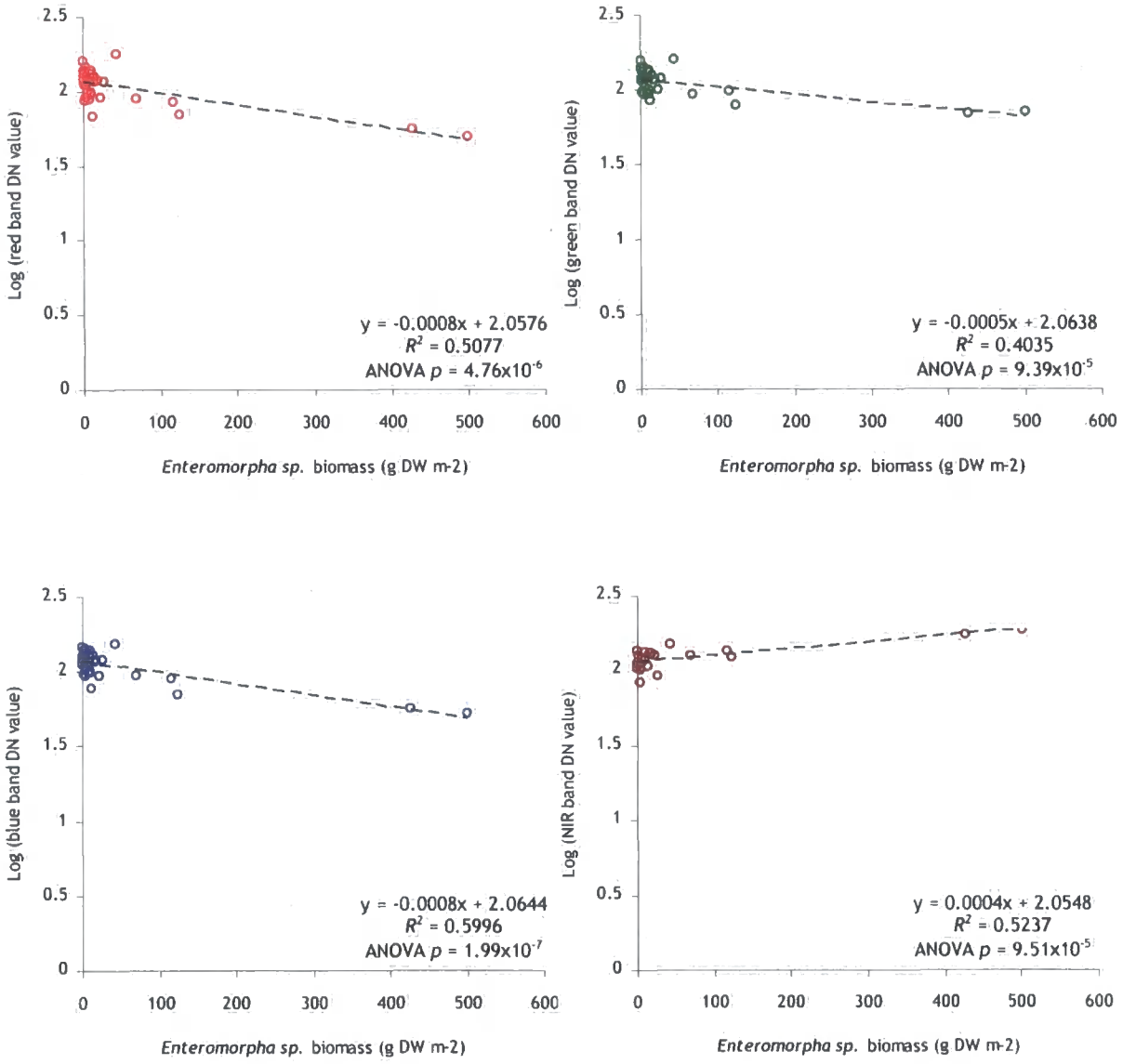

Figure 3.14 *Enteromorpha sp.* biomass against $\log_{10}$ of red, green, blue and NIR reflectivity DN for November 2006 mosaic

Unlike the true-colour bands, the biomass - $\log_{10}$ NIR reflectivity plot showed a significant reduction in coefficient of determination under log-normal conditions (R^2 = ~0.1 decrease). This would indicate that the NIR - biomass relationship is indeed linear. The gradient of the regression line also decreased in comparison to figure 3.13. This suggests that the $\log_{10}$ of NIR DN value does not respond as readily to

variations in biomass as the NIR DN value itself, and the association between the two variables is not as strong.

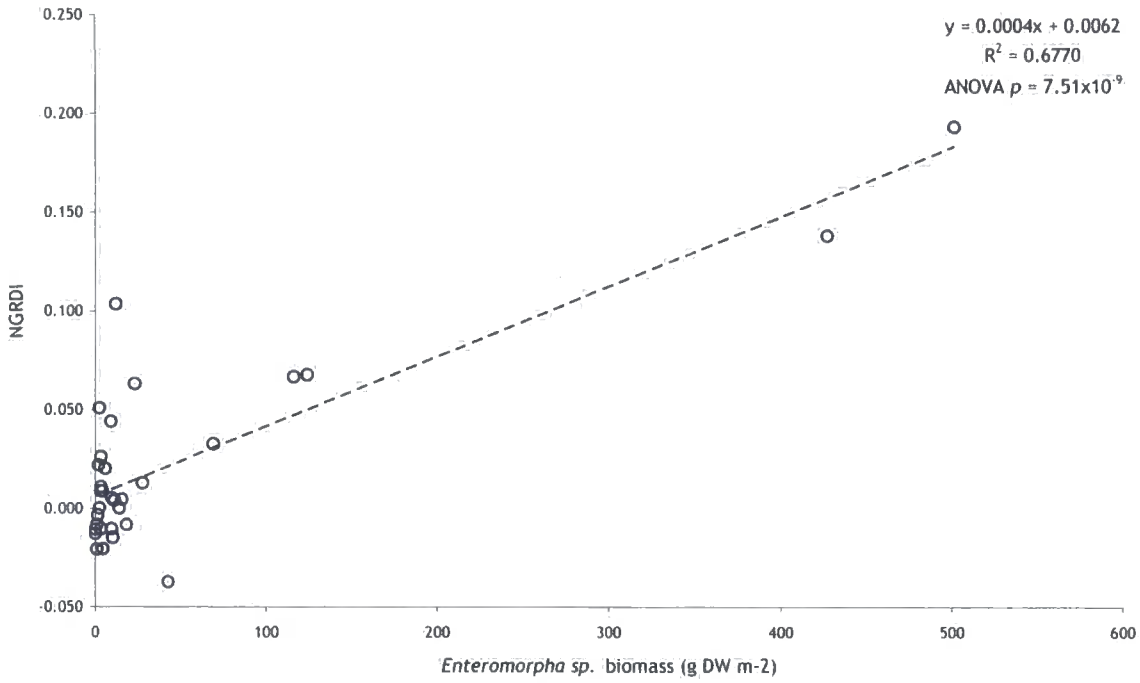

Figure 3.15 *Enteromorpha sp.* biomass against *relative* NGRDI computed on the November 2006 mosaic.

Hunt *et al.* (2005) show that the normalised green-red difference index (NGRDI) highlights the difference in spectral response between vegetation and substrate. This uses the premise that light absorbing pigments within photosynthetic organisms weaken reflectance in the red and blue wavelengths, whereas cellular refraction causes strong refraction in the green and near-infrared (NIR) (Curran & Steven, 1983). Figure 3.15 shows how *relative* NGRDI value varies with *Enteromorpha sp.* biomass. The relatively strong correlation between biomass and NGRDI (R^2 = 0.6770) highlights the positive NGRDI trend in response to macroalgal biomass. An extremely low ANOVA *p*-value of 7.51×10^{-9} highlights the significance of the relationship at the 99% confidence level. Lower biomass values show greater clustering than the simple spectral response - biomass plots, indicating a more narrow NGRDI range, although a number of outliers are present. Higher macroalgal biomass (>50 g DW m^{-2}) is shown to correspond with higher NGRDI values. The gradient of the trendline is marginally steeper than the individual spectral response - biomass plots, indicating that NGRDI varies more strongly in response to

biomass than simple spectral response - biomass plots. The majority of points also show a linear distribution along the trendline, although the two highest biomass measurements deviate further from the regression line than in the spectral response - biomass plots (see figure 3.13).

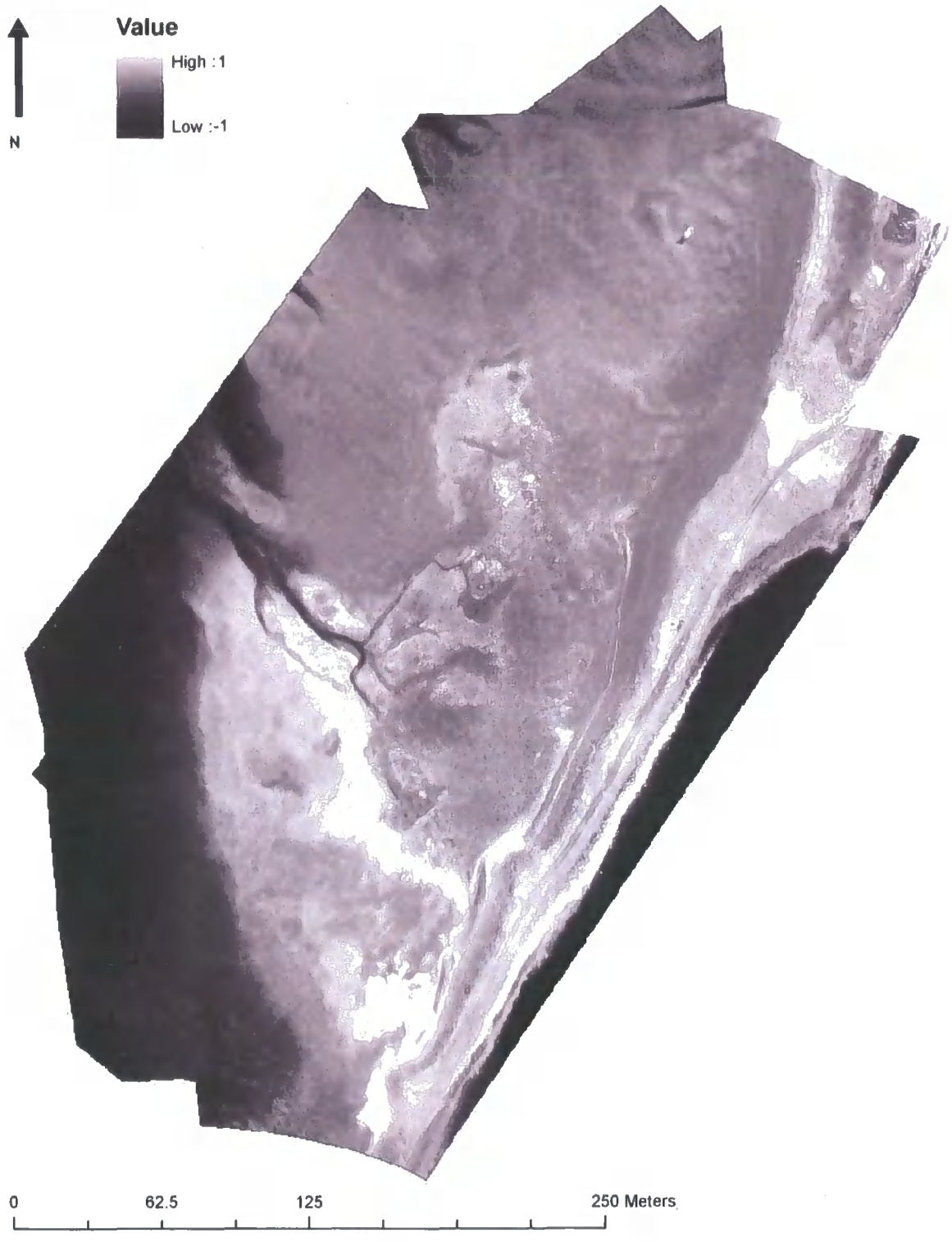

Figure 3.16 *Relative* NDVI computed from November 2006 true-colour and NIR imagery

Figure 3.16 shows the NDVI image produced by co-registering the near-infrared band from the NIR mosaic to the red band of the true-colour image. The NDVI suggests a similar distribution of *Enteromorpha sp.* to that discussed in section 3.1.1. Highest NDVI values are located towards the south of the image, and correspond to an area of dense macroalgal matting. Secondary areas of high NDVI around the drainage structure (towards the centre of the mosaic) also coincide with areas of medium to low biomass.

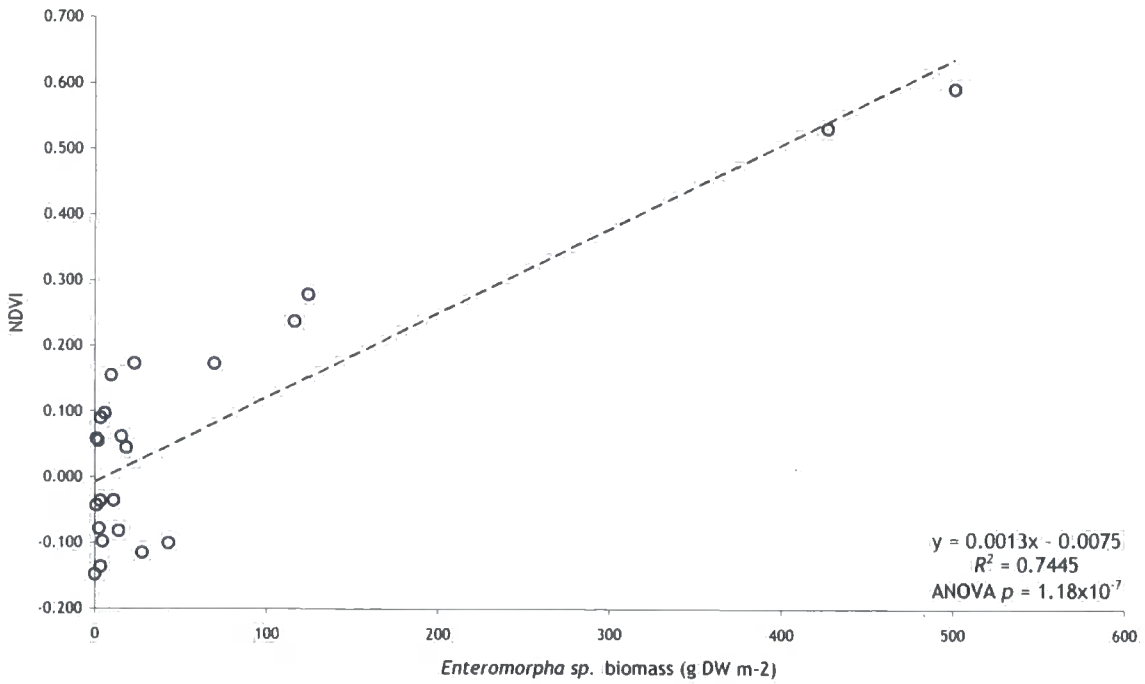

Figure 3.17 *Enteromorpha sp.* biomass against *relative* NDVI computed on the November 2006 mosaic.

The strong correlation between biomass and NDVI (R^2 = 0.7445) displayed in figure 3.17 suggests that *Enteromorpha sp.* biomass variability can be explained quantitatively by the NDVI ratio. Although lower biomass samples yielded a relatively large range of NDVI values, the proximity of moderate (50 - 150 g DW m^{-2}) and dense biomass samples to the regression line highlights a possible linear relationship between macroalgal dry weight and NDVI. It is necessary to note, that it was not possible to include a number of biomass samples in the plot, because they were concealed on the NIR mosaic by tidal inundation; this may have acted to artificially increase the coefficient of determination. However,

ANOVA $p < 0.01$, indicating that the R^2 is significant even in the absence of a number of biomass samples.

The presence of a cluster of samples within figure 3.17 which yielded zero or negative NDVI values is problematic, as it is not rationally possible to achieve a negative NDVI for a pixel that is known to be vegetated. On this premise, it is logically sound to remove such points from the regression plot. Although this acts to further decrease the size of the dataset, the remaining points allow for a more rigorous analysis of the response of NDVI to macroalgal biomass.

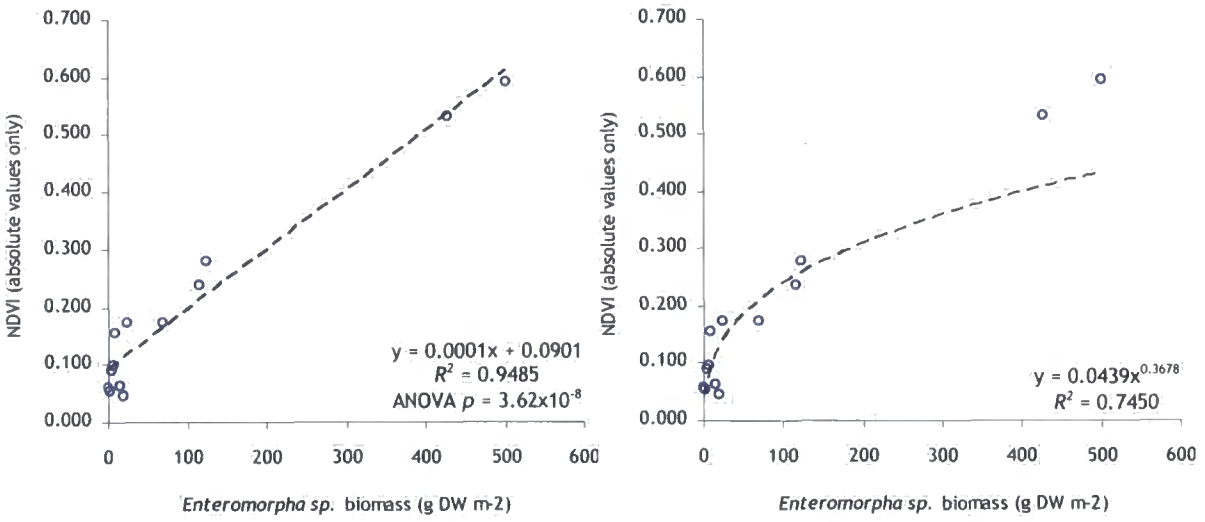

Figure 3.18 *Enteromorpha sp.* biomass against *relative* NDVI computed on the November 2006 mosaic. All negative and zero values have been removed. **(A)** linear regression model, **(B)** power regression model.

Figure 3.18 shows the same dataset with zero or negative NDVI values removed. Using a standard linear regression model **(A)**, the coefficient of determination is greatly improved upon that of figure 3.17. Although the trendline does not pass through the origin, the steep gradient shows that NDVI varies significantly with respect to biomass, and indicates that there is a very strong association between NDVI (absolute values) and *Enteromorpha sp.* This is supported by the high R^2 value, and suggests that the modified NDVI dataset can explain *Enteromorpha sp.* biomass with a high degree of accuracy. Guichard *et al.* (2000) suggested that NDVI did not respond linearly to biomass, and used a power regression

model (B) to explain biomass variability. Although the power regression trendline appears to model the low biomass values with a high degree of accuracy, it does not adequately trace the high biomass values. Because error inherent in sampling the low biomass values is likely to be much greater than that of the higher values, the validity of the model is questionable. In addition, the coefficient of determination does not show a significant improvement over figure 3.17, so the power regression model can be rejected in favour of standard linear regression.

3.4.1.2 Session 2

Spectral response - biomass plots for the June 2007 mosaicked imagery further emphasise the correlation between *Enteromorpha sp.* biomass variation and spectral response. Figure 3.19 shows DN value against macroalgal biomass for the red, green and blue bands. All three plots describe a similar pattern of spectral response: The regression line indicates a negative reflectivity trend in response to increasing macroalgal biomass, highlighting a possible correlation between visible wavelength reflectivity and *Enteromorpha sp.* dry weight. The *y*-intercept of the regression lines all show similar trends to the November 2006 imagery, with 'zero' biomass values yielding reflectivities of ~120 DN, and the relatively shallow gradient suggests that biomass variation yields a relatively narrow band of reflectivity values. Although the R^2 values indicate a relatively minor correlation (R^2 = ~0.5 - 0.6), it is superior to that yielded by the November 2006 imagery. ANOVA *p*-values for the red, green and blue reflectivity - biomass plots are also lower than those yielded by the November 2006 imagery, indicating an increased significance in correlation. Low biomass values exhibit a smaller range of spectral intensities than that of the Session 1 imagery (see section 3.4.1.1), and *Enteromorpha sp.* samples show a more even distribution. It is likely this accounts for the improvement in correlation over the first dataset. Although DN values yielded by moderate to high biomass samples (>10 g DV m^{-2}) deviate further from the regression line than in previous imagery (see section 3.4.1.1), this is again likely to be a function of the more uniform sample weight distribution.

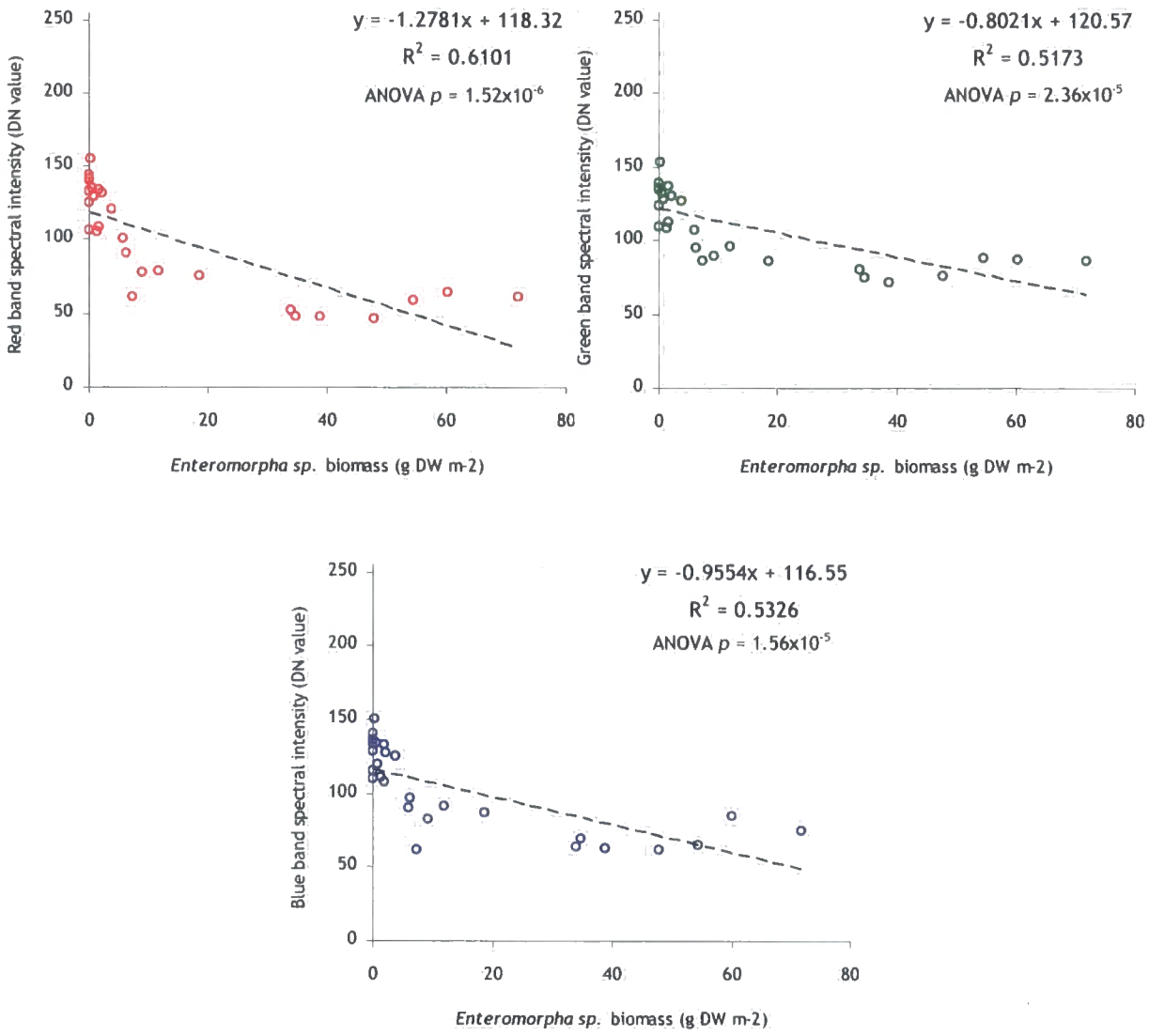

Figure 3.19 *Enteromorpha sp.* biomass against red, green and blue reflectivity DN for the June 2007 mosaic.

As noted for the November 2006 dataset, the relationship between biomass and reflectivity may not follow a linear trend. This premise is supported by dense clustering of low-biomass sample points above the regression line, in addition to a number of medium biomass points below the line for all of the plots in figure 3.19. Figure 3.20 shows *Enteromorpha sp.* plotted against $\log_{10}$ of red, green and blue DN values for the June 2007 imagery.

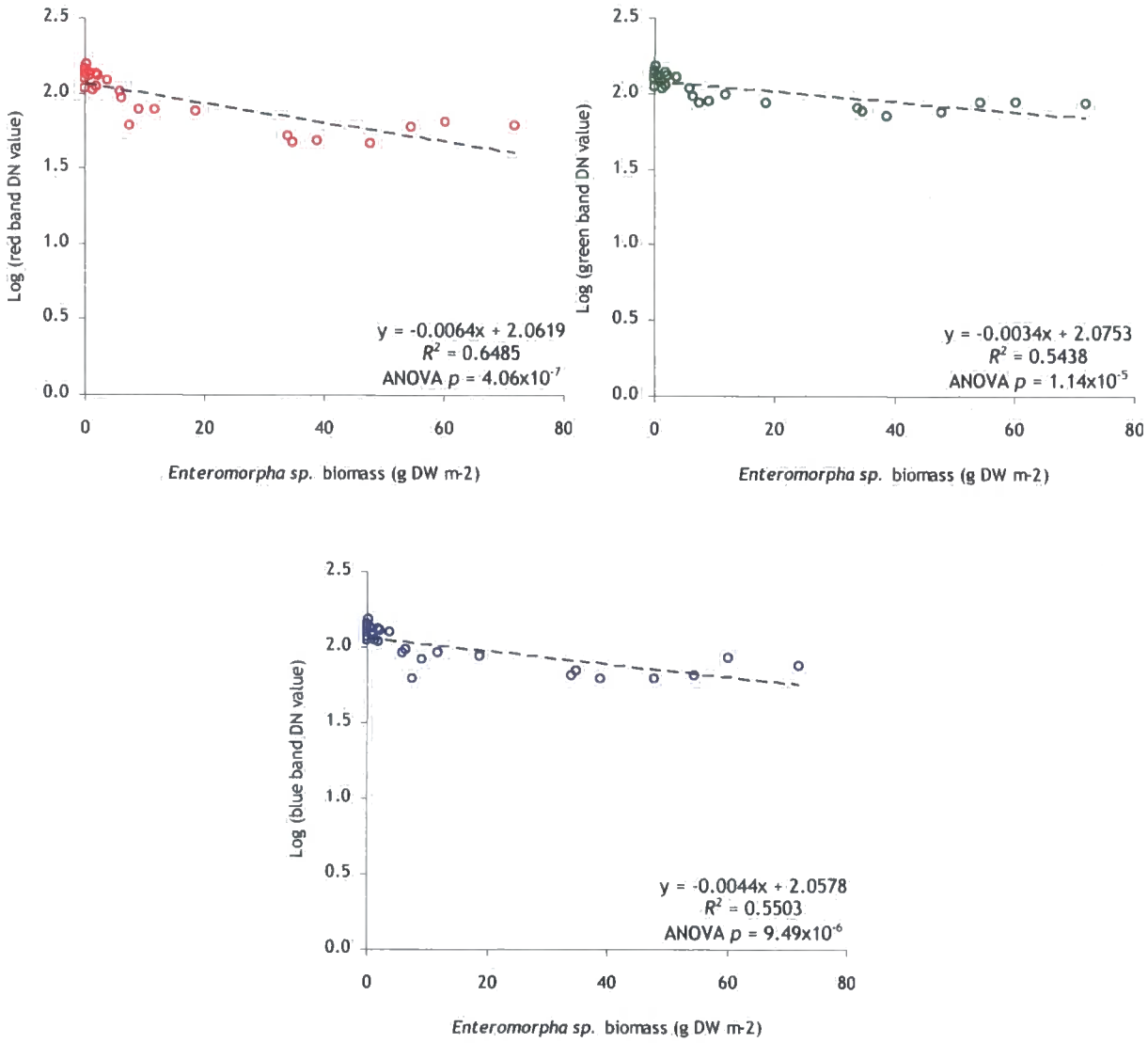

Figure 3.20 *Enteromorpha sp.* biomass against $\log_{10}$ of red, green, blue and NIR reflectivity DN for June 2007 mosaic

Log_{10} transformation of the red, green and blue bands shows a tighter clustering of low-biomass samples around the y-intercept of the regression line. A marginal improvement in correlation with macroalgal biomass (R^2 = ~0.01 increase) suggests that the biomass - reflectivity relationship may not adhere to a simple linear model. This is also supported by the close proximity of high-biomass samples to the regression line. However, the marginal increase in coefficient of determination appears insufficient to determine the nature of the relationship.

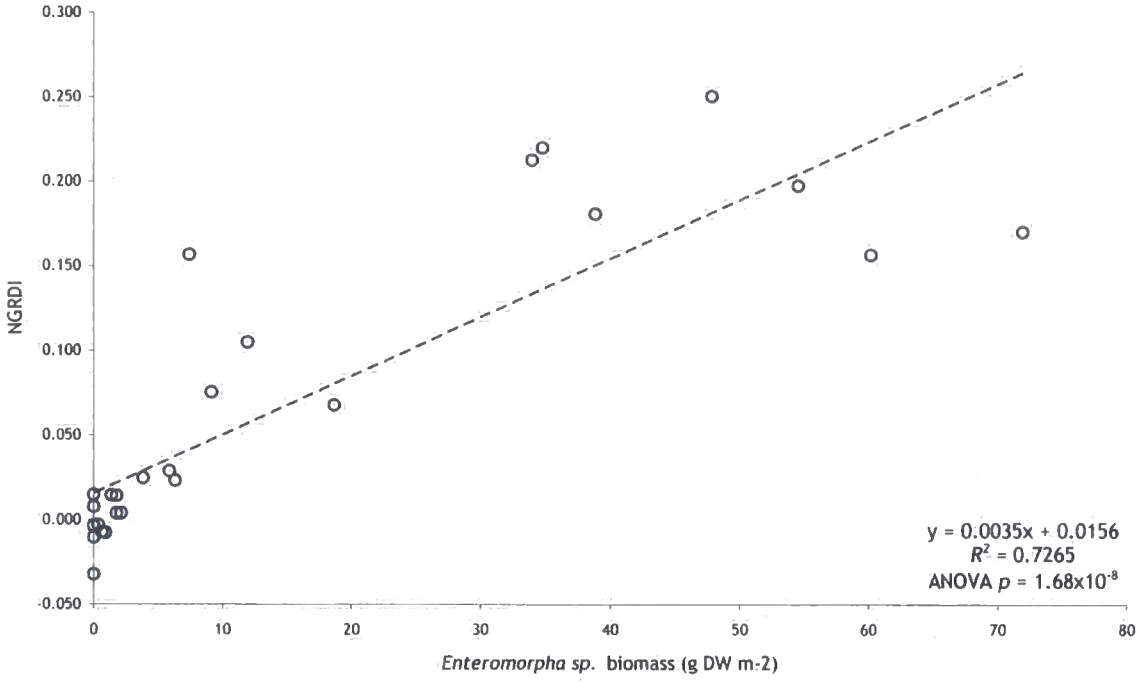

Figure 3.21 *Enteromorpha sp.* biomass against *relative* NGRDI computed on the June 2007 mosaic.

The *relative* normalised green-red difference ratio (see figure 3.21) computed on the June 2007 mosaic shows a high degree of correlation with *Enteromorpha sp.* dry weight, indicating that NGRDI can explain algal biomass variability. The coefficient of determination (R^2 = 0.7265) is similar to that shown by Guichard *et al.* (2000), suggesting that spectral response displays an analogous variability in response to biomass. However, the trendline shows a steeper gradient than that of the November 2006 imagery, indicating that the range of NGRDI values ceded may show seasonal variation. Low biomass samples show a smaller distribution of NGRDI values than the November 2006 imagery, although higher biomass samples deviate significantly from the regression line. Again, the increased regularity in sample weight distribution is likely to have improved correlation over that of the first dataset. Although the ANOVA *p*-value of 1.68×10^{-8} highlights the significance of the R^2 value, it is lower than the November 2006 NGRDI, possibly as a result of the deviation of high biomass samples.

3.4.2 Image Colour Saturation

3.4.2.1 Session 1

Table 3.2 shows the coefficient of correlation between the red, green and blue components of the true colour mosaic (see figure 3.1).

	Correlation coefficient (R^2)		
	Red	Green	Blue
Red		0.9768	0.9441
Green	0.9768		0.9345
Blue	0.9441	0.9345	

Table 3.2 Band intercorrelation of November 2006 mosaic

The high R^2 value indicates a close association between the visible wavelengths, and hence a high degree of band intercorrelation within the mosaic. Image saturation describes the purity of colours within an image and acts to reduce band intercorrelation (Laliberte *et al.*, 2007), allowing for enhanced discrimination between vegetation and substrate. Figure 3.22 shows the saturation transformation applied to the November 2006 true-colour mosaic.

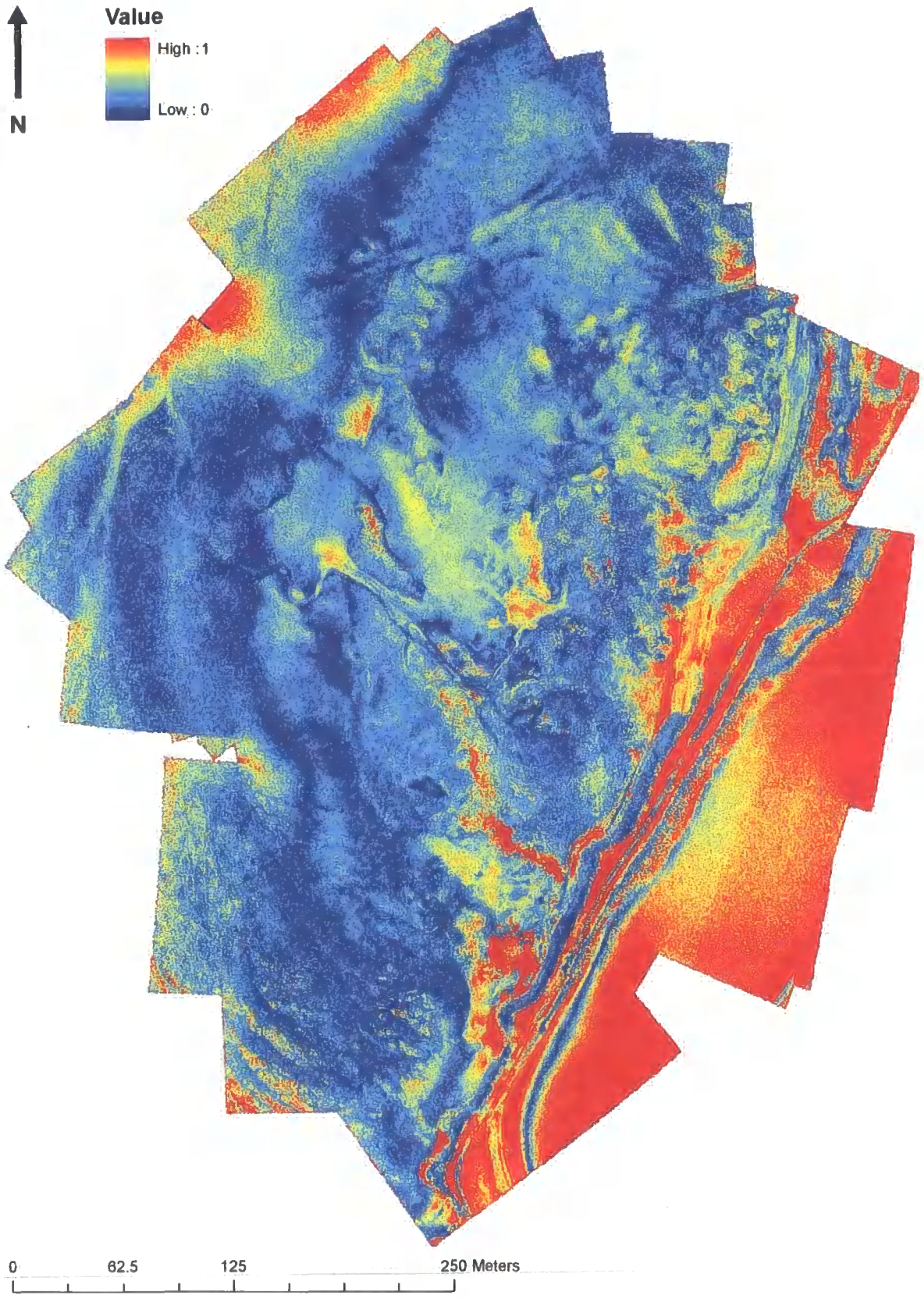

Figure 3.22 Image colour saturation computed on November 2006 true-colour mosaic

Colour saturation shows similar qualitative trends to those discussed in section 3.1.1. Highest saturation values (red/orange shading) are located towards the south of the image, and correspond to an area of dense macroalgal matting. Less dense *Enteromorpha sp.* cover is highlighted by medium saturation values (yellow shading) towards the centre and north of the image, near the drainage structure. Patches of sparse macroalgal growth identified in section 3.1.1 as areas of grey colouration towards the north-west of the site are also highlighted by orange/yellow shading, again indicating a relatively high saturation value.

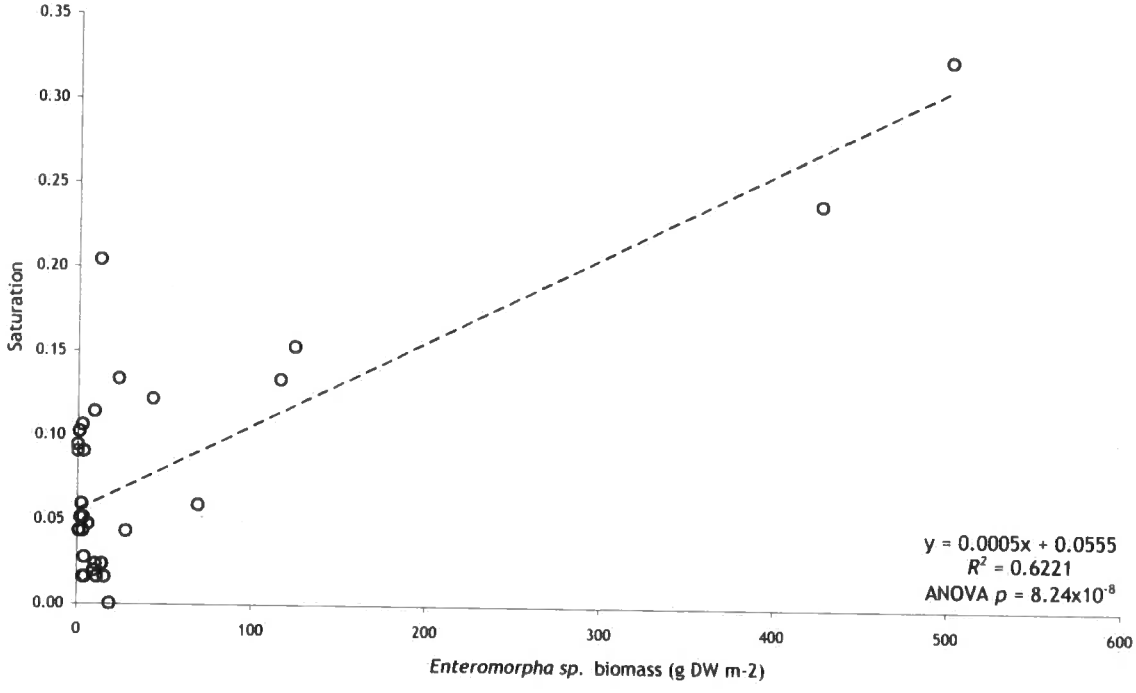

Figure 3.23 *Enteromorpha sp.* biomass against image colour saturation computed on the November 2006 mosaic.

Figure 3.23 shows a moderately strong positive correlation between colour saturation and macroalgal biomass (R^2 = 0.6221). Although ANOVA $p < 0.01$, indicating a significant saturation - biomass correlation, low biomass samples show a large distribution of saturation values, with a large number of possible outliers. As discussed in section 2.6.2, a number of filters were applied to the saturation mosaic in figure 3.22 in order to remove anomalies and compression artefacts which may account (in part) for these deviations.

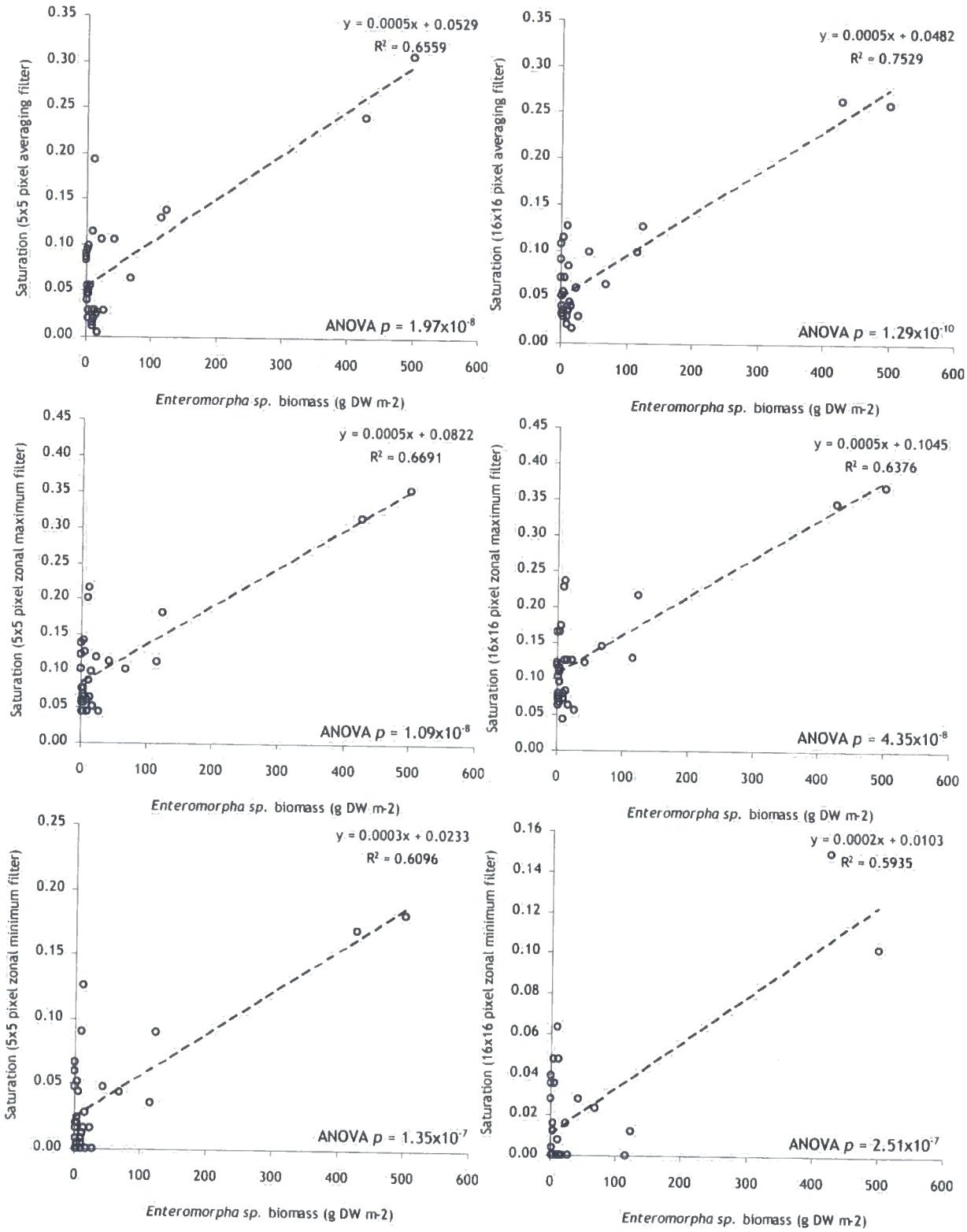

Figure 3.24 *Enteromorpha sp.* biomass against colour saturation under various filter criteria (November 2006)

Figure 3.24 shows saturation - biomass plots after applying *averaging*, *zonal maximum* and *zonal minimum* filters to figure 3.22. The 16 x 16 pixel averaging filter yielded the strongest correlation (R^2 = 0.7529). Low biomass values yielded a smaller range of saturation values with the application of *averaging* or *zonal maximum* filters, although the *zonal minimum* filter increased the number of potential outliers. The deviation of higher biomass samples (>50 g DW m^{-2}) from the regression line is also diminished under all conditions except the 16x16 pixel *zonal minimum filter*, although ANOVA *p*-values were similar under all criteria. Although the notable absence of biomass samples between ~45 and ~140 g DW m^{-2} is likely to have influenced the relationship between image saturation and biomass, figure 3.24 suggests that *Enteromorpha sp.* dry weight variations can be explained by image colour saturation.

3.4.2.2 Session 2

	Correlation coefficient (R^2)		
	Red	Green	Blue
Red		0.9714	0.9582
Green	0.9714		0.9472
Blue	0.9582	0.9472	

Table 3.3 Band intercorrelation of June 2007 mosaic

Table 3.3 shows the level of band intercorrelation between the red, green and blue components of the June 2007 mosaic (see figure 3.5). The mean correlation is marginally greater than that of the session 1 mosaic, presumably as a result of the larger expanse of uniform-coloured substrate visible.

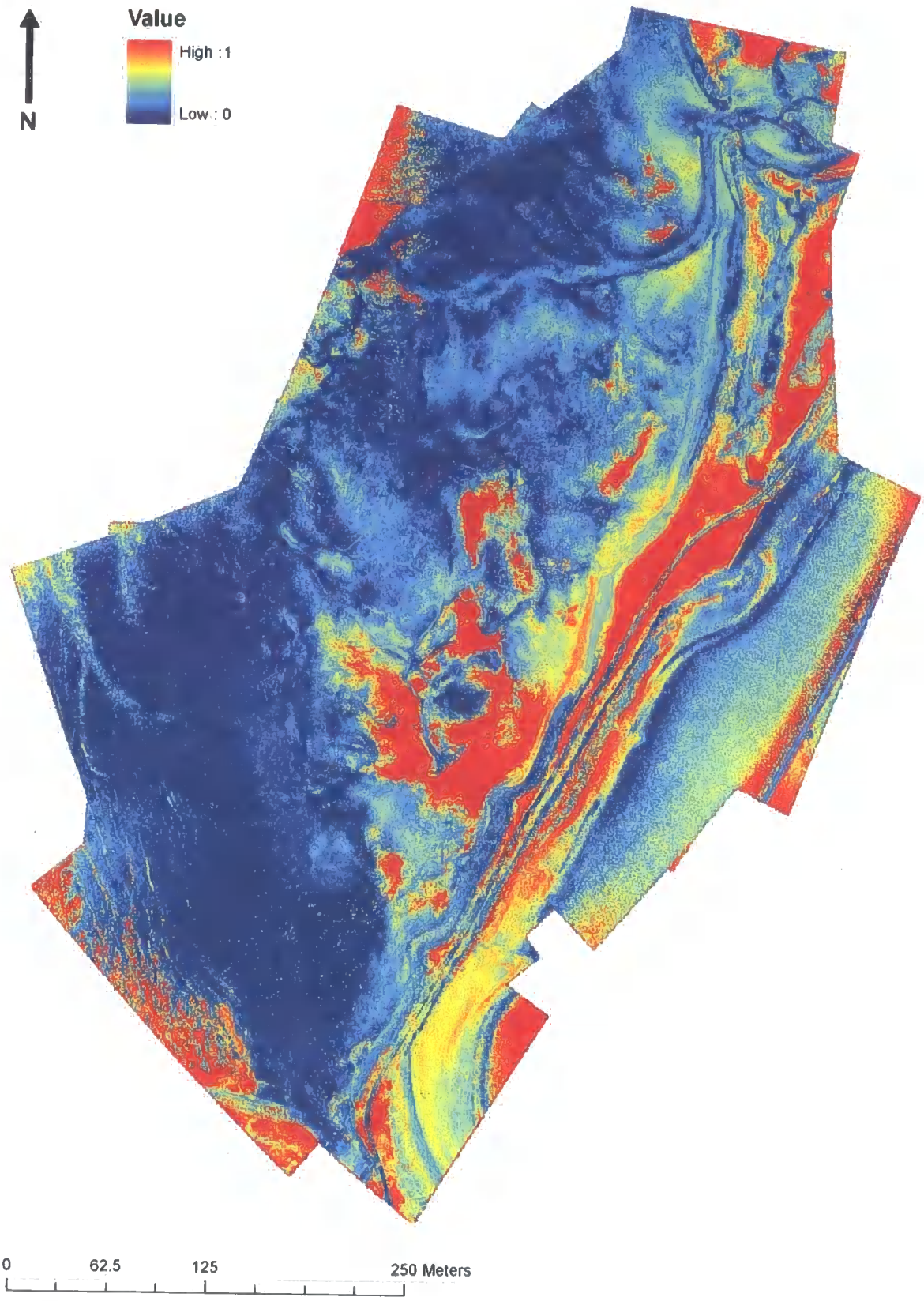

Figure 3.25 Image colour saturation computed on June 2007 true-colour mosaic

Figure 3.25 shows a colour saturation transformation applied to the June 2007 mosaic. Both *Salicornia sp.* and *Enteromorpha sp.* cover are highlighted by red and orange shading. The largest area of dense macroalgal matting and *Salicornia sp.* growth is visible as an extensive region of high saturation values (red shading) towards the centre of the image (near the drainage structure). The two further areas of dense *Enteromorpha sp.* cover towards the extreme north and south-east edges of the mosaic are also highlighted by high saturation values. The 'salt and pepper' texturing of moderate macroalgal coverage described in section 3.1.2 is also visible towards the south of the image as a number of small dotted moderate saturation values (yellow shading).

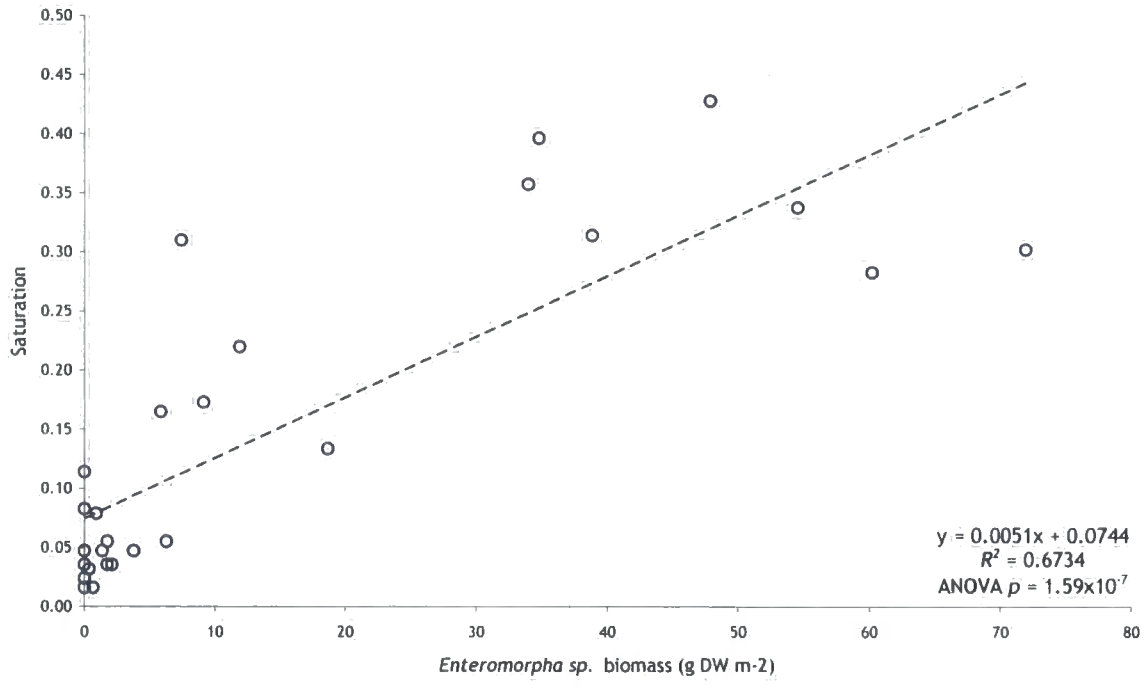

Figure 3.26 *Enteromorpha sp.* biomass against image colour saturation computed on the June 2007 mosaic.

Figure 3.26 again shows a relatively strong correlation (R^2 = 0.6734) between colour saturation and biomass. ANOVA $p < 0.01$, indicating the correlation is significant at the 99% confidence level. Lower biomass samples yielded a smaller range of saturation values than those in the November 2006 dataset. However, larger samples show a greater deviation from the regression line, necessitating the use of filters to remove potentially anomalous values caused by JPEG compression artefacts. Figure 3.27

shows the relationship between saturation and biomass after passing the dataset through *averaging*, *zonal maximum* and *zonal minimum* filters. The only increase in correlation was again produced by the *averaging filter*; Although the larger 16 x 16 pixel filter (representing ~100 cm^2 GSD @ ~200 m altitude) worked best for the Session 1 saturation mosaic, the smaller 3 x 3 pixel filter (representing ~30 cm^2 GSD @ ~230 m altitude) gave the optimum correlation for the June 2007 mosaic (R^2 = 0.6775). All other filters produced marginally lower R^2 values than the raw saturation mosaic, apart from the 10 x 10 pixel *zonal minimum filter*, which led to a significantly reduced linear correlation. Like the raw saturation mosaic, the filtered data shows tight clustering of lower biomass values. The magnitude of deviation from the regression line increases with respect to biomass; samples greater than 10 g DW m^{-2} yield a much greater range of saturation values (especially using the *zonal minimum filter*) than smaller quantities of *Enteromorpha sp.* Although the ANOVA *p*-value of 1.36×10^{-7} for the 3 x 3 *averaging filter* suggests that the significance of the relationship is similar to that of the unfiltered dataset, the 10 x 10 *zonal minimum filter* yielded a greatly reduced *p*-value of 0.00026. While this value is still lower than 0.01, suggesting the R^2 is still significant at the 99% level, it shows that image filtering may not necessarily improve correlation.

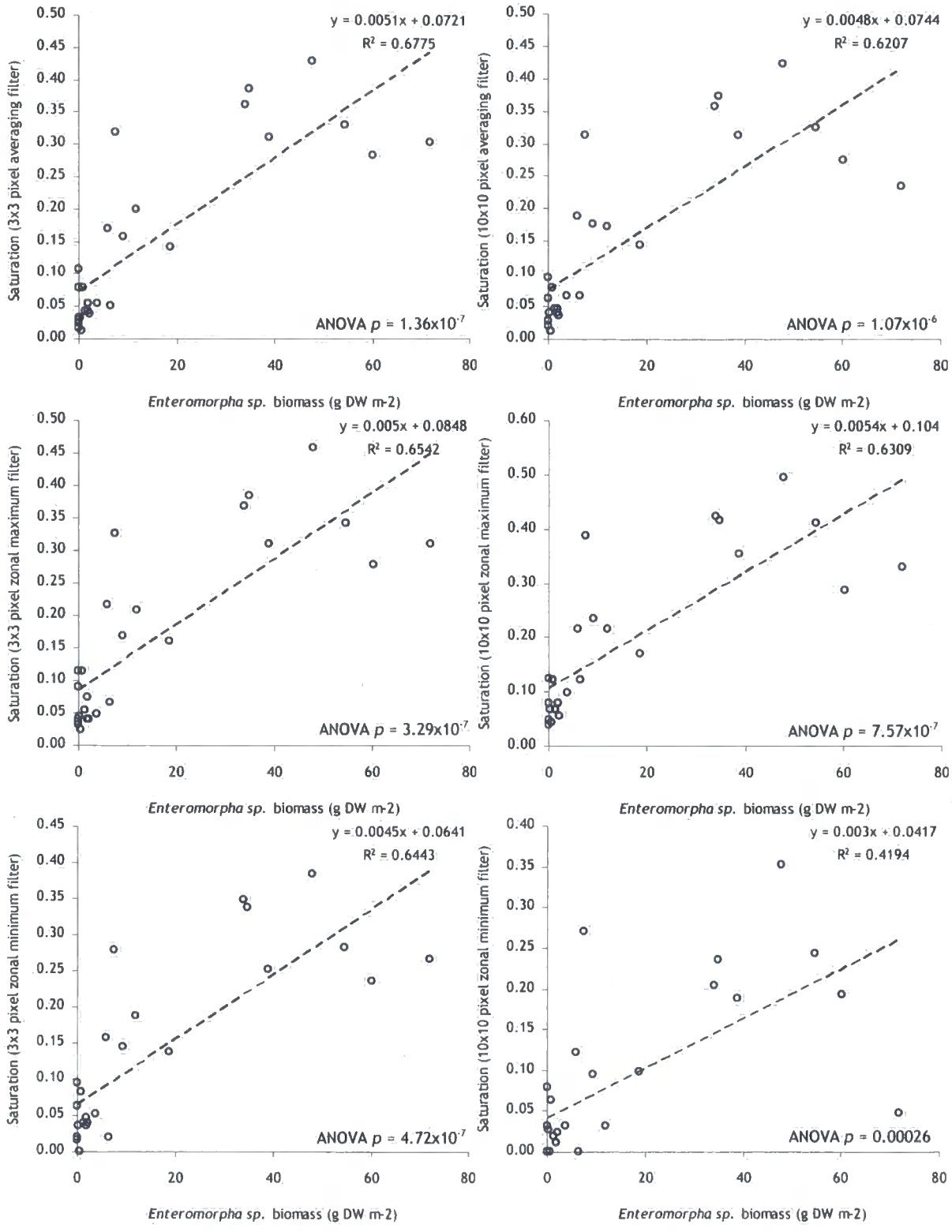

Figure 3.27 *Enteromorpha sp.* biomass against colour saturation under various filter criteria (June 2007)

3.4.3 Image Texture

3.4.3.1 Session 1

Entropy and inertia texture measures were computed for the raw image constituents of the November 2006 true-colour mosaic. The size of the 'moving window' and transposition 'step' (see section 2.6.3) were iterated in order to explore the response of texture to variations in these parameters, and an individual image texture 'map' was calculated for each of these window size/step size permutations. Because of the large number of available window/step size combinations, a total of 216 texture maps were returned for each of the texture measures (entropy and inertia).

Each texture map produced was co-registered to the true-colour mosaic (see section 2.5.2.2), and texture values extracted from *Enteromorpha sp.* sample locations. This process was performed for each permutation of the window/step size parameters, thus producing an individual set of texture values for each parameter combination. The coefficient of determination between macroalgal biomass and the texture value produced by each permutation was established, giving a total of 216 R^2 values for each texture measure (entropy and inertia).

Because of the difficulty in graphically representing the interaction between three independent variables (window size, step size and biomass - texture correlation), it is necessary to look towards alternative methods of data presentation. In order to visualise how window size and step size interact with the biomass - texture relationship, the R^2 values produced by the various permutations can be represented using a *regression surface*, a matrix whereby each column represents an individual transposition 'step' size, each row represents a different 'moving window' size, and the colour of each cell within the *regression surface* represents the coefficient of determination between *Enteromorpha sp.* biomass and the texture value produced by the window/step size permutation for that cell.

Hence, the colour of each cell within the matrix represents the biomass - texture correlation value produced by the cell's specific window/step size permutation. This allows for visual exploration of the influence of window and step size upon the biomass - texture relationship, and the identification of the window and step size combination that yields the strongest biomass - texture correlation.

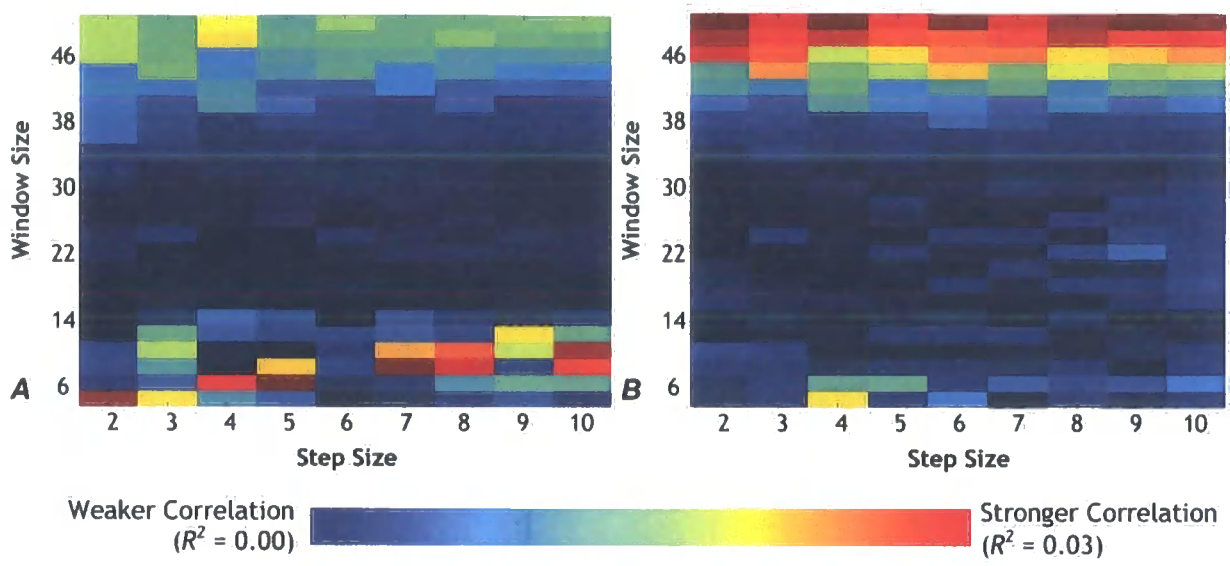

Figure 3.28 Texture regression surfaces for **(A)** entropy and **(B)** inertia measures computed on November 2006 raw imagery

Figure 3.28 shows the regression surface plots for entropy and inertia. Entropy values exhibit a generally weak correlation with biomass, although the R^2 shows a slight increase with respect to window size. The strongest correlation with biomass was produced by a window size of 6 pixels and a step of 7 pixels, giving a value of $R^2 = 0.0288$. Textural inertia shows a similar increase in correlation with respect to window size, although the increase is more uniform than entropy, with fewer of the anomalous correlation 'spikes' exhibited by lower Entropy window sizes. The strongest inertia - biomass correlation was produced by a window size of 50 pixels and a step of 10 pixels, giving a value of $R^2 = 0.0254$.

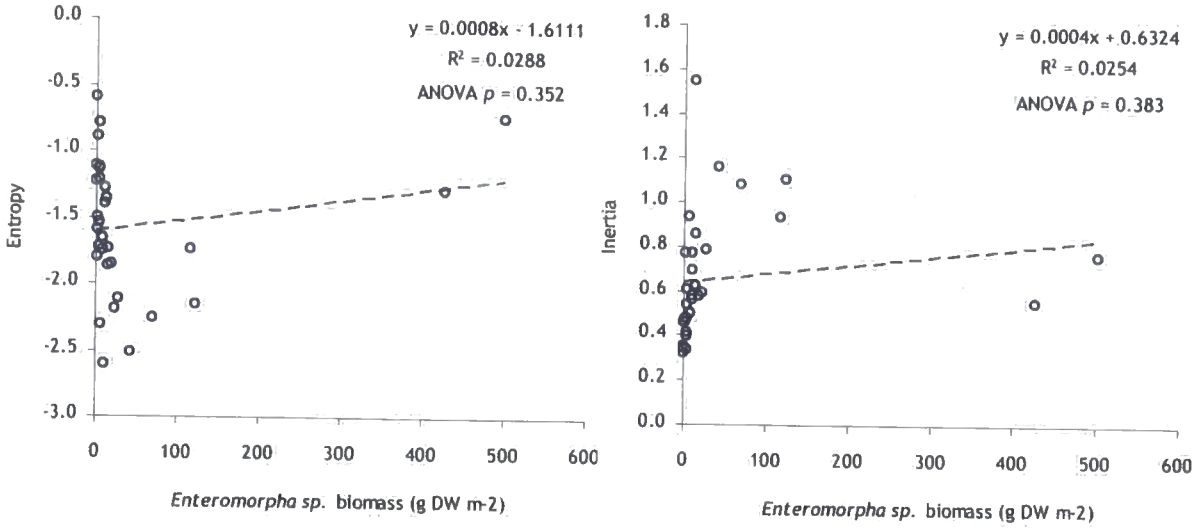

Figure 3.29 *Enteromorpha sp.* biomass against entropy and inertia measures computed on November 2006 raw imagery.

Figure 3.29 shows *Enteromorpha sp.* biomass against entropy and inertia for the optimum window/step combinations. The large degree of point dispersal and the extremely low coefficients of determination exhibited by both texture measures suggests there is no relationship between *Enteromorpha sp.* and textural variation exhibited by the November 2006 true-colour mosaic. ANOVA *p*-values of 0.352 and 0.383 for entropy and inertia respectively also show that the correlations are greater than the $p = 0.01$ threshold, and are *not* significant at the 99% level.

Figure 3.30 illustrates the entropy and inertia algorithms applied to the November 2006 true-colour mosaic. However, it is necessary to note that this is solely to illustrate the effect of texture on imagery; it is not feasible to process mosaicked imagery, because of warping introduced during the mosaicking process.

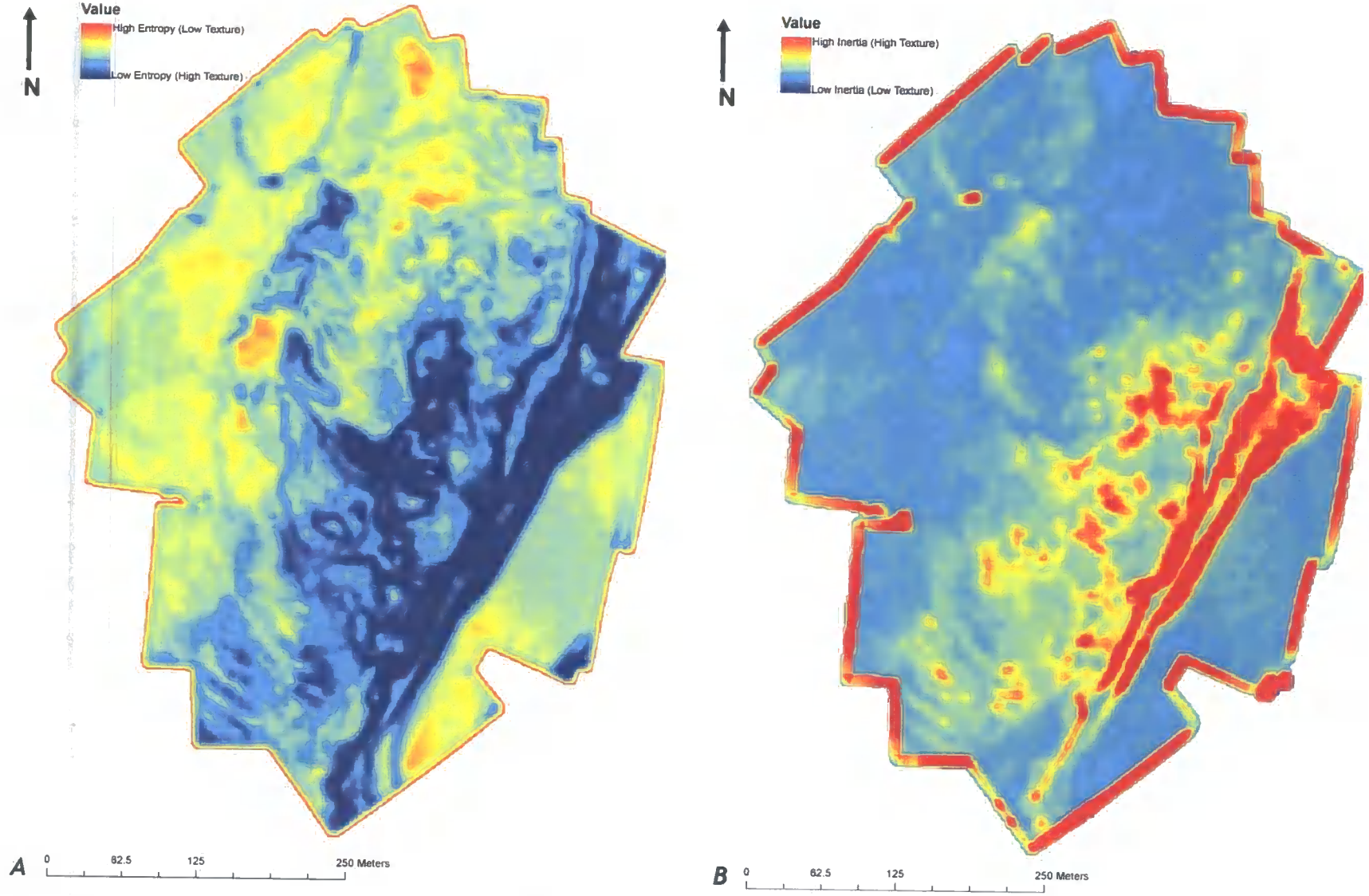

Figure 3.30 Entropy (**A**) and inertia (**B**) computed on the November 2006 mosaic. For illustrative purposes only.

3.4.3.2 Session 2

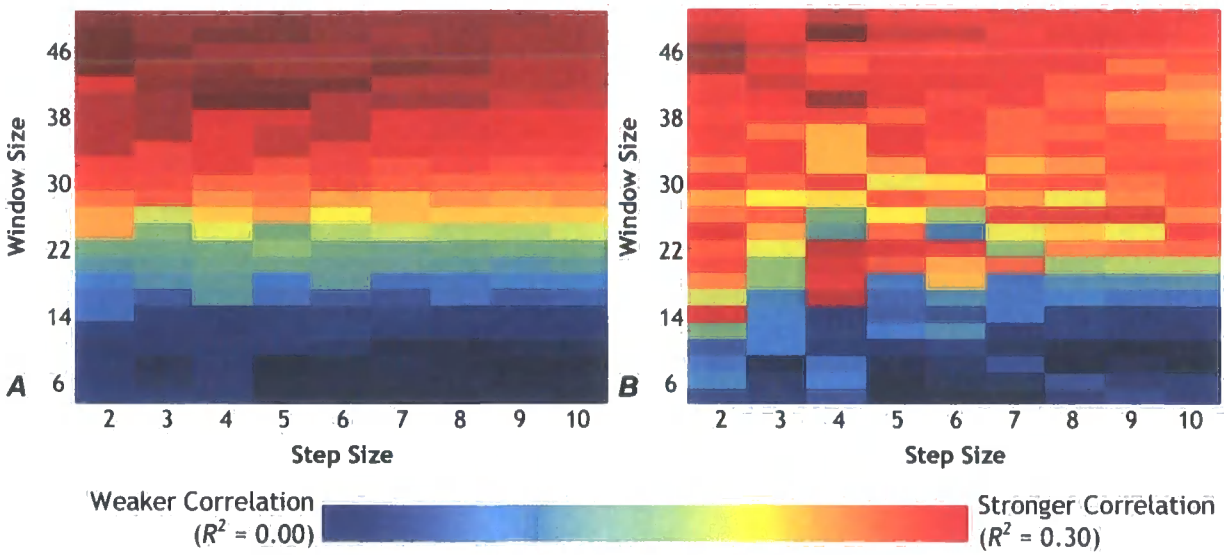

Figure 3.31 Texture regression surfaces for **(A)** entropy and **(B)** inertia measures computed on June 2007 raw imagery

Figure 3.31 shows regression surfaces for entropy and inertia computed on the June 2007 mosaic. The colour gradient again suggests entropy increasingly correlates with *Enteromorpha sp.* biomass respective of window size, although the correlation 'spikes' present in figure 3.28(A) are not visible. The strongest correlation with biomass was produced by a window size of 44 pixels and a step of 10 pixels, giving a value of R^2 = 0.2800. Inertia shows a similar trend to entropy, although the increase in correlation is less uniform. The strongest correlation with biomass was produced by a window size of 48 pixels and a step of 8 pixels, giving a value of R^2 = 0.2317. Although step size does not appear to play a significant role in determining the strength of the correlation, the R^2 value increases by an average of 0.0017 per step for entropy and 0.0045 per step for inertia respectively.

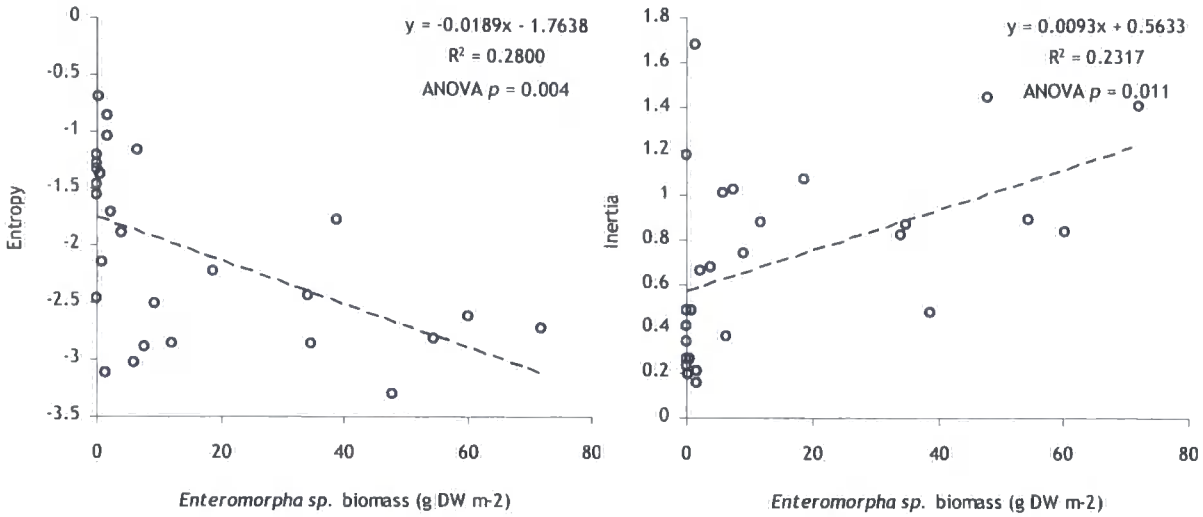

Figure 3.32 *Enteromorpha sp.* biomass against entropy and inertia measures computed on June 2007 raw imagery.

Figure 3.32 shows how image texture (entropy and inertia) vary in response to macroalgal biomass under the optimum window/step size combination. Entropy exhibits a weak negative correlation with biomass (R^2 = 0.2800), whereas inertia is positively correlated to biomass (R^2 = 0.2317), albeit weakly. Both texture measures show a high degree of scattering, similar to that produced by the November 2006 dataset. However, the more uniform distribution of biomass samples may have improved the degree of correlation. Although entropy yields a *p*-value of 0.004, suggesting the relationship is significant at the 99% confidence level, this value is low in comparison to those yielded by spectral/saturation - biomass plots. Similarly, inertia yields a *p*-value of 0.011, indicating that the R^2 value is *not* significant.

Figure 3.33 shows the entropy and inertia algorithms applied to the June 2007 colour mosaic. Again, it is necessary to note that this is for illustration purposes only, to show textural variations across the study area; distortions introduced into the imagery by successive mosaicking and georeferencing procedures render it unsuitable for the extraction of quantitative texture values.

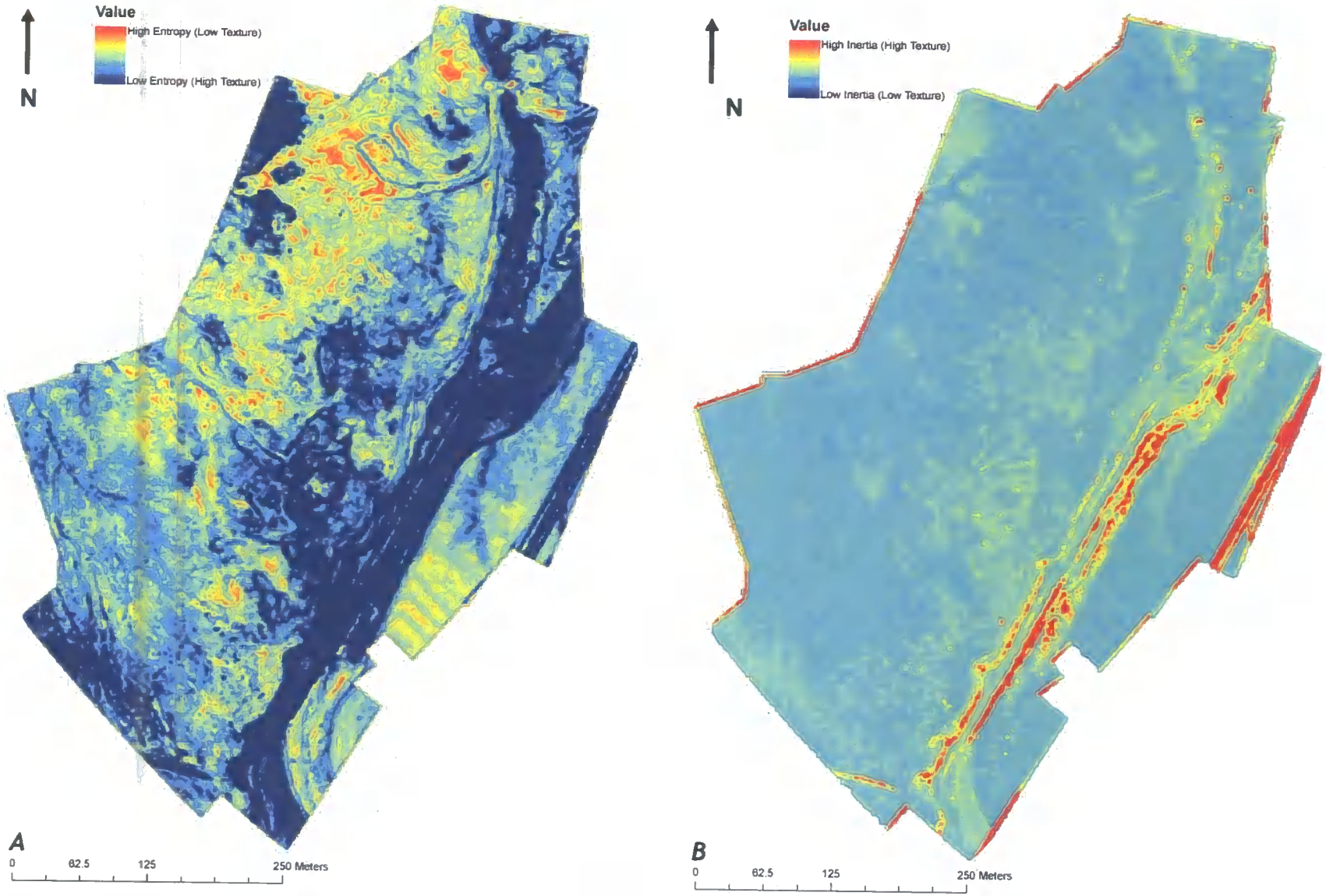

Figure 3.33 Entropy **(A)** and inertia **(B)** computed on the June 2007 mosaic. For illustrative purposes only.

3.5 Predictive biomass models

3.5.1 Session 1

The image processing techniques that yielded the optimum coefficient of correlation were used to model macroalgal biomass from the November 2006 mosaic. The regression equations determined in section 3.4 were used to predict macroalgal biomass at known sample points. Plots of observed vs. predicted *Enteromorpha sp.* biomass were then established using NGRDI, NDVI and image saturation as the predictor variables.

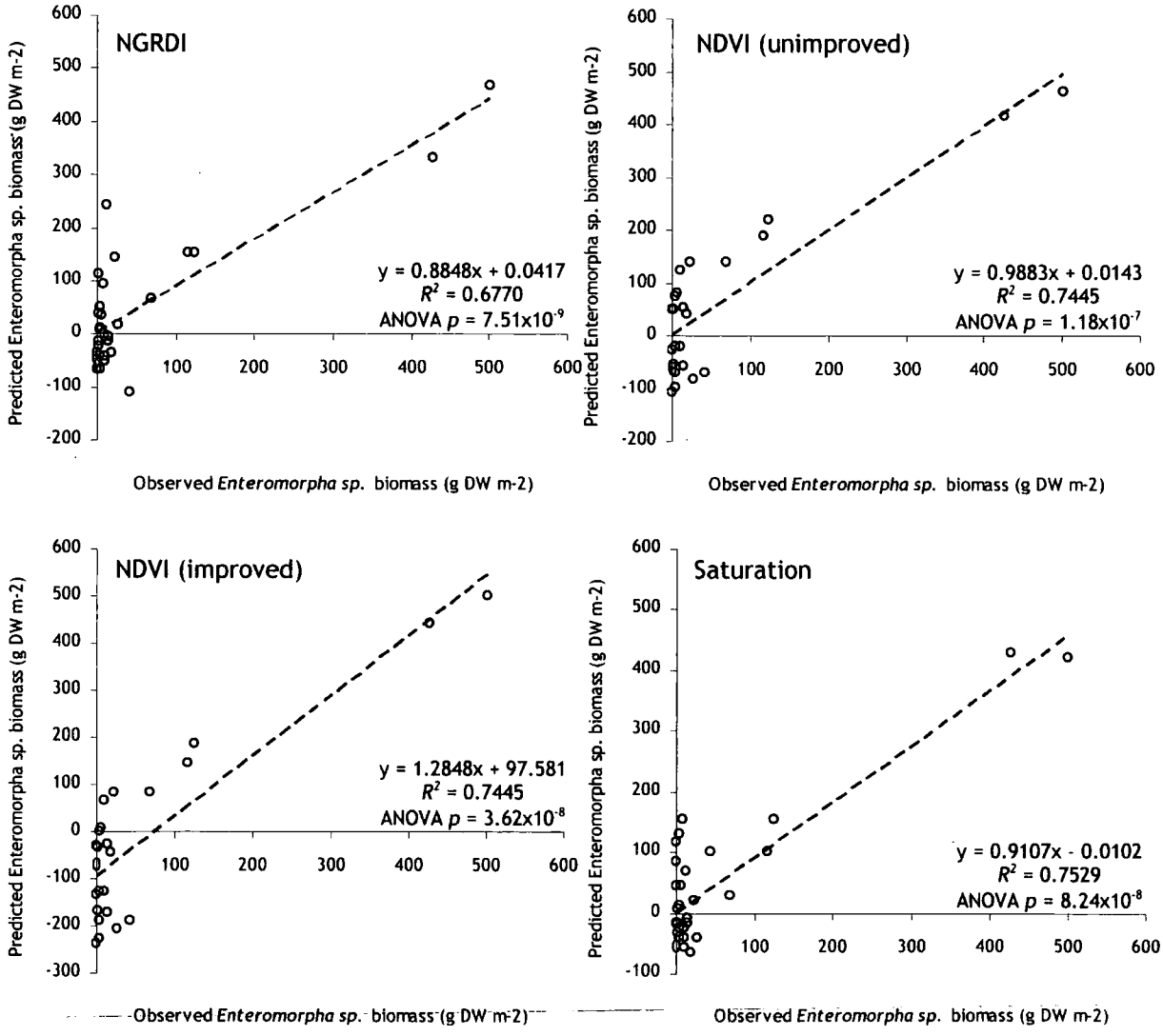

Figure 3.34 Observed *Enteromorpha sp.* biomass vs. biomass predicted from regression equations established from November 2006 imagery. See figure 3.18 for explanation of improved NDVI.

Of the four observed vs. predicted plots in figure 3.34, NDVI (unimproved) and image saturation appear to predict biomass with an *x*:*y* ratio approaching 1. The regression line gradients exhibited by NGRDI and NDVI (improved) are marginally less favourable. The proximity by which the regression line passes to the origin in the NGRDI, NDVI (unimproved) and Saturation plots also demonstrates the ability of these models to predict biomass. The NDVI (improved) plot shows less promising characteristics; the regression line intercept suggests that this model underestimates macroalgal biomass by a margin of ~97 g DW m^{-2}. Similarly, both the unimproved and improved NDVI plots appear to underestimate low to moderate amounts of *Enteromorpha sp.* biomass, as demonstrated by the position of regression line *below* samples with an observed biomass of ~20 - 100 g DW m^{-2}.

The predictive models established above were applied to the November 2006 imagery to determine a total calculation for macroalgal biomass within the study area. The regression equations determined from in section 3.4 were applied to imagery, to give 'biomass maps' for the study area. These images were then masked using the *Enteromorpha sp.* layers created through supervised classification (see section 3.2.1), to show coverage variations in macroalgal biomass across the site. Table 3.4 shows the total biomass computed for the study area under the various predictive models.

Model	Total *Entermorpha sp.* biomass (kg)	Total *Entermorpha sp.* biomass (absolute values only; kg)
NGRDI	882.924	886.100
NDVI (unimproved)	759.772	967.754
NDVI (improved)	371.488	796.295
Saturation	873.927	928.234
Average	722.028	894.596

Table 3.4 Total *Enteromorpha sp.* biomass calculated from November 2006 imagery

The total macroalgal biomass as derived using the NGRDI, unimproved NDVI and Saturation models shows good agreement, suggesting a figure of ~750 - 880 kg for the total *Enteromorpha sp.* biomass within the study area. The NDVI (improved) model shows a significantly reduced estimate. It is likely that this is a function of the intercept of the regression line illustrated in figure 3.34, leading to a gross underestimate in algal biomass. Negative biomass predictions were yielded by all models, a result of the inability of all models to accurately predict small biomass values. Negative

NGRDI/NDVI values not masked out by the supervised classification also yielded negative biomass predictions. The third column of table 3.5 shows the total biomass prediction following the removal of all negative values. This shows a closer agreement between the individual models, particularly the improved NDVI, which yielded a significantly increased biomass prediction.

Figures 3.35, 3.36 and 3.37 show the variation in *Enteromorpha sp.* cover across the study area computed from the NGRDI, NDVI (unimproved and improved) and Saturation models. Although table 3.5 indicates that the models produced *total* biomass estimates that were in good agreement, figures 3.35, 3.36 and 3.37 suggest a significant variation in the maximum and minimum biomass values predicted by the individual models. The NGRDI model yielded the highest biomass variation, a range of ~5000 g DW m^{-2}. NDVI and saturation yielded variations of ~1700 - 1900 g DW m^{-2}. Saturation exhibited the smallest range of negative biomass values. Figure 3.36 indicates that the NDVI model is weighted towards higher biomass values; the area of dense biomass towards the south of the study area is more clearly defined that in figures 3.35 and 3.37. However, it is pertinent to note that this may be due to the absence of a substantial area of low biomass to the north-west of the site that were obscured during NIR photography.

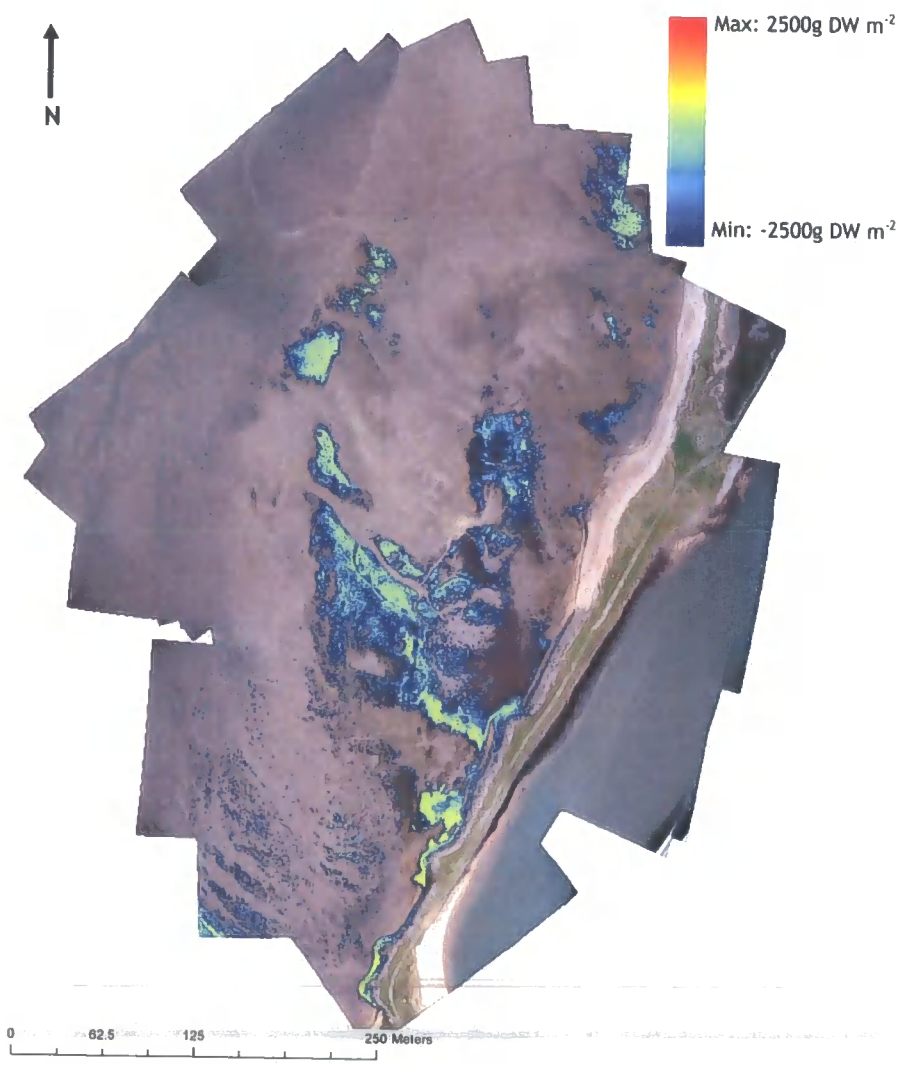

Figure 3.35 *Enteromorpha sp.* biomass variation across study area. Computed from NGRDI model.

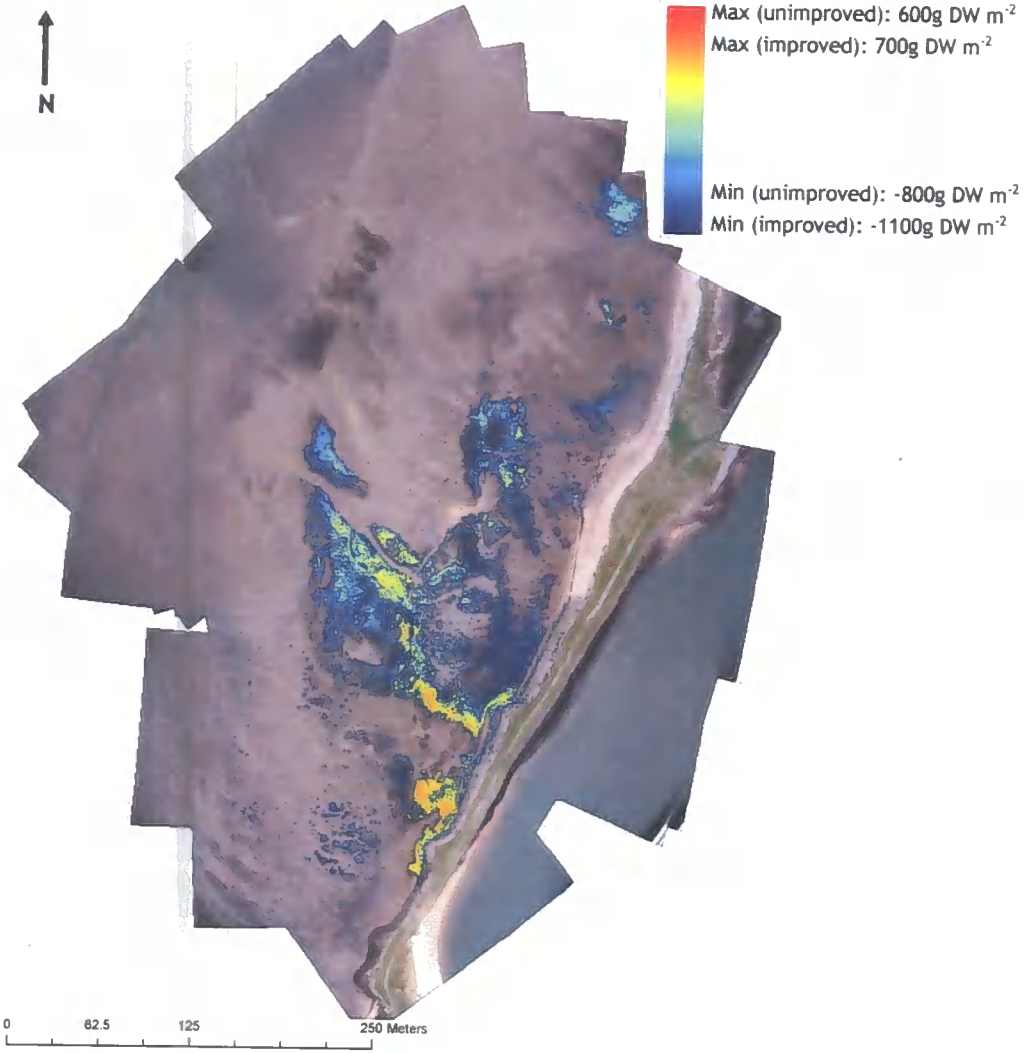

Figure 3.36 *Enteromorpha sp.* biomass variation across study area. Computed from NDVI models. Note different max/min values for unimproved and improved NDVI models

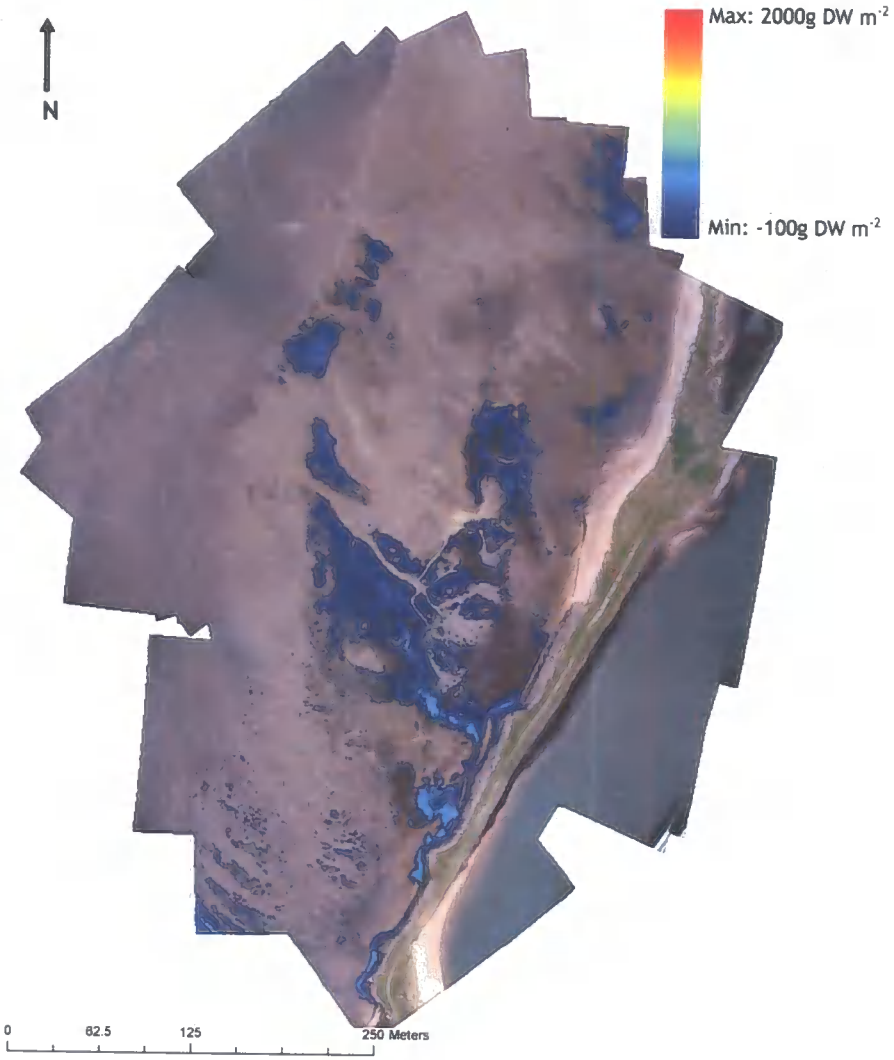

Figure 3.37 *Enteromorpha sp.* biomass variation across study area. Computed from Saturation model.

3.5.2 Session 2

Figure 3.38 shows observed vs. predicted *Enteromorpha sp.* biomass computed from the June 2007 mosaic. Near-infrared imagery was not available, so biomass estimates were only calculated using NGRDI and Saturation as the predictor variables.

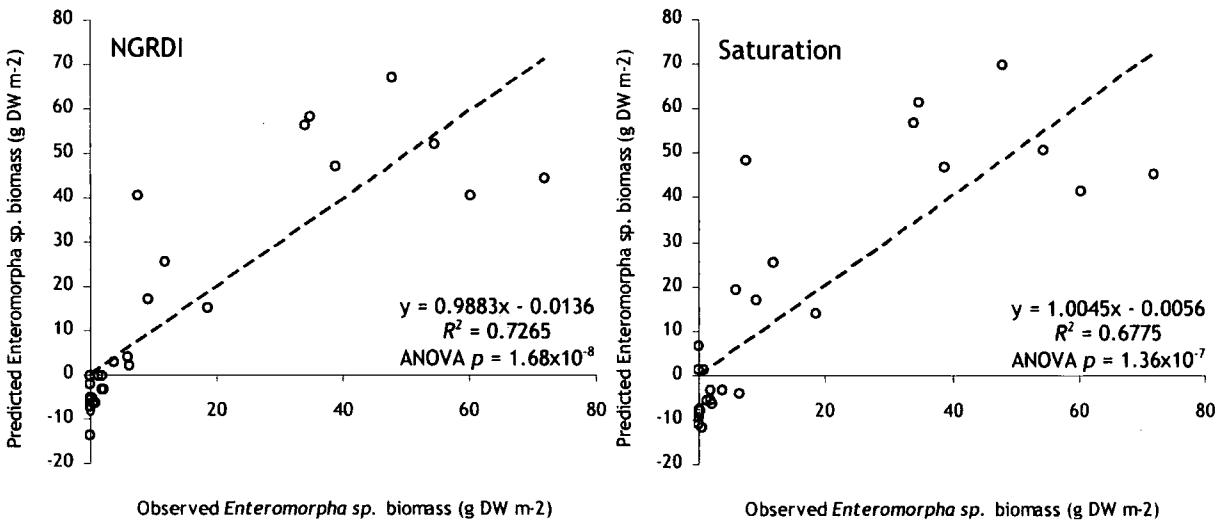

Figure 3.38 Observed *Enteromorpha sp.* biomass vs. biomass predicted from regression equations established from June 2007 imagery.

Both NGRDI and Saturation show an *x*:*y* ratio approaching 1, demonstrating a close association between observed and predicted biomass. The proximity of the regression line intercept to the origin is also a favourable indication that the models do not significantly over or under-predict *Enteromorpha sp.* biomass. However, it is necessary to note that there is significant deviation of moderate and high biomass samples from the regression for both NGRDI and Saturation. Similarly, the position of the Saturation regression line *above* a cluster of low biomass samples may indicate a difficulty in predicting low biomass.

Model	Total *Enteromorpha sp.* biomass (kg)	Total *Enteromorpha sp.* biomass (absolute values only; kg)
NGRDI	241.638	280.018
Saturation	165.721	249.118
Average	203.680	264.568

Table 3.5 Total *Enteromorpha sp.* biomass calculated from June 2007 imagery

Table 3.5 shows total *Enteromorpha sp.* biomass predicted from applying the regression equations in section 3.4 to the June 2007 true-colour imagery. There is a significant discrepancy (~76 kg) between total biomass as predicted by the NGRDI and the Saturation models. Although figure 3.38 indicates that a good degree of correlation between the observed and predicted variables for the saturation model, a cluster of low-biomass samples appear to have produced negative biomass estimates. It is likely that the significantly lower figure for overall biomass in table 3.6 is a function of this. Although negative biomass values were also yielded by the NGRDI model, figure 3.38 shows fewer negative variables. As noted for the November 2006 imagery, negative results may also represent NGRDI values that were not correctly masked out by the supervised classification. The removal of all negative biomass values from the dataset ceded a closer agreement (~31 kg) between the NGRDI and Saturation models.

Total biomass yield is significantly smaller than that calculated from the November 2006 imagery. This is to be expected, as the June 2007 imagery was taken towards the beginning of the growth season, before seasonal *Enteromorpha sp.* cover was fully established. Figures 3.39 and 3.40 show how biomass varies across the study area. Although total macroalgal biomass is lower than that computed by the previous imagery, *Enteromorpha sp.* cover seems to be significantly increased. This may simply be a result of a larger expanse of sparse macroalgal cover; this seems plausible, because new (sparse) macroalgal growth is prevalent at the start of the growth season, instead of the denser algal mats experienced later in the year. It is also possible that improved conditions allowed for better discrimination of sparse algal cover from aerial images, although this is difficult to quantify. However, it is more probable that the extensive cover is a function of poor supervised classification, leading to an insufficient mask to extract algae.

Biomass range shows good agreement between the two figures, although NGRDI exhibits a greater tendency towards negative biomass values. However, as noted in section 3.5.1, NGRDI also shows a larger amount of moderate and high biomass cover than the Saturation model, highlighting the tendency of NGRDI to predict higher values.

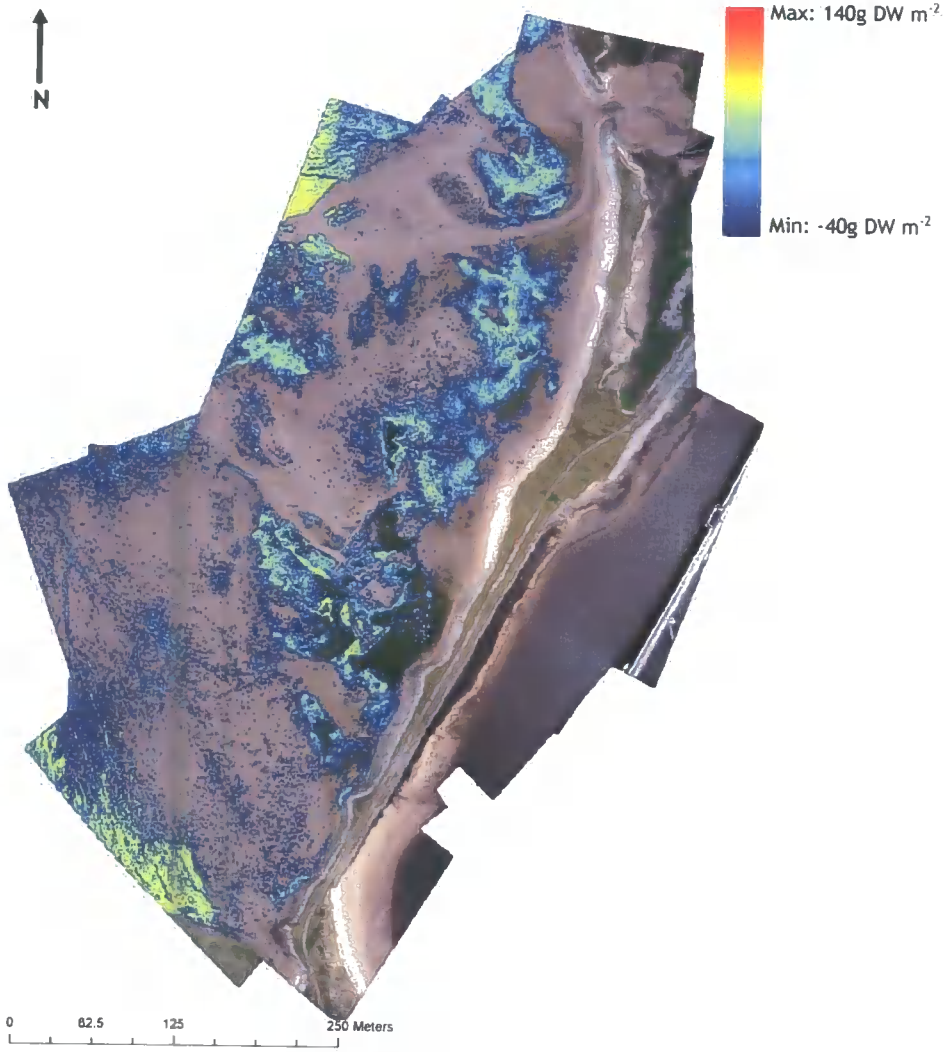

Figure 3.39 *Enteromorpha sp.* biomass variation across study area. Computed from NGRDI model.

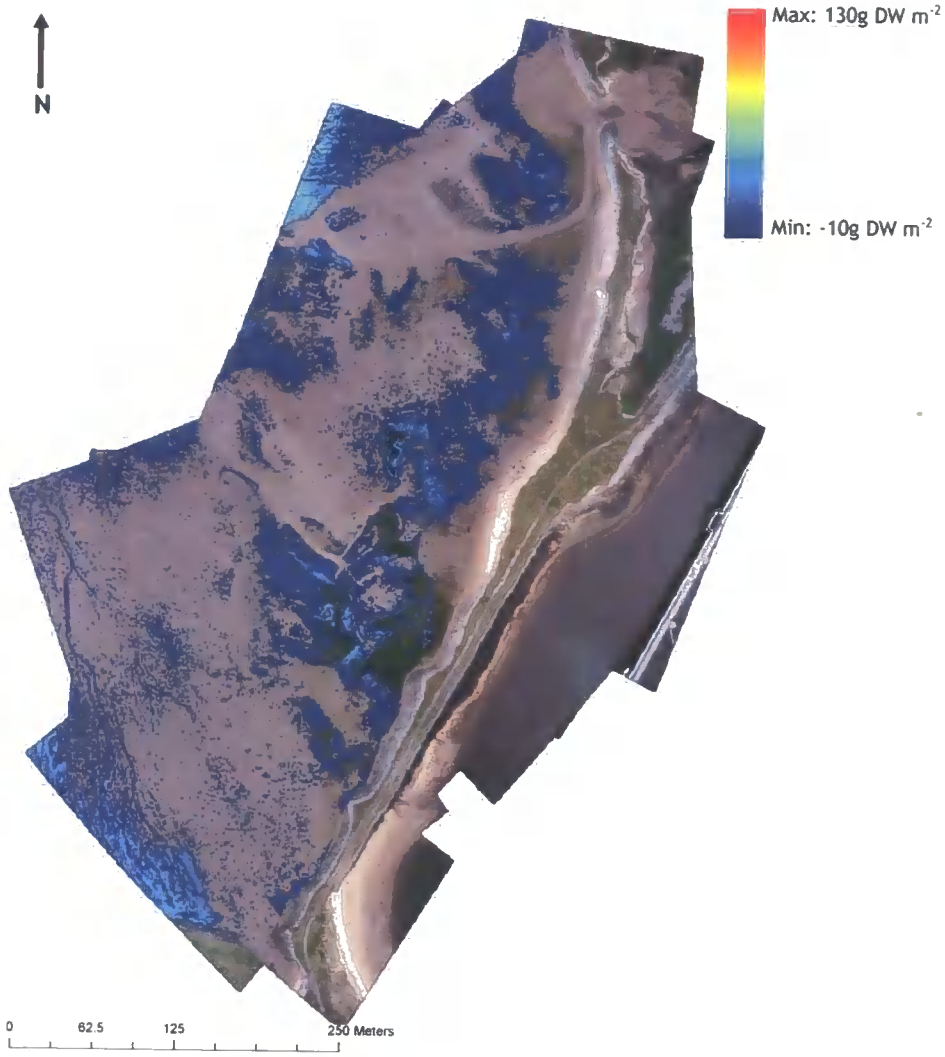

Figure 3.40 *Enteromorpha sp.* biomass variation across study area. Computed from Saturation model.

Chapter 4. Discussion

4.1 Relationship between image metrics and ground truth data

4.1.1 Spectral biomass estimation

The weak negative correlation between spectral response and *Enteromorpha sp.* biomass exhibited by the November 2006 dataset suggests that the RGB spectral channels alone do not independently explain biomass variability, and are insufficient for the quantitative estimation of macroalgal biomass from the imagery. However, the negative correlation between biomass and spectral response in the green wavelength agrees with standard convention (eg. Budd & Milton, 1982).

The June 2007 dataset showed analogous trends, with the red, green and blue channels all displaying a negative correlation with macroalgal biomass. The increase in ANOVA *p*-significance of the coefficient of determination over the November 2006 imagery is likely a product of the more uniform weight distribution of *Enteromorpha sp.* samples. Although the 'dense' biomass samples are significantly smaller than those of the November 2006 dataset (~70 g DW m^{-2}, rather than ~500 g DW m^{-2}), the spectral values yielded by the largest June 2007 samples (~80 DN) are similar to those shown by the largest November 2006 samples (~75 DN). This is a result of one of two scenarios: It is possible that ~70g DW m^{-2} represents a 'saturation' value, above which biomass cannot be estimated spectrally. In this case, it would not advisable to use linear regression to model algal biomass; this may account for the low R^2 exhibited by the November dataset. However, it is much more likely that the difference in spectral response of algal cover is a direct function of seasonal conditions; cloud cover was significantly lower during the June 2007 image acquisition session, and the reflectance of macroalgal cover is likely to have changed accordingly. The low declination of the sun during the November 2006 imagery may also have limited spectral reflectance, especially in those areas of dense macroalgal canopy, where the multiple layers of algal matting may have caused shading. Because imagery was acquired at significantly different stages in the *Enteromorpha sp.* development cycle, algal chlorophyll content is also likely to have changed,

representing seasonal variations in photoacclimation (eg. Falkowski & LaRoche, 1991). This, in turn, will have influenced the seasonal differences in algal spectral response. These sampling 'snapshots' within which imagery was acquired also only represent a small portion of the macroalgal growth cycle, and as such, it is necessary to highlight that algal reflectivity may differ significantly within other time periods. Martins & Marques (2002) note that *Enteromorpha sp.* growth is highest within June, whereas by November macroalgal coverage is relatively constant. Because of this, *Enteromorpha sp.* cover is likely to increase dramatically within June and July, and spectral reflectivity is likely to vary accordingly, whereas by November, reflectivity is likely to stay fairly consistent. Hence, the rate of change of the reflectivity-biomass relationship is likely alter significantly throughout the annual growth cycle as a result of chlorophyll content, algal mat density, canopy shading and surface roughness, and future research should take macroalgal growth models into account.

Of particular interest is the dense clustering of low-biomass samples noted for both the November 2006 and June 2007 images. Figures 3.13 and 3.19 show similar occurrences for all spectral channels, with a 'blotch' of low reflectivity / low biomass values close to the origin. Although this may represent a failure of the sampling regime to extract a consistent range of different sample sizes, resulting in excessive samples of low-biomass *Enteromorpha sp.* cover, it is more likely to represent an inability of the sensor to discriminate between different levels of 'sparse' macroalgal cover. Alternatively, this may signify that the sensor is unable to even detect small amounts of biomass against certain backgrounds. This may account for the large variation in algal *cover* shown between the November 2006 and June 2007 datasets. Although quantitative biomass estimates from June 2007 imagery indicated a lower amount of biomass (see section 3.5.2) than the November 2006 dataset, there appeared to be a considerably increased amount of *sparse* algal cover visible in the imagery. This may be a function of substrate colour; whereas the June 2007 imagery was taken at low tidal conditions, November 2006 imagery was taken under significantly raised tidal conditions, which may have caused substrate darkening. It is feasible that this rendered the sensor unable to discriminate algae from substrate, leading to an under-representation of sparse algal cover. The might therefore indicate the presence of a threshold below which it is not possible to correlate macroalgal biomass to the spectral properties of an image.

Point variance within the standard spectral reflectivity plots is also of concern. November 2006 imagery shows maximum deviation from the regression line with low-biomass samples. However,

spectral values yielded by the June 2007 mosaic indicate that high-biomass samples produced the greatest deviation from the regression line. Although the variability of low-biomass reflectivity values is likely to be a result of the sensor limitations discussed above, this does not fully explain point variance for higher biomass samples, which should to be easier to discriminate spectrally. Although it is possible that the spectral disparity of high biomass samples is a function of natural variability, it is likely that much of the variation results from incorrect georeferencing. As noted previously, the extensive algal matting shown in the November 2006 imagery was not present, and *Enteromorpha sp.* samples were taken from significantly smaller growth 'patches'. Because of this, it is plausible that any georeferencing error within the mosaic led to the extraction of spectral values from an area outside of the growth 'patch', giving an incorrect reflectivity property for the associated *Enteromorpha sp.* sample (see section 4.2.1). It is also possible that the high-biomass spectral response variability exhibited by the June 2007 imagery is the manifestation of a 'threshold' above which biomass cannot be described spectrally. Figure 3.19 indicates that reflectivity DN values for biomass of ~35 g DW m^{-2} and above show a significantly decreased rate of change than values yielded by low algal biomass, and high biomass sample points show a relatively flat distribution gradient compared to lower biomass. However, a similar 'threshold' occurrence was not observed for the November 2006 imagery, which was comprised of appreciably higher biomass values, so the causes of this distribution are unclear.

Although a log transformation of the November 2006 and June 2007 reflectivity plots acted to reduce point variance and centre the cluster of low-biomass reflectivity values around the regression line, the relatively minor improvement in regression coefficient for both image sets suggests that this method is insufficient for accurately explaining biomass variability. Log_{10} transformation of the NIR reflectivity plot in figure 3.13 actually produced an inferior R^2 value than that of the standard plot, indicating that the NIR - biomass relationship is indeed linear. Although the true-colour bands deferred marginally improved coefficients of determination, the association between biomass and log_{10} of reflectivity still appears relatively weak, and is insufficient as evidence from which to draw a conclusion as to the nature (linear or non-linear) of the reflectivity - biomass relationship.

The *relative* Normalised Green-Red Difference Index (NGRDI) for both the November 2006 and June 2007 datasets suggests that *Enteromorpha sp.* biomass variations can be adequately explained.

Although the absence of *moderate* sized samples from the session 1 dataset (see figure 3.15) is likely to have influenced the coefficient of determination, the removal of the outlying *low* biomass samples leads to a marginal *increase* in the coefficient of determination (R^2 = ~0.1 increase) and AVOVA *p*-significance ($p = 5.96x10^{-11}$) suggesting that outliers do not greatly affect the correlation. The June 2007 imagery shows a further improvement in correlation. The highest spectral values yielded by the June 2007 imagery were also similar to those of the of the November 2006 dataset, even though algal samples were of a magnitude smaller. Once again, this is likely to be a function of seasonal conditions. However, it is also likely that the NGRDI computed on the November 2006 imagery was affected by substrate darkening, resulting from surface wetness. Hunt *et al.* (2005) note a similar effect whereby the difference between green and red DN was reduced when soil was water-saturated, biasing the NGRDI calculation. Because of this, it is not feasible to directly compare the NGRDI images from the two data acquisition sessions, although both datasets would suggest that NGRDI can be used as a method with which to infer *Enteromorpha sp.* biomass from aerial photographs.

The high degree to which biomass correlated with the November 2006 relative NDVI (unimproved) would suggest that this represents another method for the modelling of biomass data. However, the loss of a number of sample points due to inundation may have acted to artificially augment the R^2. The presence of a number of negative NDVI values is also problematic. As noted in section 3.4.1.1, this is theoretically impossible, as the presence of vegetation should logically yield a near-infrared spectral response higher than that that of the red band. Although it is likely that negative NDVI values are the result of inaccurate co-registration of the NIR mosaic to the true-colour mosaic, it is possible that some anomalous NDVI values are a function of the inability of the sensor to discriminate sparse biomass samples. As suggested above, substrate darkening is likely to have influenced both the red and NIR spectral values, because the NIR imagery was obtained when the tide was significantly advanced. This may have further decreased the ability of the sensor to discriminate low-biomass samples, leading to erroneous NIR and red DN values.

The removal of all zero and negative NDVI values from the dataset led to a greatly enhanced coefficient of determination (R^2 = 0.9485; see figure 3.18A), suggesting that biomass variability can be explained with a high degree of accuracy. However, the removal of further samples from an already sample-poor dataset raises questions as to the applicability of the improved NDVI to

predicted *Enteromorpha sp.* biomass. Similarly, the high regression line y-intercept indicates that all NDVI values lower than 0.0901 would predict negative biomass values, so care must be taken when using the improved NDVI model as a predictor variable. This may also highlight the unsuitability of using simple linear regression to model the NDVI-biomass relationship, in favour of non-linear models. The absence of a second NDVI dataset from the June 2007 imagery also limits the conclusions that can be drawn from the method.

4.1.2 Image saturation biomass estimation

The moderately strong correlation between November 2006 image saturation and biomass suggests that saturation can be used to predict macroalgal biomass. Correlation with biomass was further improved by all but one of the filters that were applied to remove anomalies. Saturation is a measure of colour 'purity' (Laliberte *et al.*, 2007) which approximates human visual perception (Laliberte *et al.*, 2007); this accounts for the high saturation value produced by areas of dense *Enteromorpha sp.*, which appear as vibrant 'pure' green shades in the mosaicked imagery for the November 2006 dataset. The saturation trend exhibited by the June 2007 dataset is similar, although image filtering does not offer such a large improvement in correlation. The range of values yielded by *Enteromorpha sp.* samples is greater than the November imagery. This indicates that algal samples exhibited a more uniform spectral response than those from earlier imagery, and is likely to be a result of the improved seasonal conditions, addressed in section 4.1.1. Substrate darkening in the November 2006 dataset may also have reduced contrast between the bands, yielding less 'pure' colours, accounting for lower saturation values than those of the June 2007 mosaic. This saturation variability has ramifications for algal monitoring, because small variations in *Enteromorpha sp.* cover, substrate wetness and time of year may yield large changes in colour saturation.

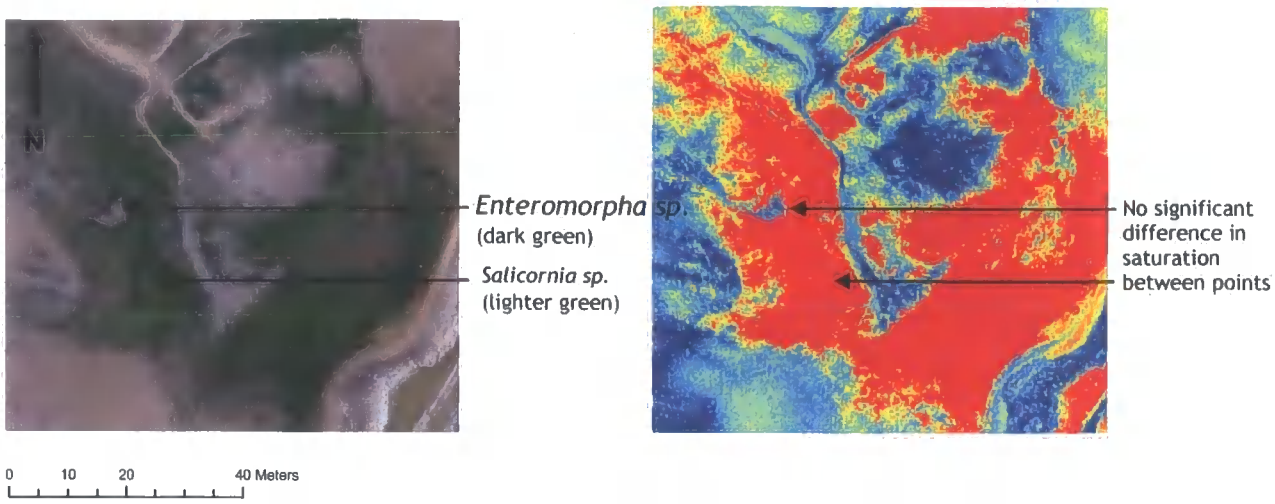

Figure 4.1 Example illustrating the inability of colour saturation to discriminate different vegetation types

Figure 4.1 also indicates that saturation cannot adequately discriminate between different species; although it is possible to discriminate *Salicornia sp.* and *Enteromorpha sp.* visually (*Salicornia sp.* appears a lighter green colour than *Enteromorpha sp.*), their 'purity' is similar, largely because the relative difference between the red, green and blue spectral response is the same. This also has implications for the use of colour saturation as an ecological monitoring tool, as it does not appear to adequately discriminate between different estuarine species.

The application of image filters to the dataset may also reduce the applicability of using colour saturation as an accurate method for monitoring algal biomass. Although filter kernel sizes were chosen to reflect the size of the sampling quadrat, the *averaging* and *zonal maximum / minimum* filters aggregate pixels within the imagery, reducing resolution. However, filtering does not produce an overly large improvement in the correlation between saturation and biomass, suggesting that such techniques may not be necessary.

4.1.3 Image texture biomass estimation

Both entropy and inertia texture measures derived from the November 2006 imagery show no significant correlation with macroalgal biomass. It is likely that this is the result of georeferencing error within the dataset. This will be addressed in section 4.2.1. The June 2007 mosaic shows a marginal increase in correlation for entropy and inertia measures over the November 2006 imagery;

as suggested in section 3.4.3.2, this is (in part) due to the more uniform sample weight distribution. However, it is also probable that the large georeferencing error induced in the November 2006 dataset was less problematic for the June 2007 dataset: In data acquisition session 1, algal samples were taken on a separate date to image acquisition, and had to then be co-registered to the mosaicked imagery. However, samples taken during data acquisition session 2 were extracted from the same location as ground control points. This meant that it was possible to visually demarcate the correct image pixel coordinates and extract texture values from these locations, without any co-registration or image transformation being necessary. This reduced error when compared with the November 2006 dataset, where it was necessary to apply an image translation to achieve desired pixel coordinates (see section 2.5.2).

It is also necessary to address the problems associated with multiple texture values for each sample point. Because raw imagery was used to compute texture values, it was necessary to process a number of overlapping images in order to achieve full coverage of the study site. Although unnecessary images were removed from the dataset (see section 2.6.3), the majority of sample points were covered by several images within the dataset (see figure 4.2).

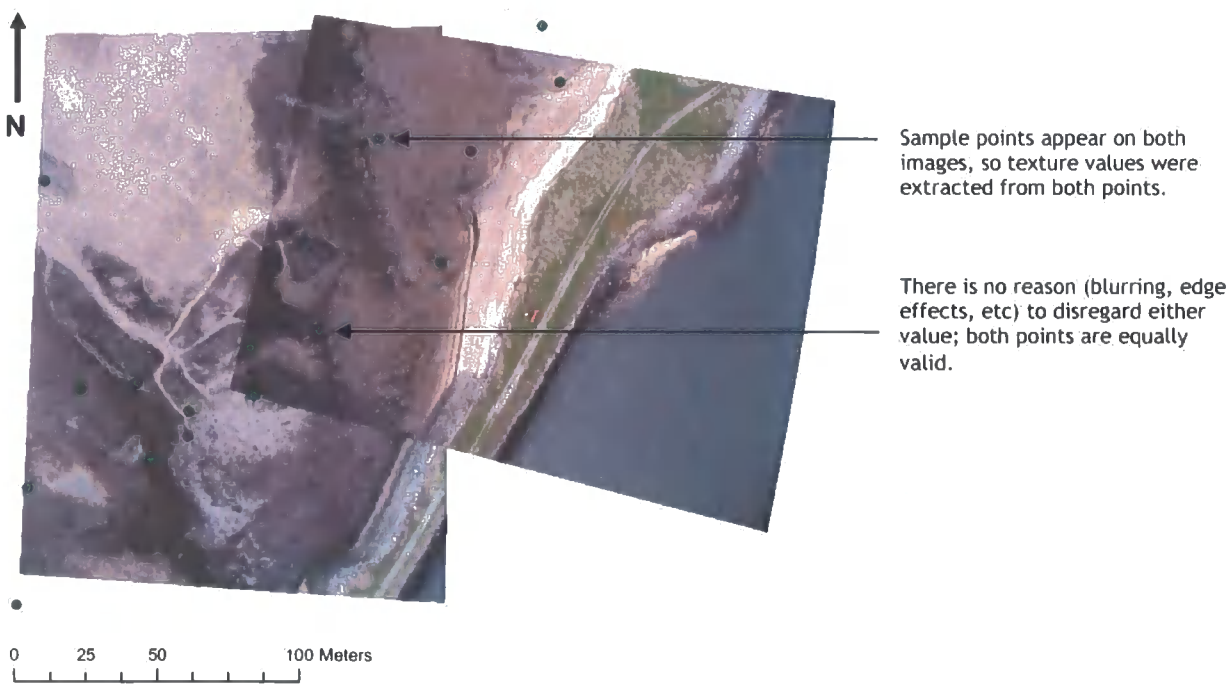

Figure 4.2 Schematic showing overlapping of macroalgal sample points

Table 4.1 is an example of the multiple texture values yielded from the raw imagery. Most of the *Enteromorpha sp.* samples show several corresponding entropy values from multiple images.

Although some images yielded similar entropy values for corresponding sample points, most images yielded large variations in texture value: Table 4.1 shows that sample point 1 (for example) yielded entropy values of -1.917 and +2.750 for images img274 and img280 respectively.

Although it was possible to disregard some texture values due to image blurring or edge effects, in the absence of more substantive information about the correct texture value to use, the texture value at each sample point was calculated as the mean of the values produced by the multiple images. Because of this, any textural 'signal' within the imagery may have been lost. Possible reasons for the differences in texture value at specific points in the imagery will be discussed in section 4.2.2

	Textural entropy value									
Enteromorpha sp. sample no.	im268	img271	img274	img280	img282	img304	img313	img330	img335	img337
1			-1.917225	-2.74984						
2			-2.938692	-2.119357						
3			-3.410507					-3.406796		
4			-2.874908					-3.346931		
5		-2.385568	-2.765948					-2.069221		
6					-1.594746	-2.085933	-1.76035	-1.97449		-2.589067
7				-2.168556	-2.518674			-1.823601		-2.259501
8	-1.539486	-0.961555			-2.665346				-2.085933	-2.547133
9	-1.79003	-1.209629							-2.518674	
10	-1.253684	-1.441354							-2.665346	
11	-2.020311	-2.328364	-1.739797							
12	-2.110958									
13		-2.418252								

Table 4.1 Example of multiple entropy values yielded for each sample point by overlapping raw images

Because of the problems alluded to above, it appears that image texture does not represent a viable method of extracting biological information from a standard 3-band digital camera. However, section 4.2.2 will offer possible solutions to the issues identified.

4.2 Adequacy of processing methodology for producing data suitable for correlation with ground truthing

4.2.1 Mosaicking and georeferencing

The satisfactory correlation of ground control/sample points with corresponding image pixel coordinates remains problematic. It was not possible to georeference single images, because of the large dataset and the limited number of ground control points (GCPs) per image, so it was necessary to create image mosaics to overcome these issues. Although image mosaics were largely acceptable, a number of visual artefacts were introduced into the imagery.

Figure 4.3 Inaccurate image 'stitches' produced by mosaicking process

Figure 4.3 shows inaccurate 'stitches' within the November 2006 and June 2007 images. The areas visible are both sections of the grassed roadway to the east of the site, and easily illustrate problems inherent in the mosaicking process. It is likely that the introduction of such errors into the mosaic decreased the georeferencing accuracy. Although the overall RMSE for the November 2006 mosaic was low (1.22 m), the error at each ground control point showed significant variability. Georeferencing accuracy was greatest towards the west of the image with an RMSE of 0.11 m, declining towards the east of the site, with an RMSE of 2.97 m. The large error to the east of the

site would therefore suggest that the accuracy with which algal sample locations can be correlated to image pixel coordinates is inconsistent.

This is illustrated by figure 4.4. Although the *Enteromorpha sp.* sample was taken from within the area of macroalgal matting, the error inherent in the georeferencing indicates that the corresponding image pixel coordinate may fall outside the area covered by algae, and the DN value or texture value extracted from said pixel coordinate may not be that produced by the algal sample itself. Because the georeferencing error was not uniform, the direction and magnitude of error varied between sample locations, so it was not possible to apply a uniform translation to the image to correct for this problem.

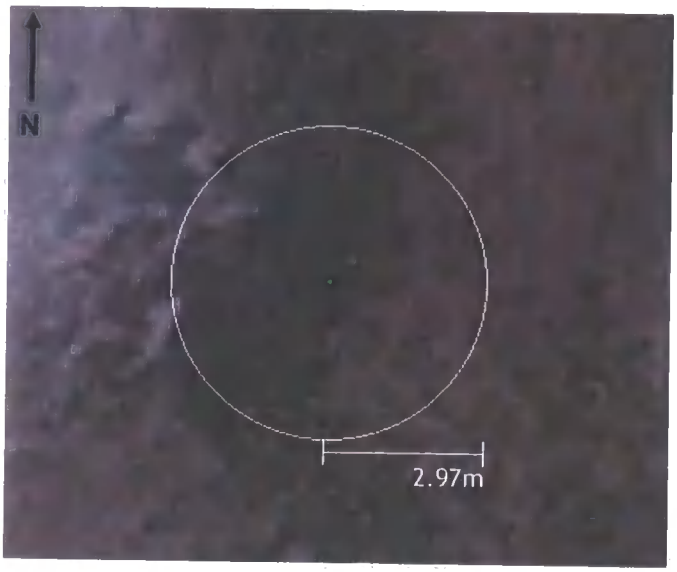

Figure 4.4 Schematic illustrating the georeferencing error at any given sample point. Extracted DN/texture value could lie anywhere within the area bounded by the circle, possibly yielding a false value.

The ground control methodology was altered for the June 2007 image acquisition session to resolve these problems. Because ground truthing (algal samples) were taken from the same location as the ground control points, it was possible to visually 'pinpoint' the corresponding image pixel locations, ensuring that the image pixel value accurately corresponded to ground truth data. However, this process (a) was time consuming, as it was necessary to manually select the correct coordinates, and (b) simply bypassed the georeferencing issues, because it did not act to reduce referencing error. Ground control points were distributed in a more uniform 'grid' pattern, with the intention of reducing the error variability caused by 'clustering' of GCPs during the November 2006 dataset.

However, both the overall RMSE (3.72 m) and the error range (0.07 - 8.49m) increased, suggesting that the distribution of ground control points is not significant.

4.2.2 Suitability of processing methodology for texture - algal biomass correlation

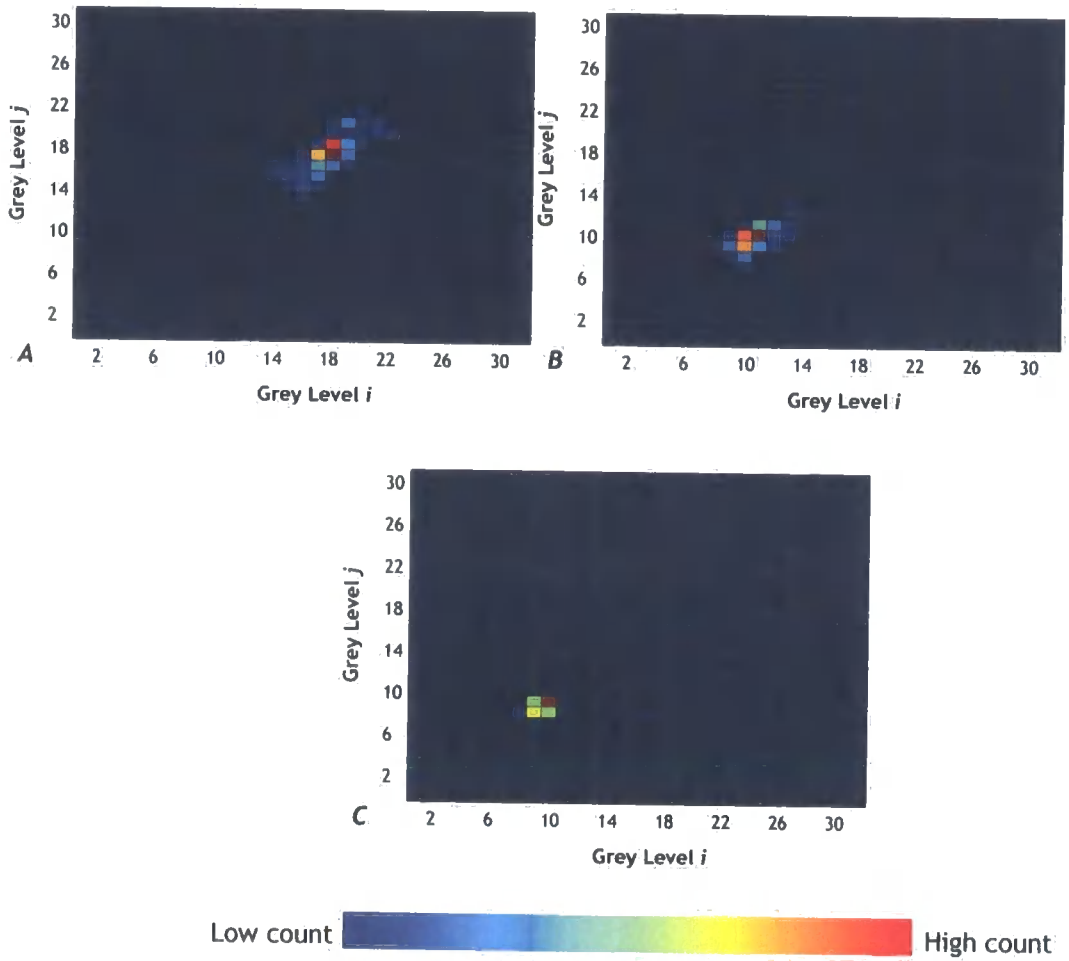

Figure 4.5 Example grey level co-occurrence matrices (GLCMs) computed on a specimen November 2006 raw image

Figure 4.5 shows example grey level co-occurrence matrices (GLCMs) for sparse **(A)**, moderate **(B)** and dense **(C)** algal cover computed from one of the November 2006 raw images. The matrices show that the incidence of neighbouring pixels with *dissimilar* grey levels decreases with respect to algal cover, suggesting that image texture is inversely proportional to macroalgal biomass. Textural

entropy computed on the GLCMs also shows an increase from -3.03 for sparse algal cover to -1.56 for dense cover.

However, although image texture may appear to relate to algal biomass in isolated 'single image' cases, section 3.4.3 indicated that both the November 2006 and June 2007 *image sets* failed to produce a significant texture - biomass correlation. The chosen image processing methodology may account for this: Because the relationship between image texture and spatial scale is critical for the adequate discrimination of dissimilar textures (De Bonet, 1997), it is necessary to use a consistent image resolution for when performing texture analysis. However, this was not feasible with imagery derived from the UAV, because it was not possible to achieve a constant flying altitude, and images from a number of different altitudes were used. It is possible that these spatial scale discrepancies between and within the raw images can account for the large variations in image texture produced by the same point on two separate images (see table 4.1).

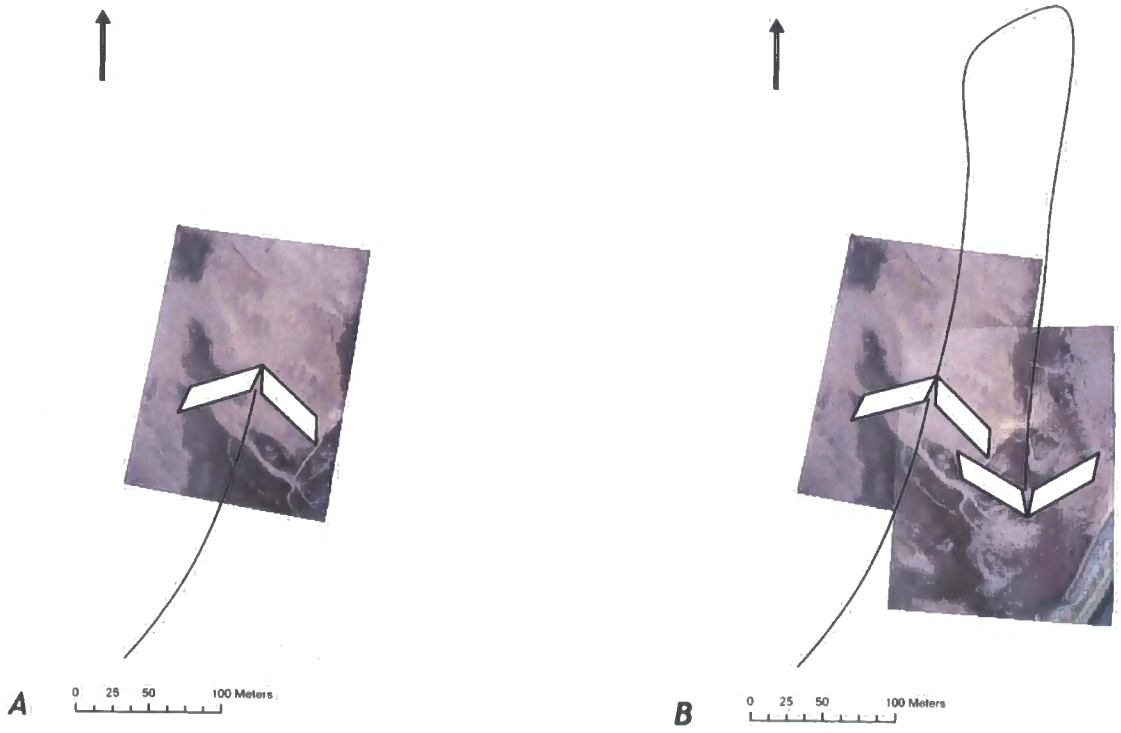

Figure 4.6 Schematic illustrating how image rotation is determined by UAV flight trajectory. Image **(A)** is acquired in a N.N.E direction on the first pass. Image **(B)** is acquired in a southerly direction on the second pass of the UAV, inducing a different image rotation.

Image rotation is also likely to account (in part) for the differences in texture between images shown in table 4.1: Images obtained using the UAV exhibited varying degrees of rotation, reflecting

the direction of flight of the aircraft (see figure 4.6). However, the 'moving window' used to compute image texture was applied in the same direction (top left - bottom right) for each raw image, indiscriminately of image rotation. Because of this, the 'window' is likely to have spanned differing pixels for the same geographic location on two images.

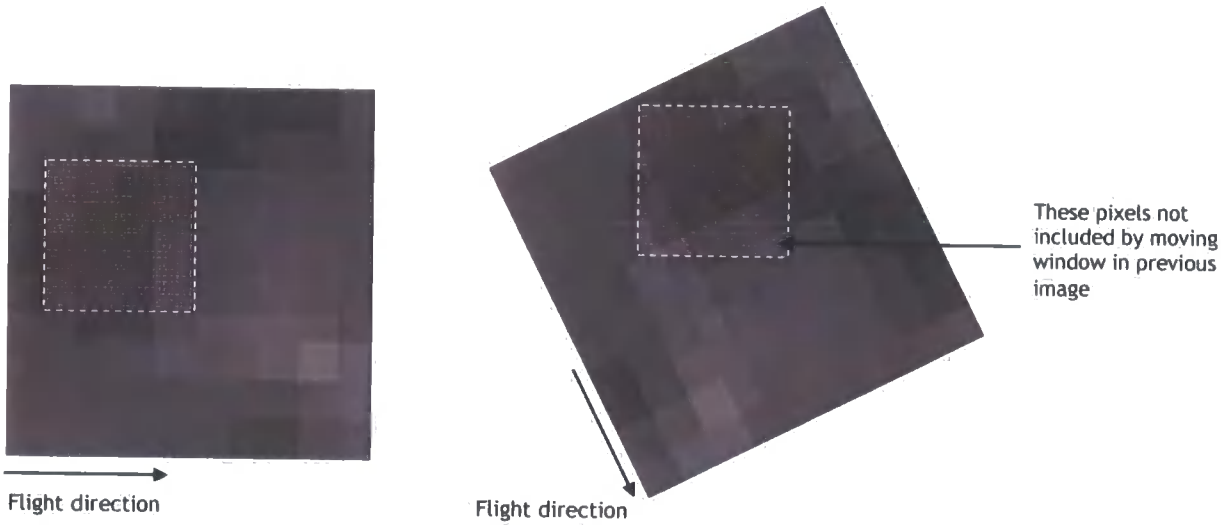

Figure 4.7 Schematic illustrating how the 'moving window' spans a different set of pixels for the same geographic location on two images with a different rotation

Figure 4.7 illustrates this effect: Because the second image was acquired on a different flight trajectory, the area bounded by the 'moving window' is different to that of the first image. This will in turn produce a different GLCM, and result in two separate entropy/inertia values for the same geographical location. Figure 4.8 is an example of this, showing the variation in GLCM for the same geographical location on two separate images.

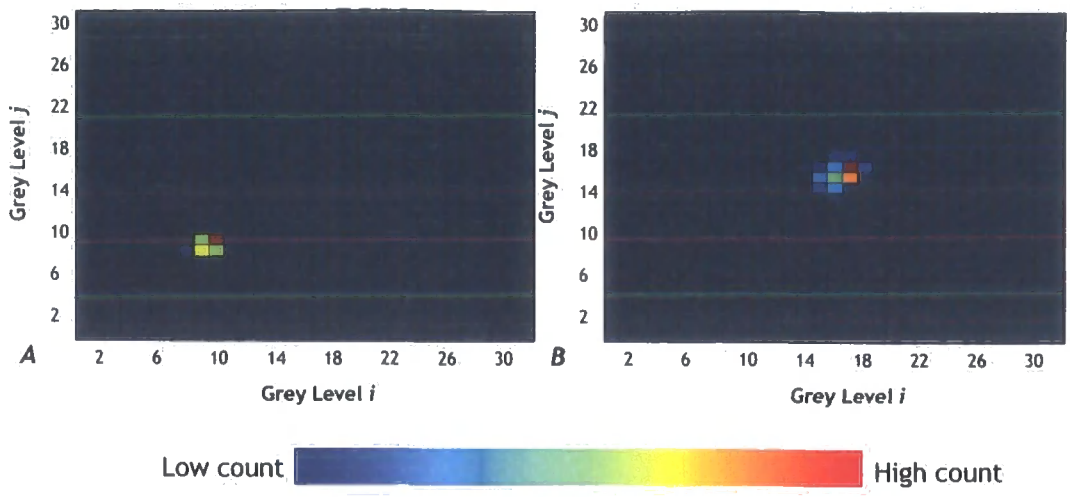

Figure 4.8 Example grey level co-occurrence matrices (GLCMs) computed on the same geographical location of two different overlapping raw images from the November 2006 dataset.

Although figure 4.8 **(A)** suggests a low incidence of neighbouring pixels with dissimilar grey levels, **(B)** shows a larger number of dissimilar neighbours. This is reflected in textural entropy values computed on the GLCM; **(A)** yields a value of -1.56, whereas **(B)** yields a value of -2.29, suggesting that texture measures show a high degree of variation between separate raw images.

Because of the large differences noted between texture values for the same geographical sample point on two images, it is likely that a combination of georeferencing error, issues of scale and issues of rotation all contributed to the lack of correlation between image texture and biomass, and can account for the discrepancies noted in section 4.1.3. Although georeferencing still remains problematic, it may be possible to account for rotation by computing the grey level co-occurrence matrix in a specific direction based on the rotation of an image. However, this would rely on the assumption that the image rotation is uniform and two-dimensional, whereas it is likely that image rotation is present in 3 axes.

4.2.3 Suitability of processing methodology for spectral/saturation - algal biomass correlation

Although the spectral characteristics of the mosaicked imagery from both data acquisition sessions appears to correlate well with *Enteromorpha sp.* biomass, it is necessary to address a number of points concerning the image processing methodology: Due to time constraints, it was not possible to radiometrically calibrate the two digital cameras flown in the UAV. Although the basic spectral response of the cameras was addressed in section 2.6.1, the NDVI and NGRDIs computed from the image datasets can only be considered relative, because of a lack of absolute spectral calibration. Hence, such data cannot be used to draw inferences as to the true biological characteristics of the *Enteromorpha sp.* Similarly, the absence of calibration limits comparisons that can be drawn with similar studies (eg. Guichard *et al.*, 2000).

'Ghosting' within mosaicked imagery was also problematic. Although the multi-band blending algorithm within the *AutoPano* (Kolor, 2007) software has been shown to perform well with remotely sensed data (Burt & Adelson, 1983), incorrect tie-points between multiple images led to the 'blending' of areas of macroalgal cover with areas of substrate (see figure 4.9).

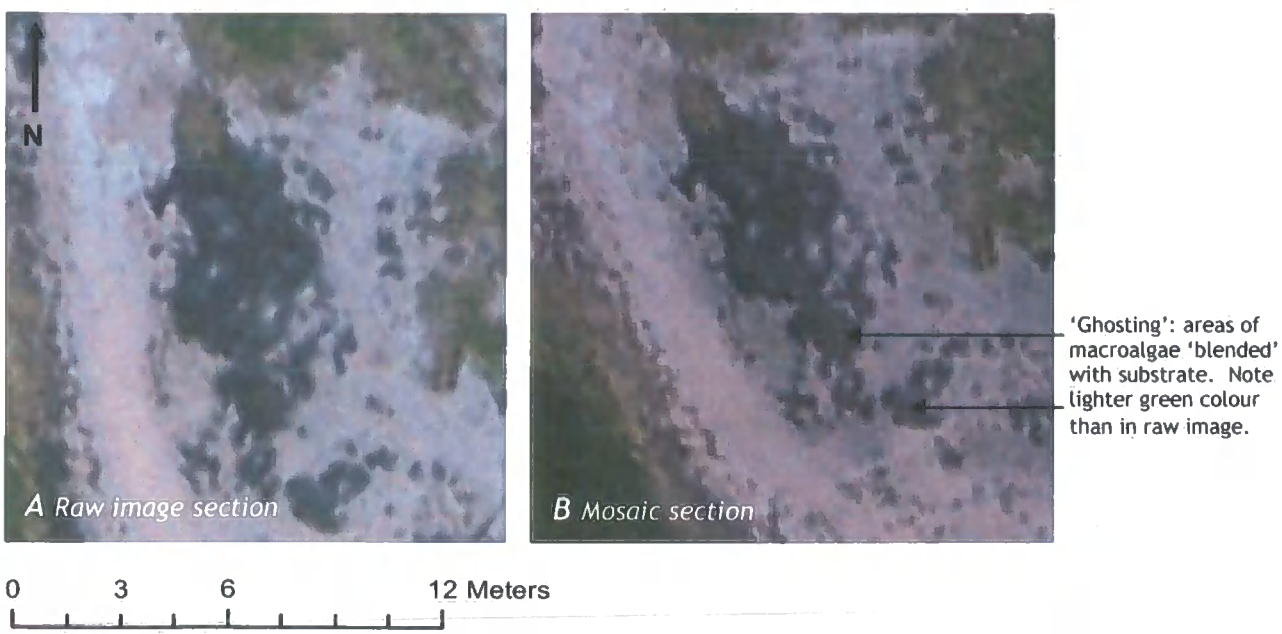

Figure 4.9 Blending of areas of macroalgal cover with areas of substrate. Produces 'ghosting' effect on mosaicked imagery, and may yield false spectral values for the area

Although this 'ghosting' effect was not visible in any areas of the mosaicked imagery used to extract values for correlation with biomass, it may be problematic if applying image classification/segmentation based on spectral features.

4.3 Estimation of *Enteromorpha sp.* biomass using image metrics

Despite the problems alluded to above, the degree to which image spectral characteristics and image saturation correlated to ground truthing highlighted their feasibility as predictor variables with which to model *Enteromorpha sp.* biomass across Seal Sands. Macroalgal biomass for the November 2006 fieldwork session was modelled through the application of the regression equations developed in sections 3.4.1 and 3.4.2 to NGRDI, NDVI (unimproved and improved) and saturation images of the November 2006 mosaic. The observed vs. predicted plots shown in figure 3.34 highlighted the close association between biomass predicted by NGRDI, NDVI (unimproved) and saturation, and *Enteromorpha sp.* observed at sample points, with *x:y* ratios approaching 1. The improved NDVI suffered from consistent underprediction of biomass. As noted in figure 3.18A, the regression line *y*-intercept of ~0.100 dictated that all NDVI values lower than this resulted in negative biomass estimations. Quantitative estimation of biomass was relatively similar for NGRDI, NDVI (unimproved) and saturation, with NGRDI and saturation yielding particularly similar values. However the improved NDVI showed a significantly decreased estimate, as a result of the above underprediction. The removal of negative values from the biomass estimate (see table 3.5, column 3) ceded increased predictions for all predictor variables, particularly for improved NDVI, giving a result in line with the other models. The average *Enteromorpha sp.* biomass yield of 894.596 kg seems plausible, although there is no past data with which to compare this figure.

Enteromorpha sp. biomass for the June 2007 mosaic was modelled using NGRDI and image saturation as predictor variables. Figure 3.38 shows an *observed:predicted* ratio approaching 1, suggesting that both NGRDI and saturation can closely approximate algal biomass, although the presence of a number of low-biomass samples below the *x*-axis indicates that image saturation may underpredict low biomass values. This is highlighted in table 3.6, which suggests that the saturation model yielded a greater number of negative biomass predictions than NGRDI. As with the November 2006

dataset, the removal of negative biomass predictions produced closer agreement between the *Enteromorpha sp.* predictions, with an average total biomass value of 264.568 kg. This value is significantly smaller than that of the November 2006 dataset, presumably because imagery was taken at difference times within the growth cycle. Again, the figure seems plausible when compared to the November 2006 biomass total, when there was visibly significantly increased *Enteromorpha sp.* cover. However, a number of issues must be addressed concerning the use of the above techniques to estimate total biomass at the site.

Sections 3.4 and 3.5 largely focus on the development of linear regression models from empirical data. However, given that light irradiance decays in proportion to the square of the distance from an object, and *Enteromorpha sp.* growth is non-arithmetic (eg. Martins & Marques, 2002), linear regression may not adequately describe the response of spectral reflectivity to algal biomass. Although the scope and time allocated to this study imposed limits on the formation of alternative methods with which to model the relationship between reflectivity and biomass, the development of generalized linear models (GLMs; eg. Donoghue *et al.*, 2004b) for *Enteromorpha sp.* - reflectivity modelling may highlight an area for future research. Similarly, prior to future model development, an analysis of the skew and distribution of the intensity/biomass datasets would be necessary in order to inform decisions regarding the most appropriate technique to model the relationship. Such an analysis may also help to highlight flaws concerning the field sampling methodology and the image selection procedure. Negative biomass predictions noted in section 3.5 may represent a limitation of using simple linear regression to describe the biomass - reflectivity relationship. Although the use of image ratios (NGRDI/NDVI) and image saturation linearly transforms the reflectivity element of the relationship, the non-linear nature of *Enteromorpha sp.* growth is still not accounted for. However, owing to time constraints, it was not possible to acquire a third dataset with which to a) validate the existing models and b) examine the suitability of the models established in sections 3.4 and 3.5 for predicting biomass at different time periods (not November/June) and in different locations.

The use of a supervised classification layer with which to mask out algal cover is of particular note. As suggested in section 3.2, both the November 2006 and June 2007 images suffered from significant misclassification. It is likely that this has introduced bias into the overall algal prediction, through the classification of substrate as algae. This could account for a large number of the negative biomass predictions noted, particularly within the NDVI imagery. It is also possible that the

classification mask is responsible (in part) for the large biomass difference between November 2006 and June 2007, because the mask may have underrepresented *Enteromorpha sp.* cover within the November 2006 imagery. As shown in figure 3.39, there appears to be significantly more extensive *Enteromorpha sp.* cover in June 2007 than in November 2006 (3.35). However, because the substrate was drier during the June 2007 data acquisition session, the sensor may have more easily discriminated algae from biomass, leading to a larger classification mask. Hence, total biomass prediction for November 2006 may actually be too low.

The decision as to whether to include negative biomass in the total estimation is also of consequence. Although it is logically not possible to achieve a negative biomass value, the high incidence with which such values occurred suggests that a large proportion of negative biomass values were *not* due to misclassification, but the result of incorrect biomass predictions by the various models. Although this was most prevalent with the NDVI (improved) model, negative values were produced by *all* predictor variables. This indicates that *all* models fail to accurately predict sparse biomass, yielding negative predictions for low values of NGRDI, NDVI and image saturation.

Figure 3.37 indicates that saturation is most efficient for prediction of sparse biomass values within the November 2006 imagery, with a maximum negative prediction of ~-100 g DW m^{-2}, whereas NGRDI is the worst predictor of low-biomass values, yielding a maximum negative prediction of ~-2500 g DW m^{-2}. Saturation is also the optimum model for the prediction of low biomass values within the June 2007 dataset, with a maximum negative prediction of ~-10 g DW m^{-2}. Although this indicates there is a wide variation in the range of biomass predictions ceded by the various biomass models, the closeness with which the total biomass calculations agree would indicate that the vast majority of algal biomass is of moderate biomass. Similarly, this also implies that *all* of the models are at their most efficient when estimating moderate *Enteromorpha sp.* biomass, accounting for the good agreement.

4.4 Performance of UAV compared to conventional remote sensing methods

The relative pros and cons of using unmanned aerial vehicles in the coastal zone were addressed in section 1.2.5. The facility to rapidly deploy and acquire data (eg. Lomax *et al.*, 2005) is of key significance with regards to image acquisition. Cloud cover of >20% is often deemed unacceptable for traditional optical remote sensing techniques (Klemas, 2001), especially within the remit of environmental change detection. The use of a UAV to acquire data may render this issue redundant because the relative ease with which the UAV could be deployed means that imagery need only be acquired when atmospheric conditions are amenable. During the November 2006 fieldwork session, imagery was acquired on an *ad-hoc* basis because of adverse weather conditions. Provided the UAV is kept in a state of readiness, it should be possible to acquire imagery without extensive prior notice, in order to take advantage of optimum weather.

The time taken *during* data acquisition is also favourably comparable to that of more traditional airborne optical surveys. Using a team of three people, it was possible to acquire imagery, ground truth samples and ground control within 5 hours.

Event	Time taken
Distribution of GCPs	60 mins
UAV pre-flight preparation	15 mins
UAV image acquisition flight	35 mins
Collection of ground truth samples	120 mins
dGPS demarcation of GCPs/ground truth locations	60 mins
Total	*4:50 hours*

Table 4.2 Approximate time taken for acquisition of UAV imagery, ground control and ground truth samples. Note that the approximate area acquired was 0.3km^2, and site access was relatively easy.

Table 4.2 shows the approximate time taken during the various stages of data acquisition during the June 2007 data acquisition session. Following the establishment of suitable ground truthing, repeat data acquisition would be reduced by approximately two hours. Similarly, the use of more permanent ground control points would negate the lengthy distribution and dGPS demarcation processes, allowing the acquisition of images on a flexible basis.

Peterson *et al.* (2003) noted that UAVs may also offer greater flexibility than traditional remote sensing approaches with regards to sensor instrumentation. This was of direct consequence to the November 2006 data acquisition session, where the use of both a near-infrared and a conventional digital camera highlighted the ease at which different sensors can be placed in a UAV. Although most airborne platforms share this flexibility (Peterson *et al.*, 2003), satellite remote sensing systems do not allow for sensor changes and adjustments. Hence, although the type of sensor which can be installed in a UAV is limited by size, weight and power requirements, the ability to offer a choice of instruments allows for comparison to be drawn with conventional aerial photography set-ups.

It is also necessary to address the disadvantages of using UAVs for macroalgal monitoring, in comparison to conventional aerial photography. Issues of achieving a consistent altitude and flight trajectory have already been discussed (see section 4.2). However, it is possible that the flight characteristics of the chosen UAV also adversely affected the imagery obtained. The placement of the sensor within the aircraft is of key importance (Hruska *et al.*, 2005); optimum sensor location should be towards the centre of mass of the airframe, to minimize the effects of pitch, roll and yaw on the images. The sensor should also be isolated from vibrations caused by the motor (Hruska *et al.*, 2005). Although the camera in the UAV was adequately isolated from the motor (see figure 2.6), it is located off-centre, within the wing of the aircraft. It is possible that this increased the incidence of off-nadir images.

Although UAV flights were operated under optimum weather conditions, it is plausible that the lightweight nature of the UAV rendered it susceptible even to light winds, introducing additional distortions into imagery. Operator skill is also of importance; a more skilled UAV operator should be able to sustain a more consistent altitude and flight trajectory, producing a more coherent series of images. This may account for the increase in georeferencing error of the June 2007 dataset over the November 2006 imagery, even though ground control was more uniformly distributed. Neither of these factors are likely to be significant for conventional aerial photography; larger aircraft are likely to be less susceptible to wind shear, and a pilots' licence ensures that all operators have achieved a 'baseline' skill level.

Although the chosen UAV has been shown to represent a significant time/cost saving over conventional remote sensing techniques with regards to image acquisition, data pre-processing may

present a significant obstacle to the rapid assimilation of data for monitoring purposes. As noted by Peterson *et al.* (2003) the distortions introduced by low level flight, the limited area covered with each image, and the large series of images generated by each flight greatly increased the amount of pre-processing necessary prior to conducting any form of image analysis. Although image acquisition was a relatively rapid process, pre-processing of data into mosaicked imagery suitable for macroalgal monitoring purposes consumed a substantial amount of time (see section 2.5 for description of pre-processing methodology). Although it was possible to automate a number of these processes, thus reducing the time taken over the second image dataset (June 2007), the synthesis of easily usable image data from the UAV was still a relatively 'hands-on' process. In comparison, both aerial photography and satellite platforms produce imagery that covers a larger GSD, reducing the need for intensive mosaicking operations. Similarly, the use of metric camera systems on standard remote sensing platforms reduces the need to remove geometric distortions in pre-processing, allowing for a faster image 'turnaround' period. Therefore, although the *acquisition* of imagery with a UAV may prove both faster and less costly than standard forms of optical remote sensing, the period between obtaining and releasing image data may be significantly greater than that of existing remote sensing platforms. This has implications for the applicability of UAVs as a tool with which to monitor and respond to rapid macroalgal growth and decline.

4.5 UAVs as a feasible source of high resolution imagery for ecological monitoring purposes

Spectral methods of extracting biological information from aerial photography have shown that a standard three-band digital camera flown on a UAV can be used to map and quantify macroalgal biomass variations. Although single bands have produced weak correlation with biomass, the extent to which *relative* NDVIs, NGRDIs and image saturation correlates to ground truth samples of *Enteromorpha sp.* highlights the viability of UAVs as an aerial photography platform. Image texture operators have shown poor correlation with biomass. However, the development of rotationally invariant texture measures may largely negate the problems noted in section 4.2.2. NGRDI, NDVI and image saturation have also shown potential for the estimation of *Enteromorpha sp.* biomass

over large spatial scales. Although a number of limitations of these techniques have to be addressed, the ability to calculate biomass remotely has diverse applicability.

Because the above techniques have only been evaluated in a controlled environment, it is necessary to discuss their relevance to the use of UAVs as a platform with which to acquire suitable ecological monitoring data. *Relative* NGRDIs and colour saturation required the least processing to produce adequate image-biomass correlations; the processing time necessary for such methods would produce data on a timescale amenable to the interannual monitoring rates required by the EU Water Framework Directive reporting cycle (Scanlan *et al.*, 2007), and such techniques may represent a workable solution for the extraction of ecological information from UAV imagery. Although the production of *relative* NDVIs also required relatively little data processing, the errors inherent in acquiring and co-registering visible and NIR datasets may limit its applicability for the derivation of ecological data from unmanned aerial vehicles, although this method may still be viable for monitoring with slower repeat rates. Because image texture showed no significant correlation with biomass, it does not appear to present a practical method of obtaining ecological data from UAV imagery. In addition to this, the deliverables of such a method are unclear; whereas the spectral techniques discussed above were used as predictor variables to produce biomass 'maps', texture processing requires raw images rather than mosaics, and the georeferencing of a large quantity of raw imagery in order to produce maps of biomass would further reduce the time/cost effectiveness of the method.

The effect of time on ecological monitoring is inherently uncertain (Urquhart & Kincaid, 1999), and the development of tools or methods for ecological monitoring must ultimately make assumptions about future ecological trends when defining the appropriate monitoring period and repeat rate. The ability to acquire, process and analyse high resolution imagery on a relatively fast survey repeat rate shows that unmanned aerial vehicles may help to reduce the uncertainty in defining appropriate survey periods and repeat rates. Similarly, Urquhart & Kincaid (1999) suggest that the design of ecological monitoring strategies often necessitates a compromise between frequent survey repetition at a single point and infrequent surveying at multiple locations. However, through the use of unmanned aerial vehicles, it may be possible to address both of these facets, by achieving both high survey frequency and wide spatial coverage.

One of the prime reasons for assessing the use of unmanned aerial vehicles for ecological monitoring was an evaluation of their ability to produce data able to 'bridge' the spatial scale gap between low

definition monitoring and experimental lab-based surveys. Guichard *et al.* (2000) suggested that resolutions of the order <0.5 m should be amenable to experimental study, allowing for the observation of local processes over a wide spatial area. Although raw imagery acquired by the UAV possessed resolutions of the order <0.07 m, the spatial coverage of single images is not sufficient for observation over a wide area. However, through mosaicking and image pre-processing, it was possible to achieve high-coverage image mosaics with resolutions of <0.1 m, indicating that unmanned aerial vehicles present a viable solution with which to achieve data of resolutions high enough to aid detailed experimental ecological monitoring.

Another key facet of remote monitoring is the necessity of providing data without causing disturbance to sensitive ecosystems (eg. Foley *et al.*, 1998) Bulk sampling of macroalgal matting was necessary to provide ground truthing, and inevitably involved a degree of intrusion into an ecologically sensitive zone. However, following the establishment of suitable ground data, unmanned aerial vehicles may be used to provide data of a resolution that was only previously achievable through intensive survey techniques, largely eliminating the environmental disturbance associated with such methods. This would enable the collection of high resolution ecological monitoring data free from anthropogenic disturbance, further increasing the appeal of the UAV as a monitoring solution.

Methods of estuarine monitoring are inherently inexact (Scanlan *et al.*, 2007), and the determination of specific techniques with which to observe macroalgal dynamics may help to standardise ecological monitoring within the coastal environment. The necessity of outlining standardised procedures for the sampling of macroalgal cover and the analysis of remotely sensed imagery must be a key aim of further research (Scanlan *et al.*, 2007). The high spatial coverage and resolution of data acquired by unmanned aerial vehicles, coupled with low operating costs and the ability to perform *ad-hoc* aerial surveys highlight unmanned aerial vehicles as an ideal tool with which to gather pilot ecological data in order to inform standardised survey techniques.

4.6 Sources of Error

Prior to reaching a conclusion, it is prudent to consider sources of error within the investigation. Error inherent within the study can be divided into two main sections: errors resulting from ground measurements, and errors that resulted from imagery.

4.6.1 Errors resulting from ground measurements

The ground measurements that were necessary for the study can be largely separated into two parts: ground control necessary for imagery registration, and ground truth sampling. The largest errors associated with ground control are likely to have arisen from dGPS/total station measurements of ground control points. Ground control collected during the November 2006 fieldwork session used a dGPS system with a typical accuracy of ±25 cm (Leica, 2006a). Ground truth sample points were also demarcated using the same system. This indicates that the error inherent in the location of ground truth/sample points on georeferenced imagery was almost as large as the sampling quadrat itself (30c m^2). However, in reality, the error term was significantly smaller; when using the dGPS, it is possible to 'occupy' a position with the dGPS rover for a number of seconds, incrementally reducing the error. Because of this, typical ground control and ground truth error during the November 2006 fieldwork session was reduced to ~7 cm. During the June 2007 data acquisition session, ground control/truthing was collected using a total station instead of a GPS system. Although the typical error was significantly smaller than that of the dGPS system (±5 mm Leica, 2006b), only the relative position of points was recorded. It was therefore necessary to transform these points to absolute geographical coordinates using a known reference point. In the absence of any nearby trig points/benchmarks, the dGPS points from the November 2006 survey were chosen. Hence, any ground control errors associated with the November 2006 survey were also replicated in the June 2007 fieldwork session.

Scanlan *et al.* (2007) notes the absence of a 'benchmark' method for the collection and preparation of algal samples. Although samples were removed following procedures suggested by Jeffrey &

Hayes (2005), consistent sampling was problematic. First, difficulties arose from the collection of firmly attached filaments of algae; in some cases, it was not possible to remove the full *Enteromorpha sp.* strand, and samples may have underestimated macroalgal cover. Second, the removal of highly dense macroalgal matting was complicated by confusion over the depth to which matting should be removed, although fieldworkers endeavoured to remove only the surface layer, as recommended by Scanlan *et al.* (2007). However, it is plausible that errors were introduced into the sampling technique by the under- or over-sampling of algal matting. In addition to errors inherent in the sampling of *Enteromorpha sp.* biomass, the lack of standardised procedures for the preparation, drying and weighing of macroalgal material is likely to have further compounded sampling error. Although samples were weighed with a milligram-accuracy analytical balance, it is probable that trace amounts of sediment and non-algal material were present, biasing dry weight values. Similarly, the sieving and washing of the *Enteromorpha sp.* is likely to have resulted in the loss of a minor amount of algal material. However, it is difficult to quantify the extent to which the chosen laboratory methods introduced error into the dataset. A more rigorous comparison of the two laboratory methods may help to highlight some potential sources of error.

4.6.2 Errors resulting from imagery

Errors associated with the mosaicking, georeferencing and texture processing methodologies have already been addressed in chapter 4. However, it is again necessary to stress that error introduced by successive mosaicking, georeferencing and processing procedures is of notable significance. Although the change in fieldwork strategy during the June 2007 largely helped to avoid the georeferencing pitfalls associated with the November 2006 dataset, the accurate extraction of pixel coordinates from known geographical location remains problematic, and although largely un-quantifiable, may account for a large proportion of error within the investigation. Similarly, the use of a commercial 'off-the-shelf' image mosaicking package rather than a bespoke remote sensing system meant that it was not possible to isolate the exact transformations/distortions introduced into the mosaicked imagery, and errors associated with this process are unknown. A lack of true

radiometric calibration of the camera equipment used onboard the UAV also means that error concerning the reflectivity values cannot be quantified.

Inaccuracies connected to the UAV flight characteristics have also been noted as a major cause of error within the image processing and analysis, particularly with regard to image texture. Because of this, numerous processing steps were necessary in order to produce workable data from the imagery. It is probable that each processing 'stage' introduced further elements of error into the dataset, through successive uncompressing and recompressing of JPEG imagery and consecutive rescaling of imagery to 8-bit unsigned integer format. Similarly, the multiple georeferencing steps necessary to produce suitable raw imagery for texture processing is likely to have further increased error.

Chapter 5. Conclusion and Future Developments

5.1 Conclusion

Data suitable for ecological monitoring must be able to highlight the causes and consequences of environmental change, with a view to further understanding the temporal and spatial behaviour of the natural world. In order to provide an alternative to more expensive remote monitoring techniques, an unmanned aerial vehicle (UAV) was used as a platform with which to acquire high-resolution imagery of macroalgal biomass at Seal Sands, Tees Estuary, UK. Imagery was acquired at two different stages in the macroalgal development cycle, in order to examine the response of *Enteromorpha sp.* under different seasonal conditions. Raw imagery derived from approximately 200m altitude did not achieve suitable ground coverage for accurate georeferencing and discrimination of macroalgal cover. However, image mosaics produced from the raw aerial photographs allowed for straightforward qualitative visual characterisation of macroalgal growth over the Seal Sands area. Photomosaics from both data acquisitions sessions were georeferenced using a number of small markers as ground control points. Although mosaics proved adequate for most quantitative analysis, distortion introduced through successive mosaicking and georeferencing procedures hindered some analysis that could be performed.

Samples of *Enteromorpha sp.* biomass were collected from Seal Sands on both image acquisition sessions in order to provide ground truthing for quantitative analysis of imagery. A number of image processing techniques were identified in order to extract suitable data from standard 3-band digital photography. Single image bands did not show a strong correlation with macroalgal biomass, and do not adequately explain *Enteromorpha sp.* variation. However, the *relative* Normalised Green-Red Difference Index (NGRDI) computed on imagery from both data acquisition sessions showed significant correlation with biomass, yielding R^2 values of 0.6770 and 0.7265 for the November 2006 and June 2007 datasets respectively. Image colour saturation also showed a strong correlation with biomass: Coefficients of determination of R^2=0.6221 and 0.6734 respectively suggested that macroalgal biomass variability could be adequately explained by colour saturation computed on mosaics from both data acquisition sessions. *Relative* Normalised Difference Vegetation Index

(NDVI) computed from the near-infrared and red components of the November 2006 mosaicked imagery correlated well with *Enteromorpha sp.* biomass (R^2 = 0.7445), although negative NDVI values within the dataset proved problematic. The removal of these values yielded a further improvement in correlation (R^2 = 0.9485). However, the loss of a number of sample points due to tidal advance, the error inherent in co-registering the NIR mosaic to the true-colour imagery and the lack of a second NIR dataset with which to draw comparisons suggests that further examination of this method is necessary. Textural analysis of the raw imagery proved inconclusive: Although entropy and inertia measures computed on both datasets did not exhibit a significant relationship with macroalgal biomass, the resolution of directional and scalar issues may improve the texture-biomass correlation in the future. Further exploration of the scale dependent nature of texture analysis may also be advisable to identify optimum image acquisition altitude.

Selected image processing techniques were used to estimate *Enteromorpha sp.* biomass for the November 2006 and June 2007 imagery. Despite a lack of previous biomass estimates for Seal Sands, estimations of 894.596 kg and 264.568 kg for the two surveys respectively, appear plausible. Although there are a number of potential issues that must be resolved prior to the use of the above techniques to predict *Enteromorpha sp.* biomass from aerial imagery, the close agreement between total biomass modelled by the various image processing techniques indicates that the technique may prove viable. The development of a composite model, combining several predictor variables may reduce endeavour to resolve issues surrounding the prediction of negative biomass values.

The time and cost associated with image acquisition was shown to compare favourably with that of conventional remote sensing techniques. Following the establishment of suitable ground truthing and permanent ground control at a site, a complete aerial survey could hypothetically be undertaken in less than half a day, with minimal associated costs. Through this, the use of unmanned aerial vehicles could make large-scale monitoring accessible to a significantly larger community, for whom conventional remote sensing would be prohibitively expensive. The conversion of raw aerial photography into image data suitable for ecological monitoring purposes was a more protracted affair. The time necessary for the production of quantitative data varied significantly with regard to the type of analysis being performed, and although the extraction of spectral data and colour saturation values from the imagery was relatively simple, the amount of labour associated with the pre-processing of raw image data into a useable form may still prove problematic. Similarly, image texture measures required the largest amount of time to compute,

but yielded the least amount of useful data, and although texture-biomass correlation may be improved with further study, the lengthy processing period necessary for the creation of texture maps is likely to be a major time/cost constraint of this method.

The ability to undertake aerial surveys on an *ad-hoc* basis allows for the adaptation and creation of bespoke ecological monitoring strategies through which the nature of environmental change could be closely observed. The relative speed with which UAV-image data can be acquired, downloaded, processed and analysed facilitates high repeat-rate monitoring on temporal scales amenable to ecological change. In terms of *qualitative* examination of imagery, unmanned aerial vehicles represent an ideal solution for the rapid response to and visualisation of short term environmental change. Similarly, due to the low cost of initial data acquisition, UAVs may prove useful for 'pilot' ecological studies, prior to the commissioning of more conventional remote sensing surveys. The relative ease with which *quantitative* data can be extracted from UAV-derived imagery suggests that unmanned aerial vehicles also have great potential as part of a 'total' ecological monitoring solution, through which data can be acquired, processed and analysed in-house, negating the costs associated with conventional surveys. As such, the benefits offered by the multiple roles for which UAVs can be used (within a remote monitoring framework) emphasises the usefulness of unmanned aerial vehicles as an ecological monitoring tool.

5.2 Future developments & recommendations

5.2.1 UAVs

The future development of unmanned aerial vehicles as an emerging technology may further enhance their applicability to large-scale remote monitoring. The advent of compact inertial navigation systems (INS) and computer-controlled flight routines may reduce the image scaling and directional issues associated with variable flight altitudes and trajectories. Similarly, the development of integrated image tagging and georeferencing software (eg. Lambers *et al.*, 2007) could significantly decrease the amount of pre-processing necessary for the establishment of image mosaics. Improved mosaicking, either through the use of 3-dimensional restitution or bespoke

remote-sensing software may also help to refine image outputs and resolve issues associated with orientation and scale, especially with regards to object-based image analysis methods (ie. texture analysis).

5.2.2 Flying conditions

Although the ability to use unmanned aerial vehicles on an *ad-hoc* basis remains one of their key attractions over more conventional remote sensing techniques, it is necessary to address suitable UAV operational conditions. Operator training is of utmost importance, and the time taken to train a UAV operator may negate much of the time and cost savings of using UAVs over conventional aerial photography. However, even when piloted by a skilled operator, atmospheric conditions may limit the usefulness of a UAV. The advent of compact commercial autopilot systems may resolve many of the issues surrounding operator cost and training.

In order to acquire usable imagery in a coastal or estuarine location, low wind speed and high visibility is essential. Although direct sunlight may introduce shadowing into imagery, clear skies are favourable to cloudy conditions, to enable increased shutter speeds and reduce image blurring. The acquisition of imagery at the minimum point within the tidal cycle is also advisable, in order to curtail the effects of substrate darkening on the spectral properties of imagery.

5.2.3 *Enteromorpha sp.* sampling

The establishment of standardised techniques for the collection and processing of *Enteromorpha sp.* ground samples is of utmost importance in enabling like-for-like surveys of estuarine algal cover. The techniques established in sections 2.3 and 2.4 go some way towards demonstrating a repeatable methodology for ascertaining biomass, but their effectiveness has not been assessed in comparison to other techniques. In order to produce effective ground control, consensus must be achieved within the literature regarding sampling strategies, algal mat extraction and biomass calculation.

This will help achieve ground truth data which is both easily replicable, and considerably less time consuming in preparation.

5.2.4 Image processing

The derivation of useful data from an extensive set of airborne digital images is of key importance for increasing the uptake of unmanned aerial vehicles as a genuine alternative to conventional airborne imaging platforms, and the development and uptake of image mosaicking tools capable of working with extensive image sets is necessary for more efficient data processing. Similarly, although image spectral processing techniques were shown to adequately correspond to biomass, the radiometric calibration of camera equipment flown onboard lightweight UAVs is advisable for the accurate determination of the true spectral properties of image data. The availability of handheld spectrometers means that ground radiometry should be a key part of any further study. Although there was insufficient time within the remit of this project to undertake such work, measurement of the true spectral response of macroalgal communities is necessary for the calculation of true NDVIs. Further research should also attempt to account for the spectral response of diatomaceous biofilms and their influence on the spectral properties of imagery.

Although NGRDI and image saturation were shown to perform well as biomass predictor variables, it was not possible to assess the usefulness of NDVI, because of the lack of a second dataset with which to draw comparisons. The acquisition of true near-infrared imagery and the establishment of an appropriate processing methodology for such data would also be a crucial component of any further research, and the development of more refined image processing methodologies is essential for aiding the widespread acceptance of unmanned aerial vehicles into the remote sensing community.

5.2.5 Macroalgal dynamics

Although much attention has been paid to unmanned aerial vehicles and their usefulness towards ecological monitoring, it is necessary to address future work involving macroalgal dynamics. Unmanned Aerial Vehicles have been shown to produce maps capable of yielding quantifiable measurements of *Enteromorpha sp.* biomass. Future research may be able to build upon these techniques with a view to achieving a monitoring solution capable of observing macroalgal communities with temporal and spatial resolution. Such a system may be help to examine the dynamics of algal blooms over one or more seasons, and may help address some of the uncertainties associated with the root causes and consequences of green tide events. Similarly, this may help to enhance understanding as to the role of macroalgal blooms within the intertidal zone so that a more holistic management of estuarine ecosystem management can be achieved.

5.2.6 Further literature

Finally, and possibly of greatest consequence, is the need for further research into the use of unmanned aerial vehicles for remote ecological monitoring. Although the current literature abounds with material detailing UAV-based research *or* remote sensing in an ecological context, there are relatively few studies which unite the two fields. A concerted effort towards the development of low-cost, high resolution ecological monitoring strategies is of importance to both the ecology and remote sensing communities, and the uptake of unmanned aerial vehicles for environmental research may help to stimulate literary debate into the use of alternative remote sensing technologies and the standardisation of survey methods.

Hence, although unmanned aerial vehicles are a relatively new technology, there is large scope for further study, and the potential of UAVs for the monitoring of environmental change and the necessity for further research must again be stressed as a potential solution to current ecological monitoring shortfalls.

Acknowledgements

I would like to acknowledge Northumbrian Water Limited for financial support which enabled this project to take place. I am grateful to SmartPlanes AB for UAV pilot training and advice concerning the image acquisition process. I would also like thank Mike Leakey at Natural England for assistance with site access. Special thanks go to David McCarthy and Natasha Barlow for all their help with fieldwork and advice during the writing up process. Finally, I would like to extend my utmost gratitude to Danny Donoghue and Patrice Carbonneau for their support, supervision and encouragement at every stage of this project, from inception to completion.

Bibliography

Adir, N, Zer, H, Shochat, S & Ohad, I (2003); *Photoinhibition - a historical perspective*; Photosynthesis Research, **76**, 1; pp 343-370

Allen, JRL (2000); *Morphodynamics of Holocene salt marshes: a review sketch from the Atlantic and Southern North Sea coasts of Europe*; Quaternary Science Reviews, **19**, 12; pp 1155-1231

Ben Moussa, H, Viollier, M & Belsher, T (1989); *Télédétection des algues macrophytes de l'Archipel de Molène (France) Radiométrie de terrain et application aux données du satellite SPOT*; International Journal of Remote Sensing, **10**, 1; pp 53-69

Berglund, J, Mattila, J, Ronnberg, O, Heikkila, J & Bonsdorff, E (2003); *Seasonal and inter-annual variation in occurrence and biomass of rooted macrophytes and drift algae in shallow bays*; Estuarine, Coastal and Shelf Science, **56**, pp 1167-1175

Bjornsater, BR & Wheeler, PA (1990); *Effect of nitrogen and phosphorus supply on growth and tissue composition of Ulva fenestrata and Enteromorpha intestinalis (Ulvales, Chlorophyta)*; Journal of Phycology, **26**, 4; pp 603-611

Bolam, SG, Fernandes, TF, Read, P & Raffaelli, D (2000); *Effects of macroalgal mats on intertidal sandflats: an experimental study*; Journal of Experimental Marine Biology and Ecology, **249**, pp 123-137

Bold, HC & Wynne, MJ (1978); *An Introduction to the Algae*; Prentice Hall, New Jersey; 706 p

Brouwer, PEM, Geilen, EFM, Gremmen, NJM & Van Lent, F (1995); *Biomass, cover and zonation pattern of sublittoral macroalgae at Signy Island, South Orkney Islands, Antarctica*; Botanica Marina, **38**, 3; pp 259-270

Brown, AR, Lewis, RE, Riddle, AM, Stanley, RD & Widdows, J (2000); *Lower Tees estuary: A scoping study of the intertidal ecosystem*; Brixham Environmental Laboratory (BL6910/B: Report to the Environment Agency), Brixham, Devon; 109 p

Brown, M & Lowe, D (2007); *Automatic Panoramic Image Stitching using Invariant Features*; International Journal of Computer Vision, **74**, 1; pp 59

Budd, JTC & Milton, EJ (1982); *Remote sensing of saltmarsh vegetation in the first four proposed thematic bands*; International Journal of Remote Sensing; **3**, pp 147-161

Burke, L, Kura, Y, Kassem, K, Revenga, C, Spalding, M & McAllister, D (2001); *Pilot Analyses of Global Ecosystems: Coastal Ecosystems*; World Resources Institute, Washington DC; 93 p

Burt, PJ & Adelson, EH (1983); *A Multiresolution Spline With Application to Image Mosaics*; ACM Transactions on Graphics (TOG), **2**, 4; pp 217-236

Cabral, JA, Pardal, MA, Lopes, RJ, Murias, T & Marques, JC (1999); *The impact of macroalgal blooms on the use of the intertidal area and feeding behaviour of waders (Charadrii) in the Mondego estuary (west Portugal)*; Acta Oecologica, **20**, 4; pp 417-427

Carbonneau, PE, Bergeron, NE & Lane, SN (2005); *Texture-based image segmentation applied to the quantification of superficial sand in salmonid river gravels*; Earth Surface Processes and Landforms, **30**, 1; pp 121-127

Carrère, V, Spilmont, N & Davoult, D (2004); *Comparison of simple techniques for estimating chlorophyll a concentration in the intertidal zone using high spectral-resolution field-spectrometer data*; Marine Ecology Progress Series, **274**, pp 31-40

Casadesús, J, Kaya, Y, Bort, J, Nachit, MM, Araus, JL, Amor, S, Ferrazzano, G, Maalouf, F, Maccaferri, M, Martos, V, Ouabbou, H & Villegas, D (2007); *Using vegetation indices derived from conventional digital cameras as selection criteria for wheat breeding in water-limited environments*; Annals of Applied Biology, **150**, pp 227-236

Catani, F, Ermini, L, Kukavicic, M, Moretti, S & Righini, R (2005); *Detecting land cover changes through remote sensing and GIS techniques*; Proceedings of the 31st International Symposium on Remote Sensing of Environment: ¤Global Monitoring for Sustainability and Security¤; ISPRS; St. Petesburg, Russian Federation; 4 p

Caughlan, L & Oakley, KL (2001); *Cost considerations for long-term ecological monitoring*; Ecological Indicators, **1**, 2; pp 123-134

Cracknell, AP (1999); *Remote sensing techniques in estuaries and coastal zones - an update*; International Journal of Remote Sensing, **19**, 3; pp 485-496

Curran, PJ & Steven, MD (1983); *Multispectral Remote Sensing for the Estimation of Green Leaf Area Index*; Philosophical Transactions of the Royal Society of London. Series A, Mathematical and Physical Sciences, **309**, 1508; pp 257-270

Davidson, NC & Evans, PR (1986); *The Role and Potential of Man-Made and Man-Modified Wetlands in the Enhancement of the Survival of Overwintering Shorebirds*; Colonial Waterbirds, **9**, 2; pp 176-188

Davidson, NC, Laffoley, DdA, Doody, JP, Way, LS, Gordon, J, Key, R, Pienkowski, MW, Mitchell, R & Duff, KL (1991); *Nature conservation and estuaries in Great Britain*; Nature Conservancy Council, Peterborough; 422 p

De Bonet, JS (1997); *Multiresolution sampling procedure for analysis and synthesis of texture images*; Proceedings of the 24th annual conference on Computer graphics and interactive techniques; ACM Press/Addison-Wesley Publishing Co; New York, USA; 361-368 p

Delauré, B, Van Achteren, T, Everaerts, J, Biesemans, J, Lewyckyj, N (2007); *Medusa - A lightweight high-resolution camera system for Earth observation from the Mercator-1 UAV*; Proceedings of the 2007 Annual Conference of the Remote Sensing & Photogrammetry Society (RSPSoc), September 11 - 14; Newcastle-upon-Tyne, UK; 6 p

Donoghue, DNM, Zong, Y, Dunford, R & Watt, P (2004a); *An investigation of the sediment budget, the fate of contaminants, and dating sediment contamination in the Teesmouth and Cleveland coast SPA; Final Contract Report for the Environment Agency (ref. 12917)*; University of Durham Geography Department;

Donoghue, DNM, Watt, PJ, Cox, NJ, Dunford, RW, Wilson, J, Stables, S & Smith, S (2004b); An evaluation of the use of satellite data for monitoring early development of young Sitka spruce plantation forest growth; Forestry; **77**, pp 383-396

Doody, JP (2004); *'Coastal squeeze' - an historical perspective*; Journal of Coastal Conservation, **10**, pp 129-138

Environment Agency (1999); *Tees Estuary - Present & Future (State of the Tees Estuary environment and strategy into the millennium)*; Environment Agency (report NE-2/00-0.25K-C-BFDU), 111 p

EDINA (2004); *Digimap*; Edina; online at http://edina.digimap.ac.uk (accessed on 17-1-07)

Eos (2003); *PhotoModeler 5.0*; Eos Systems Inc.; Vancouver, BC, Canada

Eriksson, BK, Johansson, G & Snoeijs, P (2002); *Long-term changes in the macroalgal vegetation of the inner Gullmar Fjord, Swedish Skagerrak Coast*; Journal of Phycology, **38**, 2; pp 284-296

Espinosa, F & Guerra-García, JM (2005); *Algae, macrofaunal assemblages and temperature: a quantitative approach to intertidal ecosystems of Iceland*; Helgoland Marine Research, **59**, 4; pp 273-285

ESRI (2006); *ArcGIS 9.1*; Environmental Systems Research Institute; Redlands, California, USA

Evans, PR, Ward, RM, Bone, M & Leakey, M (1999); *Creation of Temperate-Climate Intertidal Mudflats: Factors Affecting Colonization and Use by Benthic Invertebrates and their Bird Predators*; Marine Pollution Bulletin, **37**, 8-12; pp 535-545

Falkowski, PG & LaRoche, J (1991); *Acclimation to spectral irradiance in algae*; Journal of Phycology, **27**, pp 8-14

Fisher Scientific (2005); *Material Safety Data Sheet (MSDS# 89617): Ethyl Alcohol (90%)*; Fisher Scientific UK; Loughborough, UK

FMA (2004); *FS8 Co-Pilot™ reference manual*; FMA Inc.; Frederick, Maryland, USA

Foley, WJ, McIlwee, A, Lawler, I, Aragones, L, Woolnough, AP & Berding, N (1998); *Ecological applications of near infrared reflectance spectroscopy - a tool for rapid, cost-effective prediction of the composition of plant and animal tissues and aspects of animal performance*; Oecologia, **116**, 3; pp 293

Fong, P, Boyer, KE, Desmond, JS & Zedler, JB (1996); *Salinity stress, nitrogen competition, and facilitation: what controls seasonal succession of two opportunistic green macroalgae?* Journal of Experimental Marine Biology and Ecology, **206**, 1-2; pp 203-221

Forster, R & Jesus, B (2006); *Field spectroscopy of estuarine intertidal habitats*; International Journal of Remote Sensing, **27**, pp 3657-3669

Friend, PL, Ciavola, P, Cappucci, S & Santos, R (2003); *Bio-dependent bed parameters as a proxy tool for sediment stability in mixed habitat intertidal areas*; Continental Shelf Research, **23**, 17-19; pp 1899-1917

Fytianos, K, Evgenidou, E & Zachariadis, G (1999); *Use of Macroalgae as Biological Indicators of Heavy Metal Pollution in Thermaikos Gulf, Greece*; Bulletin of Environmental Contamination and Toxicology, **62**, 5; pp 630-637

Garmin (2003); *Geko 201 Personal Navigator: owner's manual and reference guide*; Garmin Ltd; Olathe, Kansas, USA

Graham, LF & Wilcox, LW (2000); *Algae*; Prentice Hall, New Jersey; 736 p

Grall, J & Chauvaud, L (2002); *Marine eutrophication and benthos: the need for new approaches and concepts*; Global Change Biology, **8**, 9; pp 813-830

Gray, JS (1980); *Why do ecological monitoring?* Marine Pollution Bulletin, **11**, 3; pp 62-65

Guichard, F, Bourget, E & Agnard, J-P (2000); *High-resolution remote sensing of intertidal ecosystems: A low-cost technique to link scale-dependent patterns and processes*; Limnology and Oceanography, **45**, 2; pp 328-338

Hanelt, D, Wiencke, C & Nultsch, W (1997); *Influence of UV radiation on the photosynthesis of arctic macroalgae in the field*; Journal of Photochemistry and Photobiology B: Biology, **38**, 1; pp 40-47

Haralick, RM & Shapiro, LG (1992); *Computer and Robot Vision*; Addison-Wesley, Reading, Massachusetts; 672 p

Haxo, FT & Clendenning, KA (1953); *Photosynthesis and Phototaxis in Ulva lactuca Gametes*; Biological Bulletin, **105**, 1; pp 103-114

Holland, KT, Puleo, JA, Plant, N & Kaihatu, JM (2002); *Littoral environmental nowcasting system (LENS)*; Proceedings of the Marine Technology Society/IEEE Conference: Oceans 2002, **1**, pp 85-91

Hong, G, R, LM & Rhodes, PA (2001); *A study of digital camera colorimetric characterization based on polynomial modeling*; Color Research & Application, **26**, 1; pp 76-84

Hruska, RC, Lancaster, GD, Harbour, JL & Cherry, SJ (2005); *Small UAV-Acquired, High-Resolution, Georeferenced Still Imagery*; Proceedings of the Wildlife Society 12th Annual Conference; Idaho National Laboratory; Idaho, USA; 13 p

Hudak, AT & Wessman, CA (2001); *Textural analysis of high resolution imagery to quantify bush encroachment in Madikwe Game Reserve, South Africa, 1955-1996*; International Journal of Remote Sensing, **22**, 14; pp 2731-2740

Hunt, ER, Cavigelli, M, Daughtry, CST, McMurtrey, JE & Walthall, CL (2005); *Evaluation of Digital Photography from Model Aircraft for Remote Sensing of Crop Biomass and Nitrogen Status*; Precision Agriculture, **6**, 4; pp 359-378

Jeffrey, DW & Hayes, M (2005); *Net Primary Productivity of Intertidal Systems: The Dublin Bay Example*; In: Wilson, JG; The Intertidal Ecosystem: The Value of Ireland's Shores; Royal Irish Academy, Dublin; pp 45-57

Kamer, K, Fong, P, Kennison, RL & Schiff, K (2004); *The relative importance of sediment and water column supplies of nutrients to the growth and tissue nutrient content of the green macroalga Enteromorpha intestinalis along an estuarine resource gradient*; Aquatic Ecology, **38**, pp 45-56

Karcher, DE & Richardson, MD (2003); *Quantifying Turfgrass Color Using Digital Image Analysis*; **43**, 3; pp 943-951

Klemas, VV (2001); *Remote Sensing of Landscape-Level Coastal Environmental Indicators*; Environmental Management, **27**, 1; pp 47-57

Kolor (2007); *AutoPano 1.3.1*; Kolor; Challes les Eaux, France

Labbé, S, Roux, B, Begue, A, Lebourgeois, V & Mallavan, B (2007); *An operational solution to acquire multispectral images with standard light cameras: spectral characterization and acquisition guidelines*; Proceedings of the 2007 Annual Conference of the Remote Sensing & Photogrammetry Society (RSPSoc), September 11 - 14; Newcastle-upon-Tyne, UK; 6 p

Laliberte, AS, Rango, A & Fredrickson, EL (2006); *Separating green and senescent vegetation in very high resolution photography using an intensity-hue-saturation transformation and object based classification*; Proceedings of the American Society for Photogrammetry and Remote Sensing Annual Conference, May 1-5; ASPRS; Reno, Nevada; 8 p

Laliberte, AS, Rango, A, Herrick, JE, Fredrickson, EL & Burkett, L (2007); *An object-based image analysis approach for determining fractional cover of senescent and green vegetation with digital plot photography*; Journal of Arid Environments, **69**, 1; pp 1-14

Lambers, K, Eisenbeiss, H, Sauerbier, M, Kupferschmidt, D, Gaisecker, T, Sotoodeh, S & Hanusch, T (2007); *Combining photogrammetry and laser scanning for the recording and modelling of the Late Intermediate Period site of Pinchango Alto, Palpa, Peru*; Journal of Archaeological Science, **34**, 10; pp 1702-1712

Larsen, PF, Barker, S, Wright, J & Erickson, CB (2004); *Use of Cost Effective Remote Sensing to Map and Measure Marine Intertidal Habitats in Support of Ecosystem Modeling Efforts: Cobscook Bay, Maine*; **11**, sp2; pp 225-242

Lee, RE (1999); *Phycology*; Cambridge University Press, Cambridge; 614 p

Leica (2006a); *Leica GPS1200 Series Technical Data*; Leica Geosystems AG; Heerbugg, Switzerland

Leica (2006b); *Leica TPS1200 Series Technical Data*; Leica Geosystems AG; Heerbugg, Switzerland

Leland, HV, Brown, LR & Mueller, DK (2001); *Distribution of algae in the San Joaquin River, California, in relation to nutrient supply, salinity and other environmental factors*; Freshwater Biology, **46**, 9; pp 1139-1167

Lewis, LJ & Kelly, TC (2001); *A short-term study of the effects of algal mats on the distribution and behavioural ecology of estuarine birds*; Bird Study, **48**, pp 354-360

Li, X-B, Chen, Y-H, Yang, H & Zhang, Y-X (2005); *Improvement, Comparison, and Application of Field Measurement Methods for Grassland Vegetation Fractional Coverage*; Journal of Integrative Plant Biology, **47**, 9; pp 1074-1083

Lomax, AS, Corso, W & F, EJ (2005); *Employing unmanned aerial vehicles (UAVs) as an element of the Integrated Ocean Observing System*; Proceedings of the Marine Technology Society/IEEE Conference: Oceans 2005, **1**, pp 184-190

Lotze, HK & Worm, B (2002); *Complex interactions of climatic and ecological controls on macroalgal recruitment*; Limnology and Oceanography, **47**, 6; pp 1734-1741

Lowe, DG (2004); *Distinctive Image Features from Scale-Invariant Keypoints*; International Journal of Computer Vision, **60**, 2; pp 91

Lu, D (2005); *Aboveground biomass estimation using Landsat TM data in the Brazilian Amazon*; International Journal of Remote Sensing, **26**, 12; pp 2509-2525

Lu, D & Batistella, M (2005); *Exploring TM Image Texture and its Relationships with Biomass Estimation in Rondônia, Brazilian Amazon*; Acta Amazonica, **35**, 2; pp 249-257

Lyngby, JE, Mortensen, S & Ahrensberg, N (1999); *Bioassessment Techniques for Monitoring of Eutrophication and Nutrient Limitation in Coastal Ecosystems*; Marine Pollution Bulletin, **39**, 1-12; pp 212-223

Malthus, TJ & Mumby, PJ (2003); *Remote sensing of the coastal zone: an overview and priorities for future research*; International Journal of Remote Sensing, **24**, pp 2805-2815

Martins, I & Marques, JC (2002); *A Model for the Growth of Opportunistic Macroalgae (Enteromorpha sp.) in Tidal Estuaries*; Estuarine, Coastal and Shelf Science, **55**, 2; pp 247-257

Martins, I, Pardal, MA, Lillebo, AI, Flindt, MR & Marques, JC (2001); *Hydrodynamics as a Major Factor Controlling the Occurrence of Green Macroalgal Blooms in a Eutrophic Estuary: A Case Study on the Influence of Precipitation and River Management*; Estuarine, Coastal and Shelf Science, **52**, 2; pp 165-177

Mather, P M (2004); *Computer Processing of Remotely-Sensed Images: An Introduction*; Wiley, Chichester, 442 p

MathWorks (2007); *Matlab R2007a*; The Mathworks; Natick, MA, USA

McGlathery, KJ (2001); *Macroalgal blooms contribute to the decline of seagrass in nutrient-enriched coastal waters*; Journal of Phycology, **37**, 4; pp 453-456

Middelboe, AL & Markager, S (1997); *Depth limits and minimum light requirements of freshwater macrophytes*; Freshwater Biology, **37**, 3; pp 553-568

Morris, EP (2005); *Quantifying Primary Production of Micophytobenthos: Application of Optical Methods*; Unpublished PhD thesis, University of Groningen, Netherlands; 184 p

Natural England (2001); *Seal Sands SSSI Designation Citation*; Natural England; online at http://www.english-nature.org.uk/citation/citation_photo/1000141.pdf (accessed on 13-06-2007)

Natural England (2007); *Condition of SSSI Units (Seal Sands)*; Natural England; online at http://www.english-nature.org.uk/special/sssi/reportAction.cfm?report=sdrt13&category=S&reference=1000141 (accessed on 13-06-2007)

Norkko, J, Bonsdorff, E & Norkko, A (2000); *Drifting algal mats as an alternative habitat for benthic invertebrates: Species specific responses to a transient resource*; Journal of Experimental Marine Biology and Ecology, **248**, 1; pp 79-104

Patricio, J, Ulanowicz, R, Pardal, MA & Marques, JC (2004); *Ascendency as an ecological indicator: a case study of estuarine pulse eutrophication*; Estuarine, Coastal and Shelf Science, **60**, 1; pp 23-35

Perry, R (2001); *OceanGLOBE*; online at http://www.msc.ucla.edu/oceanglobe/photos.htm (accessed on 17-1-2007)

Peterson, DL, Brass, JA, Smith, WH, Langford, G, Wegener, S, Dunagan, S, Hammer, P & Snook, K (2003); *Platform options of free-flying satellites, UAVs or the International Space Station for remote sensing assessment of the littoral zone*; International Journal of Remote Sensing, **24**, 13; pp 2785-2804

Pihl, L, Svenson, A, Moksnes, PO & Wennhage, H (1999); *Distribution of green algal mats throughout shallow soft bottoms of the Swedish Skagerrak archipelago in relation to nutrient sources and wave exposure*; Journal of Sea Research, **41**, pp 281-294

Plater, AJ & Appleby, PG (2004); *Tidal sedimentation in the Tees estuary during the 20th century: radionuclide and magnetic evidence of pollution and sedimentary response*; Estuarine, Coastal and Shelf Science, **60**, 2; pp 179-192

Quilter, MC & Anderson, VJ (2000); *Low Altitude Large Scale Aerial Photographs - A Tool For Range And Resource Managers*; Rangelands, **22**, 2; pp 13-17

Raffaelli, DG, Raven, JA & Poole, LJ (1998); *Ecological impact of green macroalgal blooms*; Oceanography and Marine Biology: An Annual Review, **36**, pp 97-125

Ramsar Convention (2007); *The List of Wetlands of International Importance, Article 2.1 of the Convention on Wetlands (1971), Ramsar, Iran*; http://www.ramsar.org/sitelist.pdf

Ratcliffe, D (1977); *A Nature Conservation Review*; Cambridge University Press, Cambridge; 320 p

Ritter, M & Wueller, D (1999); *Colour Characterisation of Digital Cameras by analysing the Output Data for Measuring the Spectral Response*; In: Proceedings of the Conference on Image Processing, Image Quality and Image Capture Systems (PICS-99); IS&T - The Society for Imaging Science and Technology, Savannah, Georgia, USA; pp 149-152

Scanlan, CM, Foden, J, Wells, E & Best, MA (2007); *The monitoring of opportunistic macroalgal blooms for the water framework directive (Implementation of the Water Framework Directive in European marine waters)*; Marine Pollution Bulletin, **55**, 1-6; pp 162-171

Schaadt, TJ, Foster, MS & Zimmerman, RC (2003); *SIMoN Project: Elkhorn Slough Macrophytes Progress Report (December, 2003)*; Phycology Laboratory, Moss Landing Marine Labs, California State University, 15 p

Schramm, W (1999); *Factors influencing seaweed responses to eutrophication: some results from EU-project EUMAC*; Journal of Applied Phycology, **11**, 1; pp 69-79

SmartPlanes (2006); *SmartOne UAV System*; SmartPlanes; online at http://www.smartplanes.se/ (accessed on 18-1-07)

Smith, GM, Spencer, T, Murray, AL & French, JR (1998); *Assessing seasonal vegetation change in coastal wetlands with airborne remote sensing: an outline methodology*; Mangroves and Salt Marshes, **2**, 1; pp 15-28

Somsueb, S, Ohno, M & Kimura, H (2001); *Development of seaweed communities on suspended substrata with three slope angles*; Journal of Applied Phycology, **13**, 2; pp 109-115

Spellberg, IF (1991); *Monitoring Ecological Change*; Cambridge University Press, Cambridge; 334 p

Tegler, B, Sharp, M & Johnson, MA (2001); *Ecological Monitoring and Assessment Network's Proposed Core Monitoring Variables: An Early Warning of Environmental Change*; Environmental Monitoring and Assessment, **67**, 1/2; pp 29-56

Thain, D, Tannenbaum, T & Livny, M (2005); *Distributed computing in practice: the Condor experience*; Concurrency and Computation: Practice and Experience, **17**, 2-4; pp 323-356

Trimmer, M, Nedwell, DB & Malcolm, SJ (2000); *Seasonal organic mineralisation and denitrification in intertidal sediments and their relationship to the abundance of Entermorpha sp. and Ulva sp.*; Marine Ecology Progress Series, **203**, pp 67-80

Urquhart, NS & Kincaid, TM (1999); *Designs for Detecting Trend from Repeated Surveys of Ecological Resources*; Journal of Agricultural, Biological, and Environmental Statistics, **4**, 4; pp 404

Valiela, I, McClelland, J, Hauxwell, J, Behr, PJ, Hersh, D & Foreman, K (1997); *Macroalgal blooms in shallow estuaries: Controls and ecophysiological and ecosystem consequences*; Limnology and Oceanography, **42**, 5-2; pp 1105-1118

Vane, G, Green, RO, Chrien, TG, Enmark, HT, Hansen, EG & Porter, W M (1993); *The airborne visible/infrared imaging spectrometer (AVIRIS)*; Remote Sensing of Environment; **44**, 2-3, pp 127-143

Vaughan, H, Brydges, T, Fenech, A & Lumb, A (2001); *Monitoring Long-Term Ecological Changes Through the Ecological Monitoring and Assessment Network: Science-Based and Policy Relevant*; Environmental Monitoring and Assessment, **67**, 1/2; pp 3-29

Villares, R, Puente, X & Carballeira, A (2001); *Ulva and Enteromorpha as indicators of heavy metal pollution*; Hydrobiologia, **462**, 1; pp 221-232

Vos, P, Meelis, E & Ter Keurs, WJ (2000); *A Framework for the Design of Ecological Monitoring Programs as a Tool for Environmental and Nature Management*; Environmental Monitoring and Assessment, **61**, 3; pp 317-344

Wikantika, K, Uchida, S & Yamamoto, Y (2004); *An evaluation of the use of integrated spectral and textural features to identify agricultural land cover types in Pangalengan, West Java, Indonesia*; Japan Agricultural Research Quarterly, **38**, 2; pp 137-148

Yu, Q, Gong, P, Clinton, N, Biging, G, Kelly, M & Schirokauer, D (2006); *Object-based Detailed Vegetation Classification with Airborne High Spatial Resolution Remote Sensing Imagery*; Photogrammetric Engineering & Remote Sensing, **72**, 7; pp 799-811